Universidade de Aveiro Departamento de Química
Ano 2012

Luís Manuel Cravo Pereira

Captura de Poluentes de Correntes Pós-combustão com Líquidos Iónicos

Capture of Pollutants from Post-combustion Streams with Ionic Liquids

Universidade de Aveiro Departamento de Química
Ano 2012

Luís Manuel Cravo Pereira

Captura de Poluentes de Correntes Pós-combustão com Líquidos Iónicos

Capture of Pollutants from Post-combustion Streams with Ionic Liquids

Dissertação apresentada à Universidade de Aveiro para cumprimento dos requisitos necessários à obtenção do grau de Mestre em Engenharia Química, realizada sob a orientação científica do Dr. João Manuel da Costa e Araújo Pereira Coutinho, Professor Associado com Agregação do Departamento de Química da Universidade de Aveiro, e co-orientação da Dra. Mariana Belo Oliveira, Estagiária de Pós-doutoramento do Departamento de Química da Universidade de Aveiro.

Dedico este trabalho aos meus pais e irmãos.

o júri

presidente

Prof. Doutor Carlos Manuel Santos Silva
Professor Auxiliar do Departamento de Química da Universidade de Aveiro

Prof. Doutor João Manuel da Costa e Araújo Pereira Coutinho
Professor Associado com Agregação do Departamento de Química da Universidade de Aveiro

Doutora Mariana Belo Oliveira
Estagiária de Pós-Doutoramento no Departamento de Química da Universidade de Aveiro

Doutora Ana Maria Antunes Dias
Estagiária de Pós-Doutoramento no Departamento de Química da Faculdade de Ciências e Tecnologia da Universidade de Coimbra

agradecimentos

Em primeiro lugar gostaria de agradecer ao Prof. João Coutinho pela possibilidade de ter realizado a minha tese mestrado sob a sua orientação. Os seus conselhos, perseverança e carácter único contribuíram não só para a realização de um melhor trabalho, mas sobretudo para a minha formação como pessoa e investigador.

Não posso também esquecer a excelente orientação do Pedro Carvalho. A sua extensa experiência nos mais diversos temas, o seu amplo conhecimento nas diferentes técnicas aplicadas neste trabalho e uma personalidade inigualável tornaram este percurso muito mais enriquecedor. A ele, o meu muito obrigado!

Gostaria também de agradecer à Ana Dias, à Mariana Belo e ao Fèlix Llovel pela disponibilidade, ajuda e conhecimentos transmitidos durante a modelação dos sistemas.

Nunca esquecerei os momentos que só um grupo como o Path poderia ter proporcionado. Sem nunca esquecer ninguém, gostaria de agradecer à Marta Batista, à Sónia Ventura e ao Jorge Pereira pelos seus conselhos e ocasiões de descontração, muito importantes para uma investigação saudável. Gostaria de agradecer em especial também ao Félix Carreira, companheiro para a vida, pelo seu apoio e sugestões que tanto ajudaram a ultrapassar obstáculos.

Por fim, e por isso não menos importante, gostaria de agradecer aos meus pais, irmãos e a Margarida Cabral pelo infinito e incondicional apoio que me deram durante este curso. Isto é para vocês!

palavras-chave

Líquidos iónicos, solubilidade de gases, dióxido de carbono, azoto, óxido nitroso, metano, soft-SAFT EoS, seletividades.

resumo

O aumento da emissão de poluentes nitrogenados, bem como as limitações presentes nos atuais métodos de controlo e o aparecimento de novas legislações e limites máximos de emissão, requerem o desenvolvimento de novos métodos para a redução destes poluentes.

Os Líquidos Iónicos (LIs), pelas suas características únicas e baixa pressão de vapor, têm despertado uma grande atenção durante a última década e estão a tornar-se numa nova classe de solventes muito promissores para a captura de poluentes e separação de gases, quer como fase estacionária num processo de membranas quer como absorvente num processo de extração. Não obstante, o desenvolvimento de novos processos de controlo, ou melhoria dos já existentes, requerem o conhecimento do equilíbrio gás-líquido (EGL) que é, até ao momento, ainda insuficiente.

Neste trabalho, a solubilidade de gases presentes em processos de combustão como o azoto (N_2), o metano (CH_4), óxido nitroso (N_2O) e dióxido de carbono (CO_2) num líquido iónico muito polar foram estudados através de medições do EGL. Os resultados demostram a já reconhecida elevada solubilidade de N_2O e CO_2 em LIs bem como a elevada seletividade em relação ao ar devido à baixa solubilidade do N_2 nos LIs. Foi ainda observado que, contrariamente aos outros gases, para os sistemas N_2 + LIs o aumento da temperatura provoca uma aumento da solubilidade do gás.

A descrição dos sistemas anteriores por modelos teóricos é fundamental para o projeto de potenciais técnicas de redução de poluentes. Neste sentido, a soft-SAFT EoS, que tem demonstrado ser capaz de descrever sistemas com LIs com enorme sucesso, foi usada para descrever os diferentes sistemas publicados na literatura e medidos aqui em função da temperatura, composição e pressão, permitindo deste modo estender a aplicabilidade do modelo a novos sistemas. Novos parâmetros moleculares, necessários para a descrição de cada componente, são propostos neste trabalho para o N_2O e para três dos cinco LIs estudados. Os resultados demonstraram uma boa descrição dos dados experimentais, tanto no que diz respeito ao comportamento inverso observado para o N_2 como a baixa dependência do CH_4 com a temperatura.

Finalmente, a capacidade de extração dos LIs bem como a sua seletividade é comparada com a dos solventes utilizados nos métodos de controlo atuais, como monoetanolamina (MEA) e éter monometílico de trietilenoglicol (TEGMME). Os resultados demonstram uma capacidade de extração dos LIs igual ou superior à dos solventes convencionais, aliada a uma elevada seletividade em relação ao N_2O e CO_2.

Com base neste trabalho, pode-se afirmar que os LIs, devido às suas características únicas e elevada seletividade, apresentam um grande potencial para serem utilizados na captura de poluentes.

keywords

Ionic liquids, gas solubilities, carbon dioxide, nitrogen, nitrous oxide, methane, soft-SAFT EoS, seletivities.

abstract

The increase in nitrogenated pollutants emissions, along with the limitations of the existing control methods and future stricter legislation, demands the development of new methods to reduce such pollutants.

Ionic liquids (ILs), due to their unique characteristics and low vapour pressure, have attracted a large attention during the last decade and are becoming a promising class of solvents to capture pollutants and for gas separation, either as a stationary phase in a membrane process or as an absorption solvent in an extraction process. Nonetheless, the development and/or improvement of new/existing control processes requires the knowledge of gas-liquid equilibrium (GLE) data for ILs + gas systems that are, at the moment, still scarce.

The solubilities of some common gases present in combustion processes, such as nitrogen (N_2), methane (CH_4), nitrous oxide (N_2O) and carbon dioxide (CO_2), were studied through the experimental measurement of the GLE. The results showed a high solubility of N_2O and CO_2 compared to N_2. Furthermore, a surprisingly increase of the solubility of N_2 with temperature was observed.

The description of previous systems by theoretical models stands also as a vital task for the development of techniques to reduce pollutants. In this sense, the soft-SAFT EoS has proven to be able to describe systems with ILs with a huge success and in a predictive manner. Thus, this model was used to describe the GLE data available in the literature and measured here, for different temperatures and for all concentrations and pressures ranges studied, in order to extend the applicability of the soft-SAFT EoS to describe/predict the gas + ILs systems. The molecular parameters necessary for the description of each compound were determined for the first time in this work for N_2O and three of the five ILs involved. The results showed a good description of the experimental data. In addition to that, soft-SAFT EoS successfully predicts the peculiar behaviour observed for N_2 as well as the low temperature dependence observed for the CH_4 systems.

Finally, the extraction capacity and gases selectivity in the ILs was compared with other solvents used in the reduction of pollutants, such as monoethanolamine (MEA) and triethylene glycol monomethyl ether (TEGMME). The results showed a similar or higher extraction capacity of the ILs compared to conventional solvents, combined with a high selectivity towards N_2O and CO_2.

Based on the results showed on this work, it is suggested that ILs due to their unique characteristics and high selectivity are promising agents to capture pollutants.

List of Contents

List of Figures

List of Tables

Nomenclature

List of Symbols

A	Helmholtz energy
f	Function (Chapter 1)
f	Fugacity (Chapter 4)
g_{LJ}	Radial distribution function of a fluid of LJ spheres
k_B	Boltzman's constant
k^{HB}	Association site volume
m	Number of segments
M	Number of association sites
$m_{g/s}$	Molality
m_i	Mass of component *i*
N	Number of points
p	Pressure
Q	Quadrupole
T	Temperature
x_i	Molar fraction of the component *i*
x_p	Fraction of the chain with the quadrupole
Z	Studied property
ε/k_B	Dispersive energy between segments forming the chain
ε^{HB}/k_B	Association site energy
μ	Chemical potential
ρ	Density
σ	Segment size
η	Binary parameter for correcting deviations in the molecular size
ξ	Binary parameter for correcting deviations in the molecular energy

List of Abbreviations

%AAD	Percentage average absolute deviation
$[C_2mim][CH_3OHPO_2]$	1-ethyl-3-mthylimidazolium methylphosphonate
$[C_4mim][BF_4]$	1-butyl-3-methylimidazolium tetrafluoroborate
$[C_4mim][N(CN)_2]$	1-butyl-3-methylimidazolium dicyanamide

$[C_4mim][NTf_2]$	1-butyl-3-methylimidazolium bis(trifluoromethylsulfonyl)imide
$[C_4mim][SCN]$	1-butyl-3-methylimidazolium thiocyanate
Ar	Argon
BOOS	Burners Out of Service
BSI	BioSolids Injection
C_2F_6	Perfluoroethane
CAA	Clean Air Act
CF_4	Perfluoromethane
CH_4	Methane
CO	Carbon monoxide
CO_2	Carbon dioxide
EPA	Environmental Protection Agency
EU	European Union
GLE	Gas-liquid equilibrium
GWP	Global Warming Potential
H	Henry's constant
H_2O	Water
H_2S	Hydrogen sulphide
HFC-23	Fluoroform
HNO_3	Nitric acid
IL	Ionic liquid
ILs	Ionic liquids
LJ	Lennard-jones
LNB	Low-NO_x Burner
LTOA	Low-Temperature Oxidation with Absorption
MEA	Monoethanolamine
N_2	Nitrogen
N_2O	Nitrous oxide
N_2O_4	Dinitrogen tetroxide
N_2O_5	Dinitrogen pentoxide
NH_3	Ammonia
NO	Nitrogen monoxide
NO_2	Nitrogen dioxide

NO_x	Oxides of nitrogen
O_2	Oxygen
O_3	Ozone
OFA	Over Fire Air
Pb	Lead
PM	Particulate matter
$S_{1/2}$	Ideal selectivity between the gases (1 and 2) in a specified solvent
SAFT	Statistical Associating Fluid Theory
SCR	Selective Catalytic Reduction
SH_6	Sulphur hexafluoride
SNCR	Selective Non-catalytic Reduction
SO_2	Sulphur dioxide
Soft-SAFT EoS	"Soft" statistical associating fluid theory equation of state
TEGMME	Triethylene glycol monomethyl ether
TPT1	Wertheim's first-order thermodynamic perturbation theory
US	United States
vdW-1f	Van der Waals one-fluid theory
VOCs	Volatile Organic Compounds
WHO	World Health Organization

Superscripts

assoc	Association interactions term
chain	Chain term
polar	Polar interactions term
res	Reference term

Subscripts

i	Component i
liq	Liquid phase
vap	Vapour phase

“The satisfaction and good fortune of the scientist lies not in the peace of possessing knowledge but in the toil of continually increasing it.”

Max Planck

1- General Introduction

1.1- Scope and Objectives

The increase of pollutants emissions along with the limitations presented by the existing control methods and stricter legislation to come, demands the investigation of new methods and ways to reduce some pollutant levels. This is particularly important for nitrogenated compounds, such as oxides of nitrogen (NO_x) and nitrous oxide (N_2O), whose emissions increase has an important effect on the atmosphere and human health.[1]

Ionic liquids (ILs) have attracted an outstanding attention during the last decade and are turning to be a promising class of solvents in the capture pollutants and also in gas separations due to their unique characteristics and low vapour pressure. Therefore, the possibility of using ILs as capturing agents for nitrogenated compounds is here evaluated and discussed by studying the gas-liquid equilibrium (GLE) of N_2O in several ILs. N_2O was here chosen as a representative molecule for the nitrogenated compounds due to its low adverse effects on human health when compared to NO_x.[2] Nitrogen (N_2) and carbon dioxide (CO_2), the major constituents of post-combustion streams,[3] and methane (CH_4), produced in higher concentration, for instance, during the incomplete combustion or at low temperatures combustion of natural gas streams,[4] are also investigated through the study of their GLE in the ionic liquid (IL), aiming at understanding ILs' capturing capacity/capability.

As previous works showed,[5-8] the CO_2 and N_2O selectivities towards gases like N_2 and CH_4 can be enhanced by using highly polar ILs due to the very low solubility that these later gases present on ILs. To evaluate this concept, the high pressure GLE of these four gases in a highly polar IL, 1-ethyl-3-mthylimidazolium methylphosphonate ($[C_2mim][CH_3OHPO_2]$), was studied as function of temperature and pressure. The GLE data was measured using a high pressure equilibrium cell based on the Daridon *et al.*[9-13] design and the synthetic method, which has previously shown to be adequate to accurately measure these types of systems. Additionally, gas solubilities in other ILs such as 1-butyl-3-methylimidazolium dicyanamide ($[C_4mim][N(CN)_2]$), 1-butyl-3-methylimidazolium thiocyanate ($[C_4mim][SCN]$), 1-butyl-3-methylimidazolium tetrafluoroborate ($[C_4mim][BF_4]$) and 1-butyl-3-methylimidazolium bis(trifluoromethylsulfonyl)imide ($[C_4mim][NTf_2]$) were taken from the literature[14-20] and from the research group unpublished data, and compared with those measured here.

Furthermore, the development of reliable thermodynamic models capable of estimating the solubility of gases in the ILs stands as a vital key to the pursuit of alternative solvents. The soft-SAFT EoS, proposed by Vega and co-workers[21] based on the original Statistical Associating

Fluid Theory (SAFT), is one of the most successful association EoS applied for the description of IL systems.[22-25] Therefore, binary GLE systems were modelled with the soft-SAFT EoS and molecular parameters for N_2O, $[C_2mim][CH_3OHPO_2]$, $[C_4mim][SCN]$ and $[C_4mim][N(CN)_2]$ are here reported for the first time, while CO_2, N_2, CH_4, $[C_4mim][BF_4]$ and $[C_4mim][NTf_2]$ were modelled using molecular parameters data available in the literature.[12, 22, 24, 26, 27]

In addition to that, ILs' capturing efficiency and selectivity were calculated and compared to some commons solvents used in the removal of some pollutants.

1.2- Air Pollution

According to the World Health Organization (WHO) Air Pollution is the "*contamination of the indoor or outdoor environment by any chemical, physical or biological agent that modifies the Natural characteristics of the atmosphere*", in other words, air pollution exists when one or several air pollutants are present in such amounts that they are damaging humans, animals, plants or materials.

Air pollution exists from times long before man discovered fire and started to use it for heating and preparing food. In fact, air pollution from wildfires, volcanic activity and natural biomass decomposition always existed. However, air quality, or its chemical compositions on minor constituents, drastically changed with the Industrial Revolution. The substances that promote air pollution can be in the liquid, gaseous or solid state and appear in the atmosphere as smoke, fog, dust, etc. according to their size, form and properties.[28, 29]

Among the 300+ substances considered as air pollutants, carbon monoxide (CO), sulphur dioxide (SO_2), volatile organic compounds (VOCs), particulate matter (PM), lead (Pb) and oxides of nitrogen (NO_x and N_2O), also known as "Primary pollutants", are the most important and with the higher ambient impact. Furthermore, these substances, depending on their physical and chemical characteristics, can react and transform into new pollutants. These substances, resultant from the reaction with primary pollutants, are known as "Secondary pollutants". Examples of secondary pollutant include ozone (O_3) and acids.[1]

The actual Earth's atmosphere is composed mainly by nitrogen (N_2), oxygen (O_2) and argon (Ar) and "*their abundances are controlled over geologic timescales by the biosphere uptake and release from crustal material and degassing of the interior*".[1] The next most abundant constituent is water vapour (H_2O) whose concentration is highly variable and controlled by water evaporation and precipitation. In spite of their minor concentrations, the remaining constituent gases, also known as trace gases, which include some nitrogenated compounds like NO_x and N_2O, play a

fundamental role in the Earth's radioactive balance and in the chemical properties of the atmosphere. The values of each atmosphere's constituent are shown in Figure 1.1.

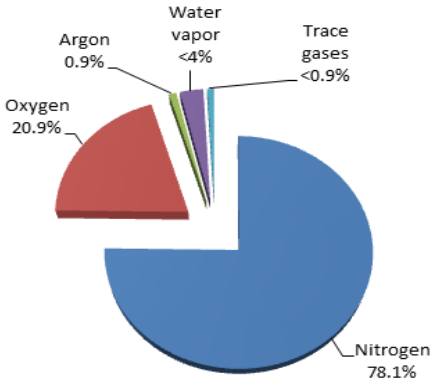

Trace Gas	Mixing Ratio	Trace Gas	Mixing Ratio
CO_2	3.4×10^{-3}	O_3	$(0.1\text{-}1.0)\times10^{-7}$
CH_4	$(1.7\text{-}3.0)\times10^{-6}$	NO_x	$(0.2\text{-}5.0)\times10^{-10}$
N_2O	3.1×10^{-7}	SO_2	3.0×10^{-10}
CO	$(0.4\text{-}2.0)\times10^{-7}$		

Figure 1.1- Composition (% v/v) of Earth's Atmosphere, adapted from Jacob *et al.*[30]

The trace gases concentrations have changed rapidly and remarkably over the last two centuries, mainly due to anthropogenic activity. Observations have shown that the composition of the atmosphere is changing on a global scale. In fact, recent measurements, combined with analyses of ancient air trapped in bubbles in ice cores, provided the record of a dramatic global increase on the concentrations of gases such as CO_2, CH_4, N_2O and various halogen-containing compounds.[1] These gases, also known as "greenhouse gases", are able to absorb infrared radiation from the Earth's surface and radiate a portion of it back to the surface, acting as atmospheric thermal insulators.

The overall effect of a gas on the Earth's temperature is measured by the global warming potential (GWP). As can be seen in Table 1.1, N_2O is one of the most important and powerful greenhouse gases, with a global warming potential 296 times higher that of CO_2; this is a result of its long residence time and its relatively large energy absorption capacity per molecule. Moreover, as it will be discussed later, N_2O can perturb in a large scale the atmospheric chemistry.

Table 1.1- Global Warming Potential (GWP) and lifetime of some pollutants, adapted from Seinfeld *et al.*[1]

Chemical species	Lifetime (year)	100-years GWP
CH_4	8.4	23
N_2O	120	296
CF_4	>50000	5700
C_2F_6	10000	11900
SF_2	3200	22200
HFC-23	260	12000
CO_2	- [a)]	1

[a)]Its removal from the atmosphere involves several processes with different time scales.

As mentioned before, the trace gases contribute to the Earth's radioactive balance but, also have an important effect in human and environmental health. According to the WHO, air pollution has caused approximately 800.000 deaths and 4.6 million lost life-years worldwide. Nonetheless, these numbers are expected to be worse than these estimations since they were estimated mainly based on the United States (US) data and extrapolated worldwide, and it is well known that this problem is not equally distributed globally, being one of the world highest levels of air pollution found in Asian megacities.[31]

As history shows, a serious consequence of exposure to air pollution occurred in the mid-20th century when cities of Europe and US suffered air pollution episodes, like the infamous 1952 London smog, that resulted in many deaths and hospital admissions[32, 33] and the recurrent smog occurrences in Los Angeles. Although the biological mechanisms are not fully comprehended, many epidemiological studies suggest[34-38] a close link between air pollution and various health outcomes (respiratory symptoms, mortality, cancer and congenital heart disease). Air Pollution may also lead to environmental degradation such as: Direct plant damage, caused by gases and acids in direct contact with leaves and needles; Soil acidification, mostly produced by acid rain but also by the harvesting of biomass by the forestry industry; Excess nitrogen, caused by nitrogen deposition leading to the fast growth of trees crowns, faster than their root systems, and Warmer climate, originating sea level rise and a probable increase in the frequency of some extreme weather events.[39]

These pollution levels seem to be linked to social and economic development mainly due to the increase use of fossil fuels for transport, power generation and products fabrications. Consequently, clean air legislation needed to be carried out in order to reduce the emission of pollutants and the infamous 1952 London smog was an important turning event in air quality control and legislation.[33] In 1956, the Clean Air Act (CAA) authorized air pollution research and left the responsibility for air pollution control to state and local governments. It was only with the 1970 CAA amendments that this responsibility was spread to other entities like the Environmental Protection Agency (EPA) created in the US.[40, 41] EPA established national ambient air quality standards to protect health and welfare and required that these standards should be achieved and maintained across the country. Other important events concerning air quality occurred during the following 30 years where the European Union (UE) and other international organisations exerted strong influence.[33]

Even though all the changes and improvements seen in the past 50 years, air pollution is still a major concern mainly due to some recurring episodes of summer smog in major cities, the well-known ozone hole over the Antarctic or even a controversial issue, climate change.

1.3- Nitrogenated Compounds

As stated before, nitrogenated compounds are considered one of the most important air pollutants. Nonetheless, N_2, the most abundant compound (78%) on Earth's atmosphere, is practically inert and, due to its chemical stability, is not involved in the atmosphere's chemistry; hence it is not an air pollutant. However, it becomes very useful to most organisms when it is fixed or converted to a form that can be used by the organisms. N_2 fixation can either occur by natural, industrial or combustions methods. The most important result in the form of N_2O, nitric oxide (NO), nitrogen dioxide (NO_2), nitric acid (HNO_3) and ammonia (NH_3).[1] Usually NO, NO_2, N_2O and other less common combination of nitrogen and oxygen (N_2O_4 and N_2O_5) are known as NO_x (oxides of nitrogen). The EPA defines NO_x as "*all oxides of nitrogen except N_2O*".[42] For simplification, this nomenclature will be adopted in this work.

NO_x are among the most important molecules in atmospheric chemistry as they play a central role in the nitrogen cycle (see Figure 8.1 in the appendix A) and, due its high reactivity, they are the main reason for ground level ozone, acid rain and smog.[1] The two primary NO_x are NO and NO_2.

NO is a colourless, poisonous gas that presents several adverse health effects, such as eyes and throat irritation, nausea, headache and gradual strength loss. In addition, prolonged exposure can cause violent coughing, difficulty in breathing and cyanosis.[2] In extreme cases it could even be fatal. NO_2 is a reddish brown and highly reactive gas and strong oxidant agent that has a suffocating odour. It is also highly toxic, hazardous and able to cause delayed chemical pneumonitis and pulmonary edema.[2] Combustions are by far the largest source of NO_x, as shown in Table 1.2. Coal-fired electric power plants and industrial combustion are the highest sources of NO_x. Furthermore, motor vehicles and other forms of transportation, including ships, airplanes and trains have also a

Table 1.2- Estimate of Global Tropospheric NO_x emission in the year 2000, adapted from Seinfeld *et al.*[1] (1 Tg nitrogen=10^{12} g nitrogen).

Sources	Emissions (Tg nitrogen/year)
Fossil fuel combustion	33.0
Aircraft	0.7
Biomass burning	7.1
Soils	5.6
Lightning	5.0

large contribution.[40, 43] Nevertheless, NO_x emissions have decreased in the last 20 years in Europe, as depicted in Figure 1.2, mainly due to the emergence of strict legislation and directives, like EURO 5 for transports and The Large Combustion Plant and the Integrated Pollution Prevention and Control for industry.[44]

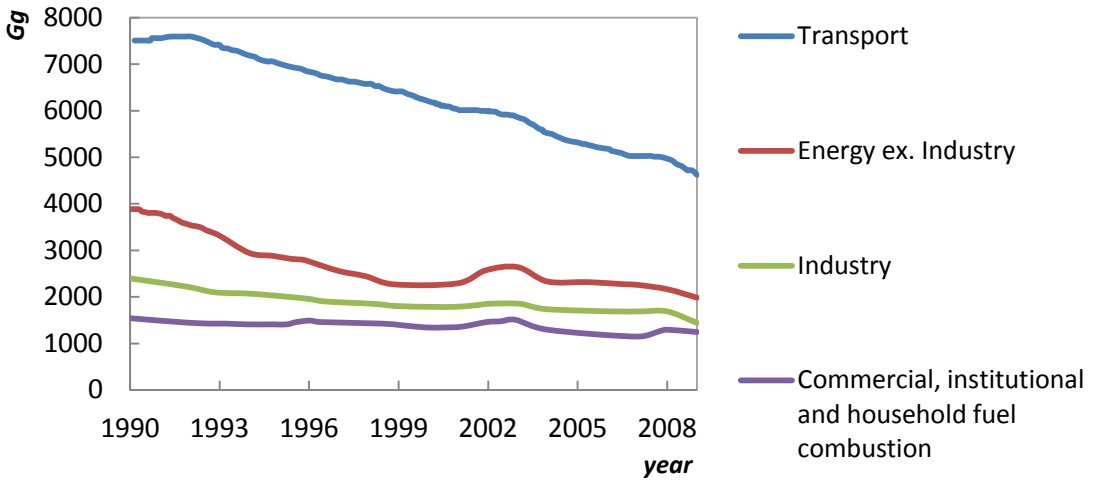

Figure 1.2- Evolution of NO_x emissions by source sector in the EU adapted from the 2011 Air Quality report[44] (1 Gg=1000 tonnes/year).

N_2O is a colourless gas, commonly referred as the "laughing gas" and it is widely employed as an anaesthetic. Also, N_2O is inert in the troposphere but in the stratosphere, it turns into the major input of NO, becoming an important natural regulator of stratospheric O_3 and, therefore, N_2O is the main responsible for the O_3 depleting.[45] Nonetheless, about 90% of N_2O is destroyed in the stratosphere by photolysis (see Figure 8.1 in the appendix A). N_2O is emitted predominantly by biological sources in soils and water,[1] while agriculture and chemical industry are the main anthropogenic sources, as depicted in Figure 1.3.

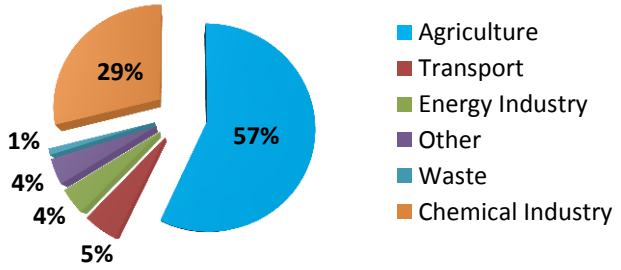

Figure 1.3- Total annual anthropogenic N_2O emission in the UE (average 1990-1998), adapted from Pérez-Ramírez *et al.*[46]

Nowadays, there is no official governmental legislation for the emission of this pollutant therefore, its increase is expected to take a rate of 0,26% per year due to anthropogenic emissions.[46] As a matter of fact, ice core records of N_2O showed a preindustrial mixing ratio of about 276 ppb, while in 2000 it was 315 ppb and in 2005 it was 319 ppb (Figure 1.4). In addition, it is expected to reach levels of 360-460 ppb by the year 2100, 11-45% higher than the actual concentration, mainly due to the larger contribution of chemical industry. One of the main

contribution comes from the HNO_3 production where N_2O is formed, resulting in emissions of 400kT per year.[46]

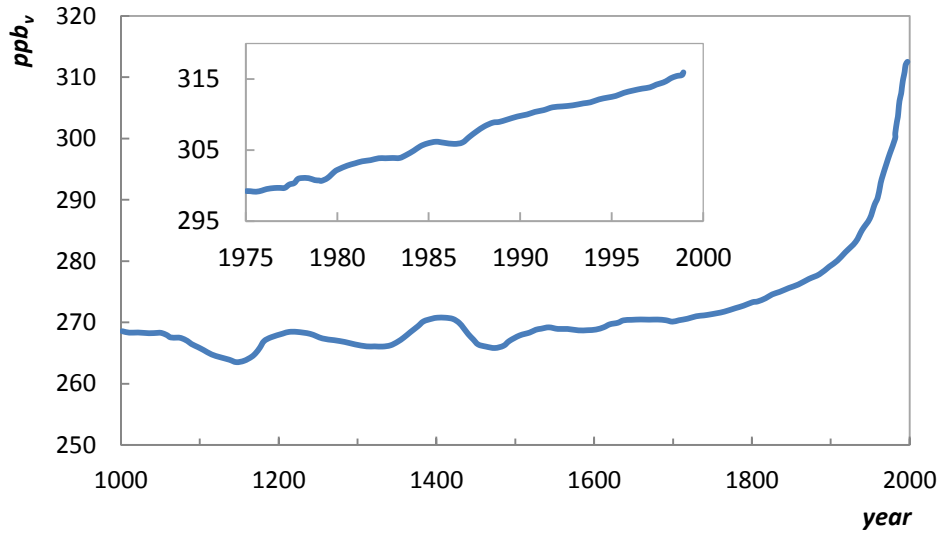

Figure 1.4- Evolution of the atmospheric N_2O concentration, adapted from Pérez-Ramirez *et al.*[46]

1.4- Control Methods for Nitrogenated Compounds

The technologies used for reducing NO_x are divided in: *i)* primary control technologies or combustion control and *ii)* secondary control technology or flue gas treatment. Primary control technologies are used to minimize the amount of NO_x initially produced in the combustion zone and involves a pre-treatment process and/or a process and combustion modifications, *i.e.*, NO_x is reduced by taking advantage of the thermodynamics and kinetics of the process by, for example, reducing flame peak temperature, reducing oxygen concentration in the primary flame zone or even, using thermodynamic and kinetic balances to promote the reconversion of NO_x back to N_2 and O_2. In the other hand, secondary control technologies are used to reduce the NO_x present in the exhaust gas from the combustion zone, *i.e.*, from the post-combustion stream. They focus mainly on converting NO_x into N_2 and O_2 using a reducing agent with or without a catalyst, or through the absorption of the species of interest.[40]

Both technologies are often used in a wide variety of combinations to achieve desired NO_x emission levels at optimal cost but, it is important to take into account that the performance of the individual technologies is not additive and varies for each combustion process.[40]

The most common techniques used for primary control are: Low-Excess Air Firing, Over Fire Air (OFA), Flue Gas Recirculation, Reducing Air Preheated, Reducing Firing Rate, Water/Steam Injection, Burners Out of Service (BOOS), Reburning, Low-NO_x Burner (LNB), Ultra Low-NO_x Burner, Injection Timing Retard, Air/fuel Ratio Changes, Low Emission Combustion, Low-NO_x

Burners with Indirect Firing, Low-NO_x Precalciners, Mid-kiln Firing. For secondary control there are: Selective Non-catalytic Reduction (SNCR), Selective Catalytic Reduction (SCR), Reburning, Low-Temperature Oxidation using Ozone, Scono$_x^{TM}$, Low-Temperature Oxidation with Absorption (LTOA) and Biosolids Injection (BSI).[40, 43] In Table 1.3 is listed a summary of some NO_x control techniques and respective removal efficiency.

Table 1.3- Summary of NO_x removal efficiency reported in the literature for diverse techniques.

Techniques	Reported NO_x removal efficiency
Low-Excess Air Firing	15-55%[a)]
Low NO_x Burner	40-65%[a)]
	14-50%[b)]
Over Fire Air	Additional 10 to 25% beyond LNB[b)]
Selective Non Catalytic Reduction	30-50%[a)]
	10-90%[b)]
Selective Catalytic Reduction	70-90%[a)]
	80-95%[b)]
Reburning	58-77%[a)]
	39-67%[b)]
Low Temperature Oxidation with Absorption	99%[a)]
Burners Out Of Service	15-30%[a)]
Water/Steam Injection	20-30%[a)]
Biosolids Injection	50%[b)]
Injection Timing Retard	15-30%[b)]
Air/fuel ratio Changes	50+%[b)]
Low Emission Combustion	80+%[b)]

[a)] Data from Schnelle. *et al.*[40]; [b)] Data from Srivastava *et al*.[43]

As shown in Table 1.3, some techniques achieve high NO_x reduction but require proper care to be taken in operating and maintaining the combustion process in order to attain the desired range of emissions. SNCR and SCR, besides LTOA, provide high NO_x reduction so they are the most popular control techniques along with LNB and OFA.[43]

On the other hand, HNO_3 production is one of the main contributors for increasing N_2O emissions, as it is formed during its synthesis, being then released from reactor vents into the atmosphere. Production of weak HNO_3 is based on the *Ostwald process* and consists on some basic chemical operations: Catalytic oxidation of NH_3 with air into NO; Oxidation of NO into NO_2 and Absorption of NO_2 in water to produce HNO_3. The N_2O formation depends totally on the NH_3 oxidation process and it can result in other products depending on the process temperature, as follows:

$$NH_3 + O_2 \xrightarrow{9Pt/1Rh} \begin{cases} N_2 \\ N_2O \\ NO \end{cases}$$ **Eq. 1.1**

For the three previous paths, at low temperatures (423-473 K) N_2 is the principal product formed, while at higher temperatures N_2O formation is initiated, reaching its maximum at 675 K. The desired product, NO, starts at 573 K and its yields continuously increase with temperature. Catalyst selectivity is important as well as composition and state (age), for achieving NO yields of 95-97%, typical values under industrial conditions. There is still others undesired reactions, involving by-products and unreacted NH_3, that can lead to an increase of N_2O emissions.[46] Thus, a great effort has been made to develop N_2O abatement systems capable of achieving high efficiency (>90% N_2O conversion) and selectivity (0.2% NO loss).

Nowadays, apart from process optimization, that will not be addressed here, only a few techniques, such as Thermal Decomposition, SCR, SNCR and Catalytic Direct Decomposition, are used for N_2O abatement from industrial sources.[46] Thermal Decomposition of N_2O is based on raising the temperature of the exhaust gases to the required 1023-1273 K, at this point it decomposes in N_2 and O_2.[47] However, this technique seems to be prohibitive because it requires a high-temperature heat exchanger which can represent a huge investment and operational costs. Thus, other techniques like SNCR and SCR are preferred. They were already referred as control techniques for NO_x and both are based in the use of a reducing agent in the presence or not of a catalyst (normally metal-zeolites). Propane, propene, natural gas or NH_3 are normally used as reducing agents for SCR, while hydrogen (H_2), natural gas or naphtha are used for SNCR. SNCR has conversion efficiencies of about 70% while SCR has highest (up to 100%), but requires an optimal temperature control (650-793 K) and a periodically replacement of the catalyst due to its high sensitivity to impurities present in the treated effluent.[46] Finally, Catalytic Direct Decomposition is based in the N_2O decomposition without a reducing agent, so they could be more attractive and economical than the previous options. However, none of the studied catalyst showed a good activity and stability under realistic industrial conditions. Some of the catalysts already studied include transition (Cu, Co and Ni) and noble metal-based catalysts (Rh, Ru and Pd) on different supports (ZnO, CeO_2, Al_2O_3, TiO_2, ZrO_2, calcined hydrotalcites and perovkites).[46]

1.5- Control Methods Insufficiency

The available techniques, already implemented in industry and capable of reducing nitrogenated compounds to values permitted by the actual legislation, do not guarantee the total pollutants removal and all present several problems and limitations. In addition, it is expected that the dependency on fossil fuels will be maintained as recently showed by the 2012 Annual Energy Outlook report[48] (Figure 1.5). These projections are only for the US, however this scenario would not be very different from the rest of the world.

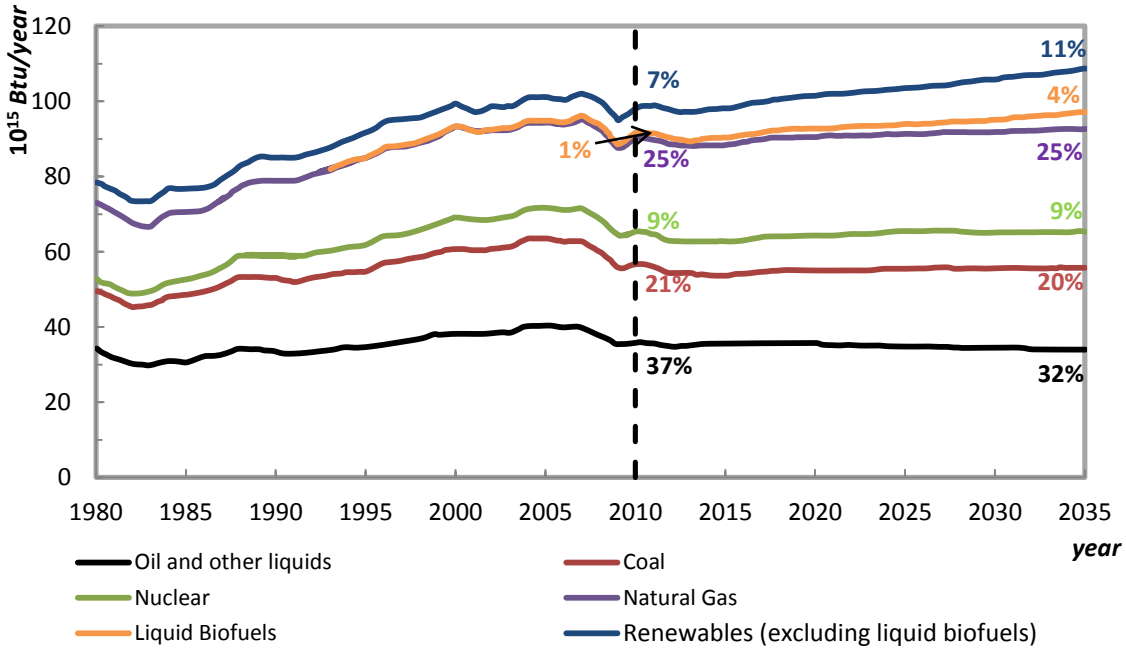

Figure 1.5- US primary energy consumption forecast till the year 2035 adapted from the Annual Energy Outlook 2012.[48]

Moreover, stricter legislation will continue to appear and environmental problems will not disappear leading to an increasing need for better and more efficient control methods. A possible solution could be the development of a new control method that could be combined with the existent techniques, for example an absorption or membrane process. These techniques could replace or be combined with existent control strategies in industrial sources such as large boilers, furnaces and fired heaters, combustion turbines, large internal combustion engines, cement kilns and exhaust streams from HNO_3 production. The potential uses of these two techniques would imply the use of a resistant material and a high boiling temperature solvent like ILs.

1.6- Ionic Liquids

ILs are salts composed of large organic cations and organic or inorganic anions that cannot form an ordered crystal and thus remain liquid at or near room temperature (by definition are liquid at temperature below 373 K). Although the combination of cations and anions allows one the synthesis of more than 10^6 different ILs, only a small amount (≈1000) of these compounds are described and characterized in literature.[49] In fact, most of the ILs studied are based on the ammonium, phosphonium, pyridium or imidazolium cation, and on the tetrafluoroborate $[BF_4]^-$, hexafluorophosphate $[PF_6]^-$, trifluoromethylsulfonate $[CF_3SO_3]^-$ or bis(trifluoromethylsulfonyl)imide $[NTf_2]^-$ anion.[49] Illustrative examples of some of these cations and anions are showed in Figure 1.6.

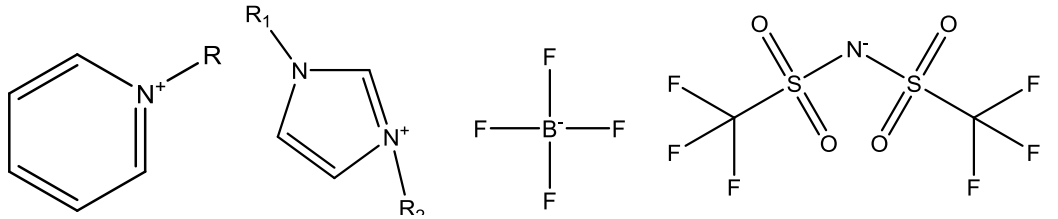

Figure 1.6- Cations and anions commonly used to form ILs.

These unique compounds were first reported by Paul Walden[50] in 1914 when he studied the physical properties of ethylammonium nitrate ($[EtNH_3][NO_3]$). His intention was to investigate the electric conductivity and the molecular size of some organic ammonium salts.[49] Even though his clear exposition and discovery of a new class of liquids, only in 1934 were they cited in a patent where it was claimed that they could be used for dissolving cellulose.[51] Over the years that followed, more studies were carried out and, by the mid-1990s, the concept of ILs was well-known mostly for their electrochemical applications.[49]

The attention of a larger community was attracted when the first water and air stable ILs were developed and these new solvents were touted as "green" and they emerged as "designer solvents". This designation was first used by Seddon *et al.*[52] when reporting the use of ILs as solvents for reaction optimization, achieving control over yield and selectivity. Since a large number of cationic and anionic structures combinations are possible, desired physicochemical properties of ILs for a particular process can be easily tuned and/or obtained by manipulating the ions that compose them.[52] For instance, hydrophobicity, viscosity or density can be adjusted by changing the alkyl chain of the cation,[53-56] or their water miscibility by changing the anion,[49] or a

more important property for this work, the gas solubility can be manipulated by the anion/cation selection.[5, 57]

The ionic nature of these liquids results in several physical and chemical advantages over conventional and molecular organic solvent such as negligible flammability and vapour pressure, thermal stability and highly solvating capacity either for polar and nonpolar compounds.[58-60] These unique characteristics raised the attention both from the academia as well as from the industry.

Due to the ILs unique features, they have been intensively applied in different areas like multiphase bioprocess operations,[61] chromatographic separations,[62] mass spectrometry analysis,[63] batteries and fuel cells,[64] solar cells,[65] separation of biomolecules,[66] organic synthesis,[67] chemical reactions,[68] catalysis,[69] liquid-liquid extractions of metal ions[70, 71] and organic compounds.[72, 73] Furthermore, their unique and outstanding characteristics could allow them to be used in several control process for pollutant, as absorption solvent in an extraction process or as stationary phase in a membrane process, just to mention some. In fact, a large number of studies have been performed concerning pollutants solubility on ILs, namely for CO_2,[17-19, 74-83] CH_4,[6, 84-88] H_2S,[83, 89] SO_2,[8, 90] CO,[76, 91-93] and NH_3.[8] These studies have shown good results at low temperatures, indicating that this class of solvents are feasible to be used to capture and/or separate these pollutants. However, no studies have been made for NO_x and, up to now, only four studies with N_2O were reported.[5, 14, 16, 18] Of these studies, the most interesting is the study conducted by Revelli *et al.*[14] where the solubility of N_2O in five imidazolium-based ILs was investigated, showing that it was possible to dissolve, at low pressure, up to 105 grams of N_2O per kilogram of IL.

The ILs exclusive characteristics and good solubility towards various gases make them promising agents for the capture of nitrogenated gases. However, a more complete solubility study is needed in order to develop techniques for reducing these compounds. Moreover, solubility data are important to develop thermodynamic models and correlations able to describe and/or predict such systems and therefore to reduce the need for an exhaustive study. To this purpose, several different theoretical approaches, correlations and equations of state (EoS) have been already applied to ILs + gases systems. Those with the best results are the soft-SAFT EoS,[22-25, 94, 95] γ - ϕ approach[96] and general correlations.[7]

1.7- Soft-SAFT EoS

Among the EoS used to describe gas solubilities in ILs, the Statistical Associating Fluid Theory (SAFT)[97-100] is becoming very popular due it success in predicting not only gas solubilities but also other ILs thermodynamic properties.[95] This theory has generated a family of SAFT-type equations based on Wertheim's first-order thermodynamic perturbation theory (TPT1) for associating fluids.[101-104] The soft-SAFT EoS, proposed by Vega and co-workers,[21, 26, 105, 106] is one of the most successful equations of this type. They were able to successfully predict the phase equilibrium behaviour of binary and ternary mixtures involving non-associating compounds like *n*-alkanes and 1-alkanes, and associating compounds like 1-alkanols,[21] as well as their critical lines and partial miscibility.[106] Later, the same study was extended with success for some heavy *n*-alkanes by Pàmies *et al.*[26] Recent works,[22-25] extended the soft-SAFT EoS applicability to more complex fluids, like ILs, with great success. Contrarily to classical models, which in most cases are based on the use of several temperature and composition dependent parameters, SAFT-type equations are able to describe IL + gas systems with a simple model and non-temperature dependent parameters.[94] Moreover, classical models required the use of ILs' critical properties that, lacking a better expression, are challenging to determine, making its determination possible through indirect estimated models that present large uncertainties.[94]

As all SAFT-type equations, the soft-SAFT EoS is written in term of the residual Helmholtz energy (A^{res}), defined as the molar Helmholtz energy of the fluid relative to that of an ideal gas at the same temperature and density. This energy can be calculated by the sum of each independent microscopic contribution. The general expression of the SAFT equation is:

$$A^{res} = A^{total} - A^{ideal} = A^{ref} + A^{chain} + A^{assoc} + A^{polar} \qquad \textbf{Eq. 1.2}$$

where the superscripts *ref*, *chain*, *assoc* and *polar* refer to the contribution from the reference term, the formation of the chain, the association and the polar interactions, respectively. A hypothetical model of an associating molecule modeled by the SAFT approach is depicted in Figure 1.7, where the number of segments (m), the segment size (σ), the dispersive energy between segments (ε/k_B), the energy (ε^{HB}/k_B) and volume (k^{HB}) of association per site are molecular parameters needed to model compounds by soft-SAFT EoS.

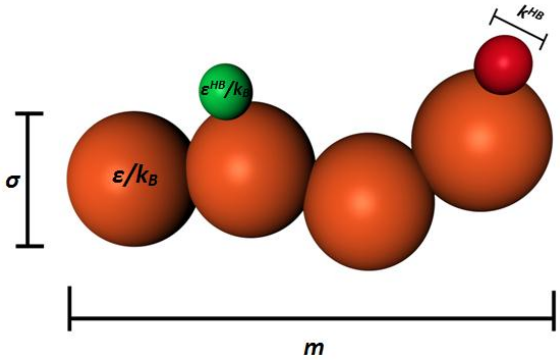

Figure 1.7- Molecule model within the soft-SAFT approach.

While the original SAFT uses a reference fluid based on hard-spheres, the soft-SAFT EoS uses a Lennard-Jones (LJ) spherical fluid, a "soft" reference fluid, which takes into account the repulsive and attractive interactions of the segments forming the chain and is modelled by the Lennard Jones EoS.[107] This equation was obtained by fitting simulation data in Benedict-Webb-Rubbin EoS and posterior parameters determination and can be extended to mixtures by applying the van der Waals one-fluid theory (vdW-1f).[108] The expressions for the size and energy parameters are:

$$\sigma = \frac{\sum_{i=1}^{n}\sum_{j=1}^{n} m_i m_j x_i x_j \sigma_{ij}^{\,3}}{\sum_{i=1}^{n}\sum_{j=1}^{n} m_i m_j x_i x_j} \qquad \textbf{Eq. 1.3}$$

$$\varepsilon/k_B \times \sigma^3 = \frac{\sum_{i=1}^{n}\sum_{j=1}^{n} m_i m_j x_i x_j \varepsilon_{ij} \sigma_{ij}^{\,3}}{\sum_{i=1}^{n}\sum_{j=1}^{n} m_i m_j x_i x_j} \qquad \textbf{Eq. 1.4}$$

where the subscripts i and j refers to the species in the mixture, and the unlike parameters, σ_{ij} and ε_{ij}, are calculated using the generalized Lorentz-Berthelot combining rule. The corresponding expressions are:

$$\sigma_{ij} = \eta_{ij}\frac{\sigma_{ii}+\sigma_{jj}}{2} \qquad \textbf{Eq. 1.5}$$

$$\varepsilon/k_{B\,ij} = \xi_{ij}\sqrt{\varepsilon/k_{B\,ii} \times \varepsilon/k_{B\,jj}} \qquad \textbf{Eq. 1.6}$$

where η and ξ are the binary adjustable parameters for the species i and j. These parameters are used to correct possible deviations in molecular size and energy of the segments forming the two compounds in the mixture. Moreover, when both binary adjustable parameters are set to 1, soft-SAFT EoS is used in a pure predictive manner.

The reference term usually varies in different SAFT's versions. On the other hand, the chain and association terms are normally identical and are derived from the Wertheim's theory (TPT1):

$$A^{chain} = \rho k_B T \sum_i x_i (1 - m_i) \ln g_{LJ} \qquad \textbf{Eq. 1.7}$$

$$A^{assoc} = \rho k_B T \sum_i x_i \left(\sum_\alpha \ln X_i^\alpha - X_i^\alpha + \frac{M_i}{2}\right) \qquad \textbf{Eq. 1.8}$$

where ρ is the molecular density, k_B is the Boltzmann's constant, T is the temperature, x_i is the molar fraction of component i, m is the chain length, g_{LJ} is the radial distribution function of a fluid of LJ spheres at density $\rho_m = m\rho$ and evaluated at the bond length σ, M_i is the number of association sites in component i, and X_i^a is the mole fraction of molecules of component i nonbonded at site α, which extends over all i compound in the mixture.

Finally, main polar interactions can also be taken into account in the model by introducing a new parameter, the quadrupole moment, *Q*. The calculation of this parameter is based on setting the fraction of segments in the chain that contains the quadrupole, and it is defined in the model as x_p. Usually, these two parameters are previously calculated and fixed, and are correlated by the following equation:

$$Q = Q_{exp} \times x_p \qquad \textbf{Eq. 1.9}$$

where Q_{exp} is the experimental quadrupole for the molecule of interest and Q and x_p are molecular parameters for the model. Moreover, its use is required when modelling some fluids of linear symmetrical molecules like carbon dioxide, nitrogen and acetylene, and others like benzene, ethylbenzene, n-propybenzene and toluene, where this property is important.[12, 22, 23, 27, 109] Although the quadrupole moment for N_2O was already studied,[110, 111] it remains unknown its effect on the soft-SAFT EoS prediction.

In order to apply Sof-SAFT EoS for a particular system, a molecular model for each compound must be chosen (sites for each molecule and allowed interactions among the sites) as well as obtain the molecular parameters. In this sense, molecular parameters of pure compound are calculated by fitting experimental data for vapour pressure and saturated liquid density over a determinate range of temperature using the functions[21]:

$$f_1(\sigma, \varepsilon/k_B, m,\ \varepsilon^{HB}/k_B, k^{HB}) = \sum_i^N \left[\rho_i^{exp} - \rho_i^{calc}\left(p_i^{exp}, T_i^{exp}\right)\right]^2 \qquad \textbf{Eq. 1.10}$$

$$f_2(\sigma, \varepsilon/k_B,\ m,\ \varepsilon^{HB}/k_B,\ k^{HB}) = \sum_i^N \left[\mu_{i,liq}^{calc}\left(p_i^{exp}, T_i^{exp}\right) - \mu_{i,vap}^{calc}\left(p_i^{exp}, T_i^{exp}\right)\right]^2 \qquad \textbf{Eq. 1.11}$$

where N is the number of experimental points, p_i^{exp},T_i^{exp},ρ_i^{exp} are the vapour pressure, the liquid density and the temperature corresponding to the experimental point i, and $\mu_{i,liq}^{calc}$,$\mu_{i,vap}^{calc}$, ρ_i^{calc} are the chemical potentials of the liquid and vapour phase and the saturated liquid density, respectively, predicted by the EoS at the temperature T_i^{exp} and pressure p_i^{exp}. These two functions are minimized using the Marquart-Levenberg algorithm[112] and the process stopped when f_1 or f_2 are less than 10^{-6}. For binary mixtures, the same fitting procedure is used along with the two binary parameters given in Eq. 1.5 and Eq. 1.6, and the next two functions:

$$f_1(\sigma, \varepsilon/k_B, m, \varepsilon^{HB}/k_B, k^{HB}) = \sum_i^N \left[x_i^{exp} - x_i^{calc}\left(p_i^{exp}, T_i^{exp}\right)\right]^2 \qquad \textbf{Eq. 1.12}$$

$$f_2(\sigma, \varepsilon/k_B, m, \varepsilon^{HB}/k_B, k^{HB}) = \sum_i^N \left[y_i^{exp} - y_i^{calc}\left(p_i^{exp}, T_i^{exp}\right)\right]^2 \quad \textbf{Eq. 1.13}$$

Generally, ILs are well modelled by using all five molecular parameters (*m, σ, ε/k_B, k^{HB}* and *ε^{HB}/k_B*) and gases by just three or four parameters (*m, σ, ε/k_B* and *Q*).[22, 23]

2- Molecular Models

2.1- Introduction

The selection of a reliable coarse-grained model able to represent the basic physical features of the compound to be described stands as a key element for the accurate predictions from any molecular-based EoS. soft-SAFT EoS relies on the pre-adjustments of molecular parameters for each pure compound. The molecules are represented through the molecular parameters: *m*, the chain length; *σ*, the segment size; *ε*, the energy parameter of the segments making the chain; *Q*, the quadrupolar moment; x_p, the fraction of segments in the chain that contains the quadrupole; k^{HB}, the volume of association and ε^{HB}/k_B, the association energy per site. Additionally, the description of the pure compound vapour pressure and liquid density is evaluated by the percentage average absolute deviation (%*AAD*), defined as the difference between experimental data and the predictions given by soft-SAFT EoS, and was calculated by:

$$\%AAD\ Z = \left|\frac{1}{N}\sum_{i=1}^{N}\frac{Z^{exp}-Z^{calc}}{Z^{exp}}\right| \times 100 \qquad \textbf{Eq. 2.1}$$

where *N* stands for the number of points considered and the subscript *exp* and *calc*, are the experimental and calculated values by the model, respectively, for the studied property, *Z*.

2.2- ILs Molecular Parameters

Although successfully applied for a wide set of compound families, like associating and non-associating hydrocarbons,[21, 106, 113] polymers[27, 109] and perfluoalkanes,[12] soft-SAFT EoS has only recently been extended to ILs by Vega and co-workers. [22-25]

Imidazolium-based ILs with PF_6 and BF_4 anions were modelled[22, 25] as LJ chain with one associating site, "*A*", where the "A" site represents the specifics interactions due to the IL chargers and asymmetry (Figure 2.1). On the other hand, imidazolium-based ILs with NTf_2 anion were modelled[23-25] with three associating sites, one "A" and two "*B*" sites, where the "*A*" would mimic the specific interactions due the nitrogen atom with the cation and the "*B*" sites would represent the delocalized charge due the oxygen atoms on the anion (Figure 2.2). Also, only AA or AB interactions, between different ILs molecules are allowed.

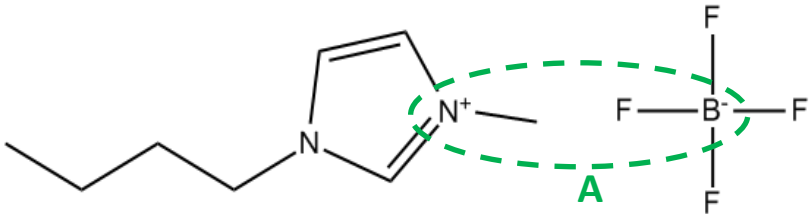

Figure 2.1- Proposed association scheme for [C_4mim][BF_4] by Andreu *et al.*[22]

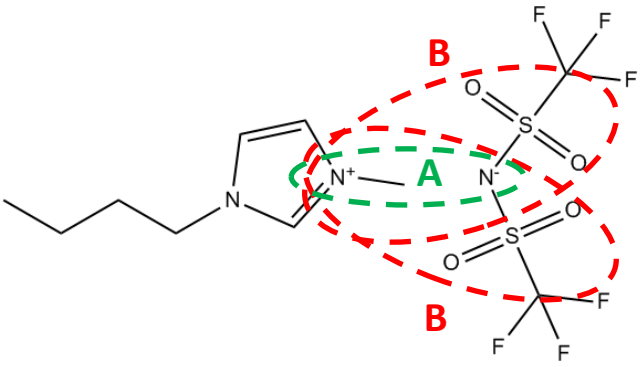

Figure 2.2- Proposed association scheme for [C_4mim][NTf_2] by Andreu *et al.*[23]

Once the ILs association scheme was selected, the molecular parameters, m, σ, ε/k_B, k^{HB} and ε^{HB}/k_B were determined. Following the Vega and co-workers suggestion, the association parameters (ε^{HB}/k_B =3450 and k^{HB}=2250) were transferred from those of 1-alkanols,[114] reducing thus, to a minimum, the number of fitted molecular parameters. Afterwards, the remaining molecular parameters (m, σ and ε/k_B) were obtained by fitting them to experimental density data at atmospheric pressure.[115, 116] Furthermore, recently, Llovel *et al.*[24] recalculated the molecular parameters for the NTf_2 family using the previously discussed scheme of association and new available experimental density data.[117] In addition to that, similarly to what was done for other compounds,[21, 27, 109] a correlation between the molecular parameters and the molecular weight of the ILs was established for the PF_6, BF_4 and NTf_2 families,[22, 23 24] improving the predictive ability of the soft-SAFT EoS.

The adjusted molecular parameters for [C_4mim][BF_4] and [C_4mim][NTf_2] are listed in Table 2.1 and allowed a good description of the ILs density, as depicted in Figure 2.3, with an %*AAD* of 0.31% and 0.06%, respectively.

Table 2.1- Molecular parameters for [C_4mim][BF_4]and [C_4mim][NTf_2] taken from the literature.[22, 24]

	m	σ (Å)	ε/k_B (K)	ε^{HB}/k_B (K)	k^{HB} (Å^3)
[C_4mim][BF_4]	4.495	4.029	420.00	3450	2250
[C_4mim][NTf_2]	6.175	4.211	399.40	3450	2250

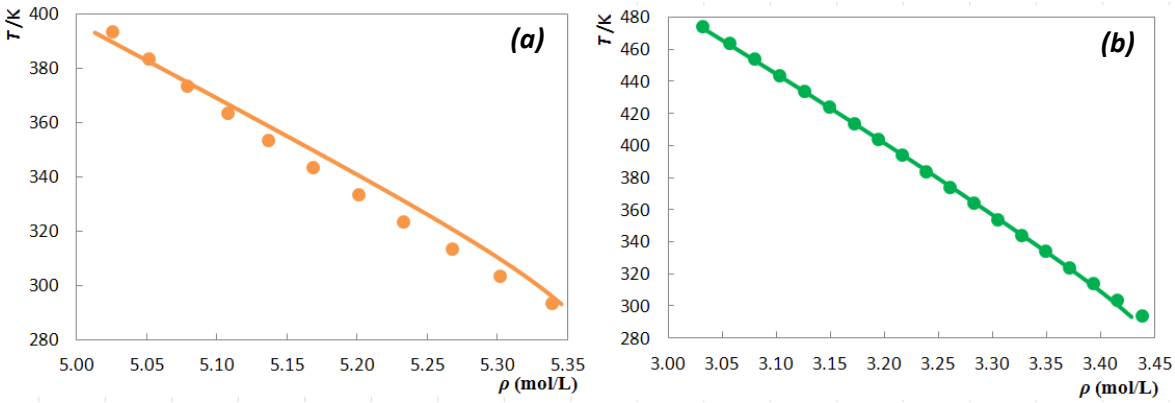

Figure 2.3- [C_4mim][BF_4] *(a)* and [C_4mim][NTf_2] *(b)* temperature-density diagrams.[117, 118] Solid lines represent soft-SAFT EoS predictions.

The set of molecular parameters used allowed a good description of the phase behaviour of some compound such as CO_2 in [C_4mim][BF_4][22] and CO_2, Xe, H_2, H_2O, methanol and ethanol in [C_4mim][NTf_2].[23, 24] Therefore, these set of parameters will be used for modelling binary mixtures in this work.

Molecular parameters for [C_4mim][SCN], [C_2mim][CH_3OHPO_2] and [C_4mim][$N(CN)_2$] were not available in the literature. Therefore, they are here determined for the first time.

Following the above mentioned approach, the ILs were modelled as a LJ chain with two association sites; one "*A*" and one "*B*" site, as depicted in Figure 2.4.

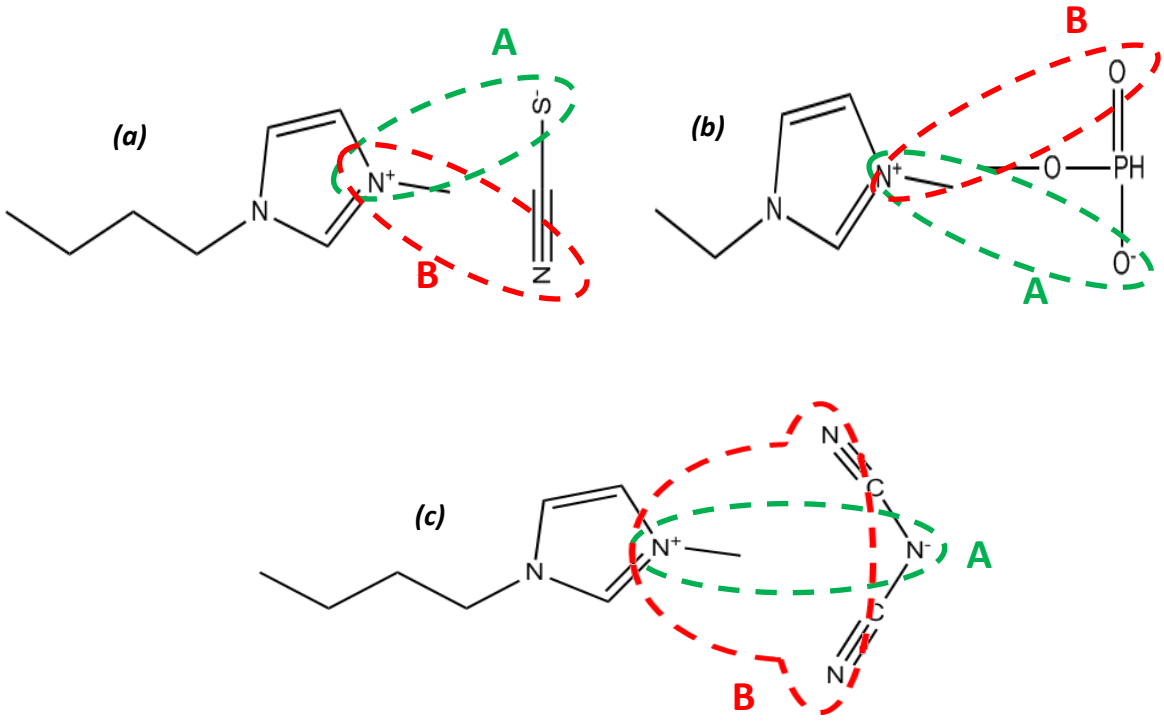

Figure 2.4- Scheme of association adopted in this work for the ILs [C_4mim][SCN] *(a)*, [C_2mim][CH_3OHPO_2] *(b)* and [C_4mim][$N(CN)_2$] *(c)*.

In all the cases, the "A" site mimics the strong interactions due the anion's sulphur (Figure 2.4-a), oxygen (Figure 2.4-b) or nitrogen (Figure 2.4-c) atom with the cation. On the other hand, the "B" site represents the delocalized charge due to the nitrogen (Figure 2.4-a and Figure 2.4-c) or oxygen (Figure 2.4-b) atoms in the anion. Moreover, the association parameters, ε^{HB}/k_B and k^{HB}, for $[C_4mim][SCN]$ and $[C_4mim][N(CN)_2]$ were also transferred from those of 1-alkanols,[114] as done for other ILs and thus fixed to 3450 K and 2250 Å^3, respectively. However, the $[C_2mim][CH_3OHPO_2]$ high polarity, according to their experimental solvatochromic parameters[119, 120] and an unpublished correlation from our research group, lead to higher values for the association parameters (ε^{HB}/k_B=4450 and k^{HB}=3950).

Once established the association scheme and the association parameters, the remaining molecular parameters (*m*, σ and ε/k_B) were determined by fitting them against experimental density data.[54, 121, 122] Despite density data for temperatures lower than 290 K was available, only density higher to that temperature was used for the fitting, in order to maintain the validity of the Johnson equation[107] used for the reference fluid in soft-SAFT EoS. The adjusted molecular parameters are listed in Table 2.2.

Table 2.2- Adjusted molecular parameters for $[C_4mim][SCN]$, $[C_4mim][N(CN)_2]$ and $[C_2mim][CH_3OHPO_2]$.

	m	σ (Å)	ε/k_B (K)	ε^{HB}/k_B (K)	k^{HB} (Å^3)
$[C_4mim][SCN]$	4.385	4.050	414.35	3450	2250
$[C_2mim][CH_3OHPO_2]$	5.405	3.686	414.35	4450	3950
$[C_4mim][N(CN)_2]$	4.508	4.077	412.00	3450	2250

These sets of parameters allowed a good description of the density of $[C_4mim][SCN]$, $[C_2mim][CH_3OHPO_2]$ and $[C_4mim][N(CN)_2]$ in a wide range of temperatures, as depicted in Figure 2.5 to Figure 2.7, with an %*AAD* of 0.08%, 0.65% and 0.16%, respectively. However, soft-SAFT EoS presents strong deviations when the prediction is extended for temperatures lower than 290 K, as depicted in Figure 2.6 and Figure 2.7. Nonetheless, this strong deviations do not come as a surprise since the applicability of the soft-SAFT's reference fluid equation is limited to $T=0.7\times\varepsilon/k_B$,[107] and therefore, for $[C_4mim][SCN]$ and $[C_2mim][CH_3OHPO_2]$ ILs the limit temperature is 290.05 K and 288.40 K for the $[C_4mim][N(CN)_2]$.

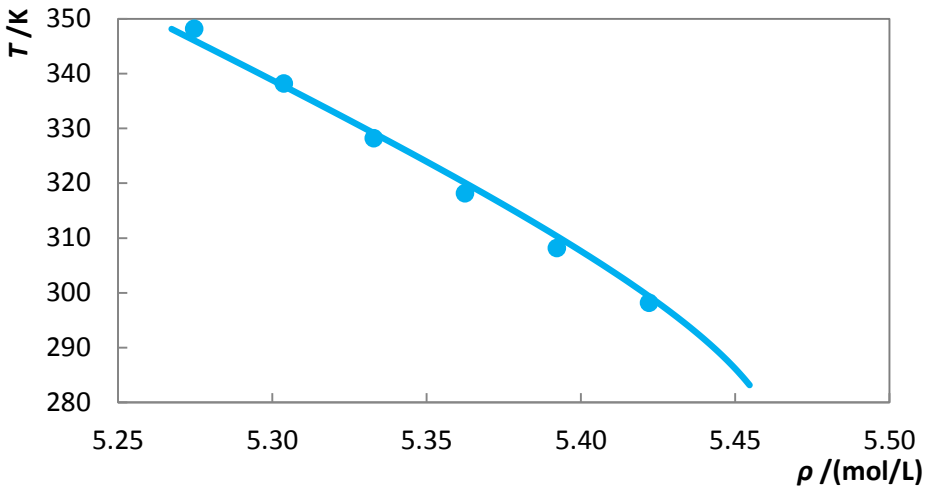

Figure 2.5- Temperature-density diagram for [C_4mim][SCN].[54] Solid lines represent soft-SAFT EoS predictions with a limit temperature of application of 290.05 K.

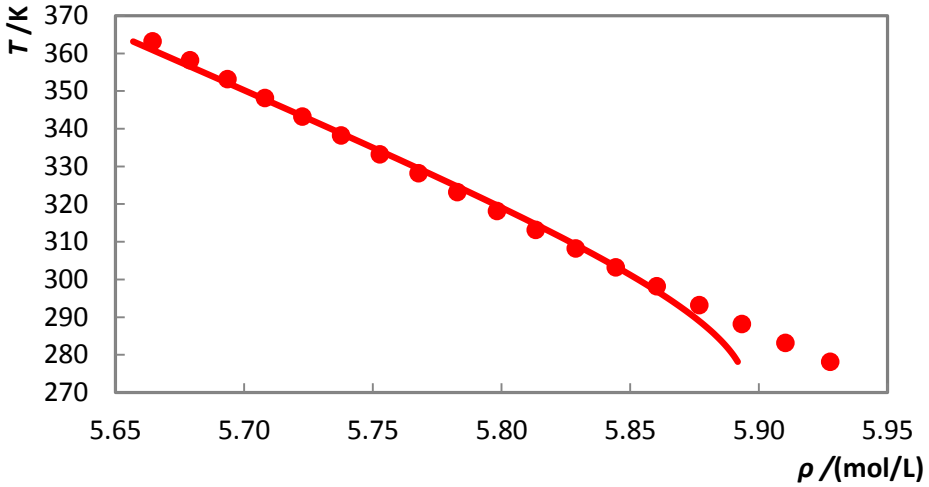

Figure 2.6- Temperature-density diagram for [C_2mim][CH_3OHPO_2].[121] Solid lines represent soft-SAFT EoS predictions with a limit temperature of application of 290.05 K.

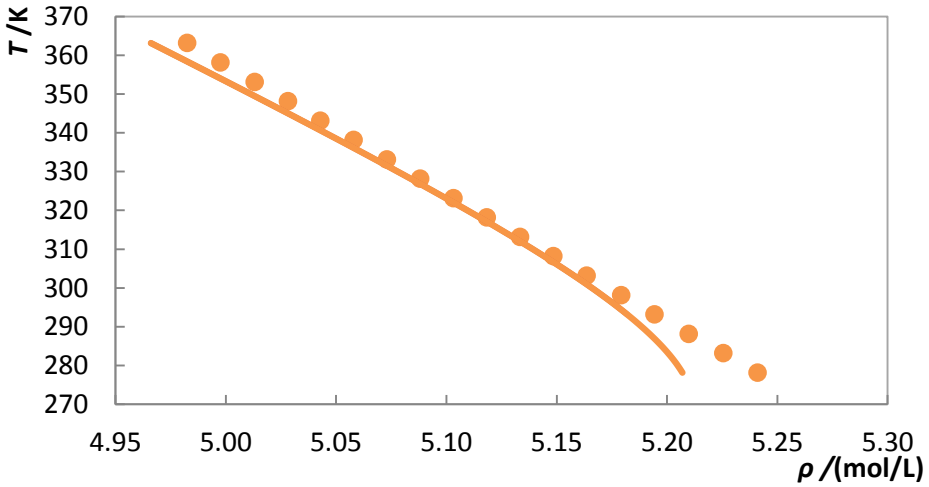

Figure 2.7- Temperature-density diagram for [C_4mim][$N(CN)_2$].[122] Solid lines represent soft-SAFT EoS predictions with a limit temperature of application of 288.40 K.

2.3- Gases Molecular Parameters

Soft-SAFT EoS molecular parameters for gases are widely available in the literature. Vega and co-workers[21] proposed molecular parameters for the n-alkanes series, which included CH_4, while trying to predict the behaviour of some binary and ternary systems with associating fluids like 1-alkanols. On a later work,[26] the authors proposed new parameters for the n-alkanes series and a new set of molecular parameters for CH_4. These molecular parameters are used here to model the CH_4 for the studied systems (Table 2.3).

Pedrosa *et al.*[27, 109] proposed molecular parameters for CO_2 and N_2 when modelling theirs phase behaviour in ethylene glycol oligomers. Later, Dias *et al.*[12] proposed similar molecular parameters for the CO_2 to describe its solubility in perfluoalkanes. Furthermore, in all the above mentioned works, the authors modelled the CO_2 molecule as a non-associating compound and as LJ chain in which explicit quadrupolar interactions were taken into account, with the molecular parameter x_p fixed to ⅓, representing the molecule as three segments with the quadrupole in one of them. [12, 27, 109] Similarly, the N_2 molecule was also modelled as a non-associating compound and as a LJ chain with quadrupolar interactions but with the molecular parameter x_p fixed to ½.[27] Moreover, the quadrupole moment used, Q=4.4 x 10^{-40} C.m^2 for CO_2 and Q=1.2 x 10^{-40} C.m^2 for N_2, are in good agreement with those reported in the literature.[123] Once the parameters Q and x_p are fixed, the molecular parameters (m, σ and ε/k_B) were adjusted (Table 2.3) by fitting them against experimental vapour-pressure and saturated liquid densities, reported in the literature.[124]

The calculated %*AAD* (Table 2.3) are higher than the ones reported however, still a good description of the pure compounds is obtained as depicted in Figure 2.8. Furthermore, contrary to the proposed molecular parameters for CH_4 and N_2, CO_2 molecular parameters were already successfully used to describe its phase behaviour in ILs systems.[22, 23] Therefore, these set of parameters will be used in this work for modelling their phase behaviour in the binary systems and their applicability will be verified.

Table 2.3- Soft-SAFT molecular parameters for CH_4, CO_2 and N_2 taken from the literature.[12, 26, 27]

	m	*σ* (Å)	*ε/k$_B$* (K)	*%AAD P (%)*	*%AAD D (%)*
CH_4	1.000	3.728	147.20	9.81	3.68
CO_2	1.571	3.184	160.20	0.33	5.90
N_2	1.205	3.384	89.16	0.31	1.91

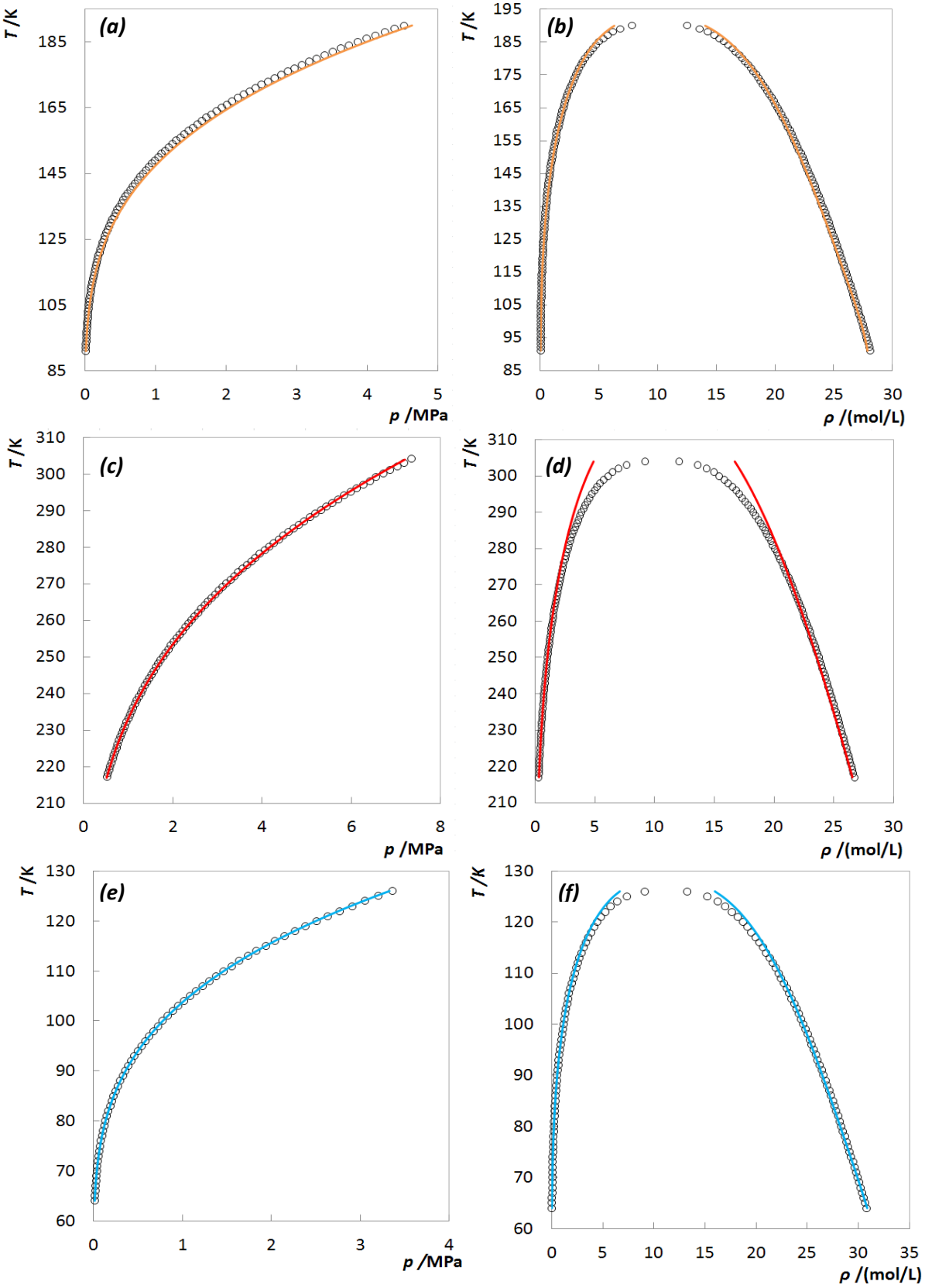

Figure 2.8- CH_4 temperature-pressure *(a)*, CH_4 temperature-density *(b)*, CO_2 temperature-pressure *(c)*, CO_2 temperature-density *(d)*, N_2 temperature-pressure *(e)* and N_2 temperature-density *(f)* diagrams. Experimental data was taken from NIST database.[124] Solid lines represent the soft-SAFT EoS predictions.

Although molecular parameters for N_2O have already been reported by Arce *et al.*[125] for PC-SAFT EoS, to our knowledge it has never been modelled before with soft-SAFT EoS. Thus, the molecular parameters for this compound were fitted against its vapour-pressure and saturated-liquid density data, taken from NIST database.[124]

Although presenting a linear structure similar to that of CO_2, N_2O presents a resonance structure, as depicted in Figure 2.9. Thus, although expecting a non-association scheme similar to that of the CO_2 molecule, three different approaches were, nonetheless, evaluated for the determination of the x_p parameter. First the N_2O molecule was modeled as a LJ chain with no explicit quadrupolar interactions, although a couple of studies report an experimental quadrupole for the N_2O molecule within 11.03 x 10^{-40} and 12.30 x 10^{-40} C.m^2.[110, 111] On the second approach the N_2O molecule was modeled as a LJ chain in which quadrupolar interactions were taken into account and with a molecular parameter x_p fixed to ⅓, mimicking the N_2O molecule resonance structure as three segments with the quadrupole in one of them. And finally, considering the N_2O molecule as a LJ chain in which quadrupolar interactions are taken into account and with a molecular parameter x_p fixed to ½.

Figure 2.9- N_2O molecular structure.

The best suitable molecular parameters (*m, σ* and ε/k_B) and quadrupole values used, for these approaches, are listed in Table 2.4 and all the set of results are listed in Table 8.1 in the appendix B.

Table 2.4- Set of adjusted molecular parameters for N_2O.

Set	*m*	*σ* (Å)	ε/k_B (K)	x_p	*Q* (10^{-40} C m^2)	*AAD P (%)*	*AAD D (%)*
1	1.197	3.612	167.42	½	5.50	7.65	1.73
2	1.130	3.699	168.83	½	6.00	7.55	1.76
3	1.751	3.078	159.90	⅓	3.67	7.07	1.39
4	1.656	3.153	159.83	⅓	4.10	7.29	1.51
5	1.490	3.300	159.44	⅓	5.00	7.55	1.60
6	1.415	3.306	190.43	⅓	4.10	0.77	2.64
7	1.655	3.105	192.48	-	-	6.73	2.91
8	2.484	2.646	158.82	-	-	4.54	0.98

As listed in Table 2.4, globally, the set 6 and 8 allowed the best description of N_2O behaviour with a %*AAD* of 0.77 % and 4.54 % for the vapour pressure, respectively, and 2.64 % and 0.98 % for the density, respectively. However, other combinations between the five

molecular parameters are also able to predict the N_2O behaviour with a relatively low %*AAD*. Therefore, all previously listed molecular parameters can potentially be used to describe the N_2O phase behaviour in binary systems.

In order to know which set of parameters would describe best the binary systems, several soft-SAFT EoS calculations, in a pure predictive manner (η and ξ are fixed to 1), were made for the systems N_2O + $[C_4mim][BF_4]$ and N_2O + $[C_4mim][NTf_2]$ using the available, and already presented, molecular parameters for the ILs and the different sets for N_2O. Afterward, the predictions were compared with experimental measurements available in the literature.[16, 18] The results are depicted in Figure 2.10.

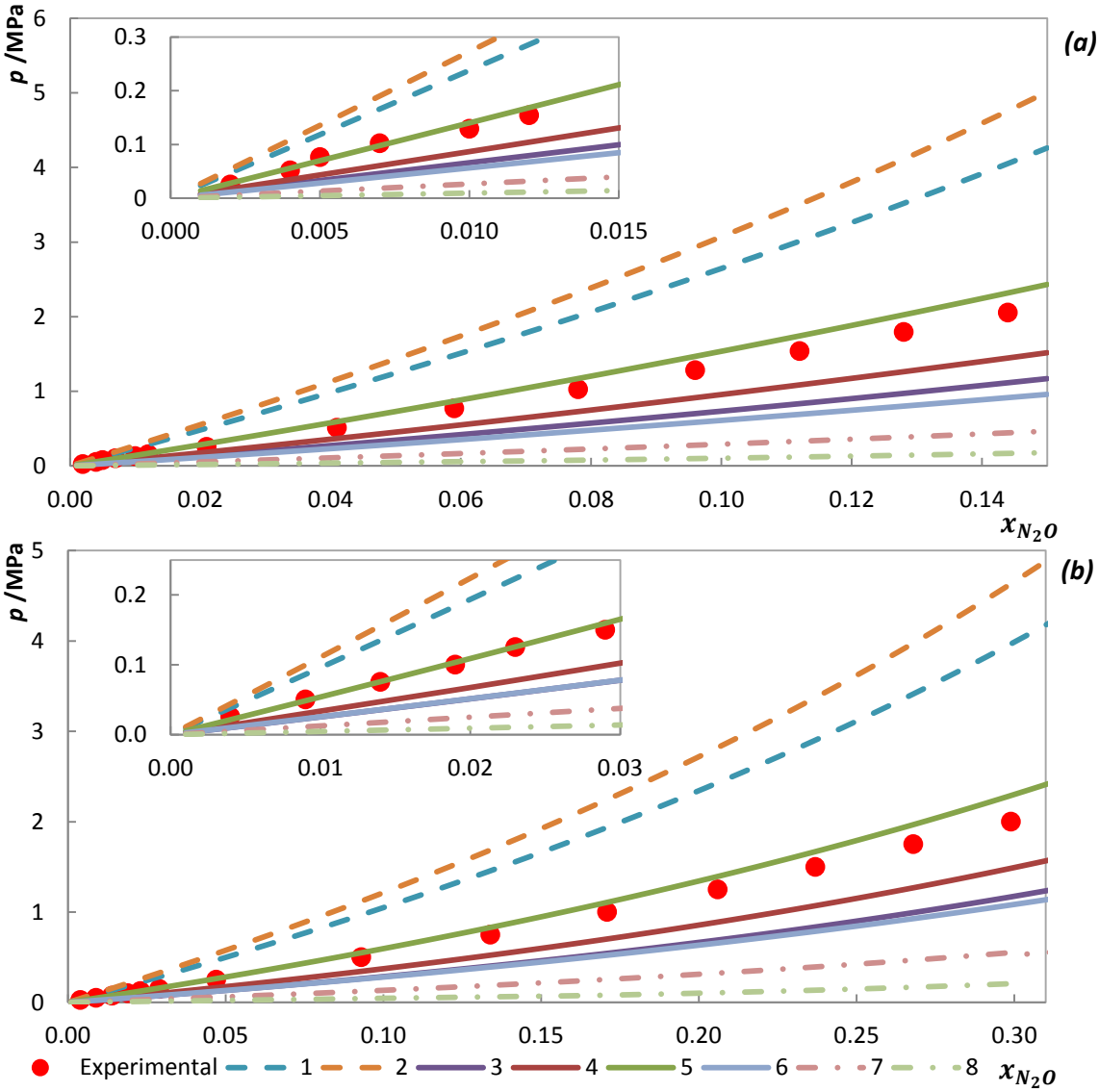

Figure 2.10- *px* diagrams for N_2O in the ILs $[C_4mim][BF_4]$[16] *(a)* and $[C_4mim][NTf_2]$[18] *(b)* at 323 K. Solid lines represent soft-SAFT EoS predictions at 323 K using the different sets of parameters for N_2O listed in Table 2.4 and both binary parameters fixed to 1.

As illustrated in Figure 2.10, fixing x_p to ½ (set 1 and 2) for the N_2O molecule, soft-SAFT EoS predicts a significant lower solubility of the gas in the ILs. On the contrary, fixing x_p to ⅓ (set 3, 4 and 5) allows a better description of the gas phase behaviour in both ILs, despite the upper prediction for the set 3 and 4. In addition to that, a higher quadrupole moment leaded to under prediction of N_2O solubility in both approaches (x_p=½ and x_p=⅓) and both ILs. Furthermore, the set 6 and 8, which allowed the lowest *%AAD* in the description of the pure gas, gave a poor description of the binary systems.

All things considered, fixing x_p to ⅓ conducted to a better description of the binary systems. Moreover, by fixing the quadrupole moment to 5 x 10^{-40} C.m^2 (set 5), an excellent prediction of N_2O solubility in both ILs is achieved. However, using this value for the quadropole moment would correspond to an experimental quadrupole of 15 x 10^{40} C.m^2. In this sense, the set 4, in which the exact experimental quadrupole value is used (Q_{exp}= 12.3 x ⅓ x 10^{-40}), is preferred.

Thus, the set 4 will be used for modelling N_2O phase behaviour in the binary systems. The soft-SAFT prediction for N_2O vapour pressure and density using this set is depicted in Figure 2.11.

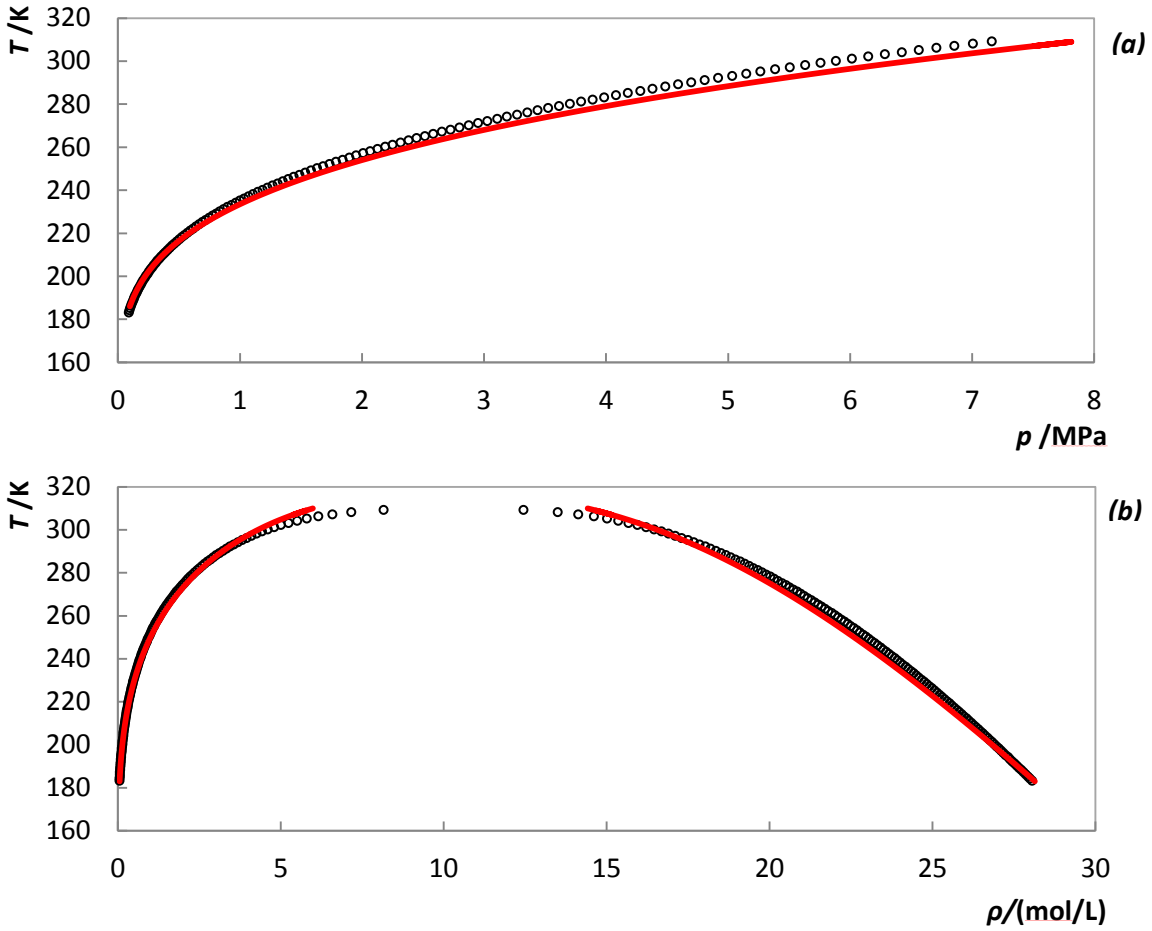

Figure 2.11- Temperature-pressure *(a)* and temperature-density *(b)* diagrams for N_2O taken from NIST database.[124] Solid lines represent soft-SAFT EoS prediction using the parameters set 4 for N_2O.

3- Gas Solubilities

3.1- Introduction

Gas solubilities measurements in ILs are necessary in order to develop techniques for capturing some pollutants like CO_2 and N_2O from post-combustion streams. Moreover, solubility studies of other compounds, like N_2 and CH_4, in ILs also stand as a vital key in order, not only to understand the ILs' capturing capability but also, to understand the ILs sorption mechanism. Therefore, solubility studies of N_2O, N_2, CH_4 and CO_2 in $[C_2mim][CH_3OHPO_2]$ were performed following the method and methodology described next.

The development of new or existing models able to describe or predict GLE data stands as a fundamental leap in the development of capturing systems and techniques. Thus, experimental solubility data measured here as well as unpublished data from our research group for $[C_4mim][N(CN)_2]$, measured with the same method and methodology, and GLE data available in the literature[14-20] were used to investigate and extend the applicability of the soft-SAFT EoS to describe/predict the gas + ILs systems.

3.2- Materials and Experimental Equipment

3.2.1- Materials

In this study, the ionic liquid (IL) $[C_2mim][CH_3OHPO_2]$ was acquired from Solvionic with mass fraction purities higher than 98 %. The IL was further purified by drying under high vacuum (10^{-3} Pa) and moderate temperature (323 K) for a period of 48 hours. The purities of the ILs were checked by ^{1}H NMR, ^{13}C NMR and ^{19}P NMR after the purification step. The final purity is estimated to be better than 99%. The final IL water content was determined with a Metrohm 831 Karl Fischer coulometer, indicating a water mass fraction of 143.85×10^{-6}. This purification procedure assures that water and volatile compounds are removed and the influence of these impurities is minimized. [126-128]

The gases CO_2 and CH_4, were acquired from Air Liquide with purity higher than 99.998% and 99.995%, respectively, while N_2O and N_2 were acquired from Praixair with purity higher than 99.998%.

3.2.2- Experimental Equipment

The high pressure equilibrium cell, used in this work, is based on a cell designed by Daridon *et al.*[9-13] and consists of a horizontal hollow stainless-steel cylinder, closed at one end by a movable piston and at the other end by a sapphire window, from which the operator follows the behaviour of the sample with pressure (0 to 100 MPa) and temperature (293 K to 363 K), as depicted in Figure 3.1.

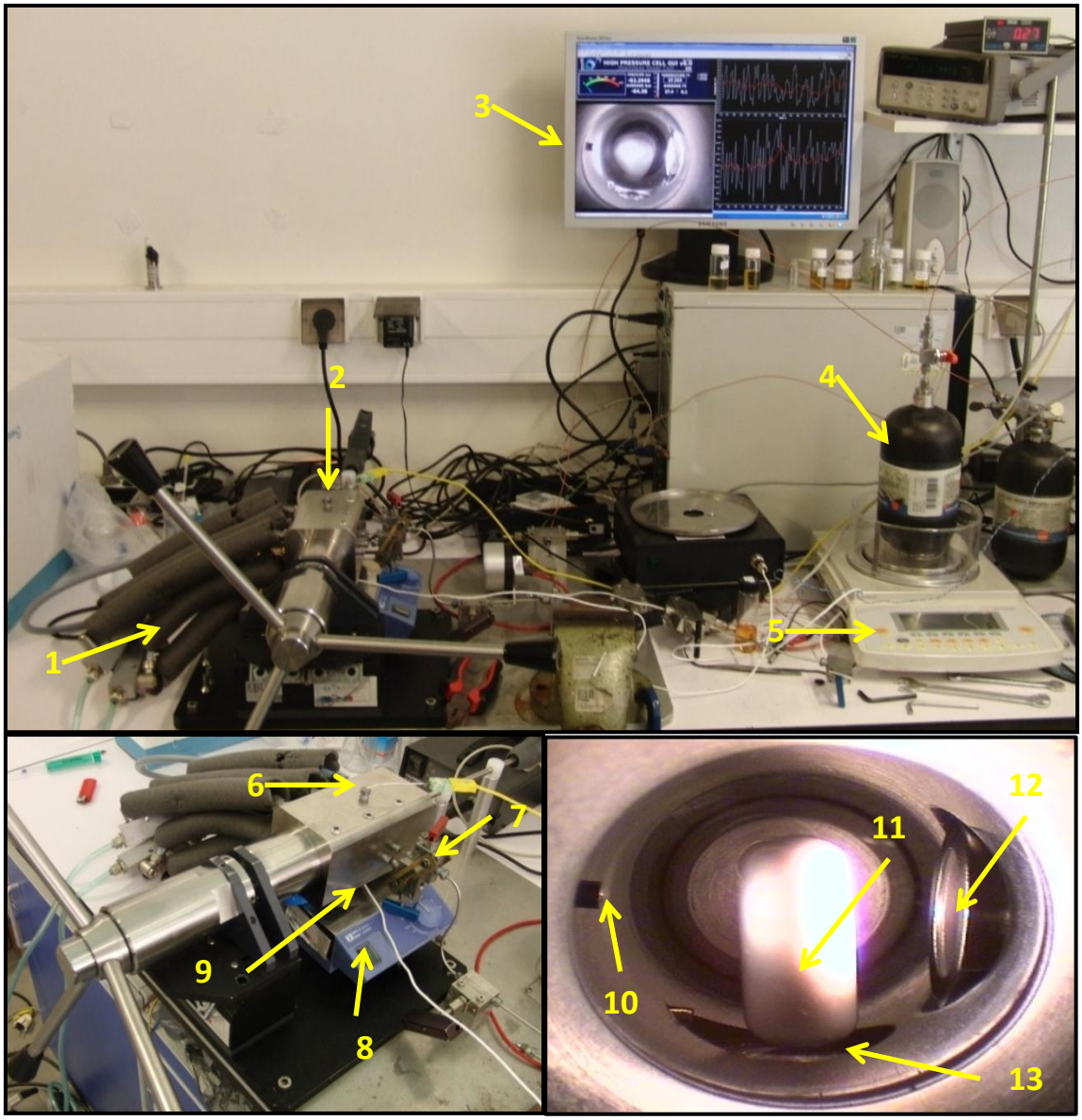

Figure 3.1- Components of the high pressure cell: 1) Thermostatized bath circulator; 2) High pressure cell; 3) Video and data acquisition; 4) Gas storage; 5) Analytical balance; 6) Temperature sensor; 7) Valves; 8) Magnetic stirrer; 9) Piezoresistive pressure transducer; 10) Gas entrance; 11) Magnetic bar; 12) Light source from an optical fiber cable; 13) Pressure probe.

The change of the phase behaviour, inside the cell, with the pressure and temperature is followed by an endoscope plus camera video which is connected to a computer screen. Moreover, the magnetic bar placed inside the cell allows the homogenization of the mixture by the action of an external magnetic stirrer. In addition, a minimal internal volume of 8 cm^3 and a maximum of 30 cm^3 allied with the magnetic bar, help to minimize the presence of temperature gradients within the sample in the cell and a good homogenization of the system. The cell is thermostatized by circulating a heat-carrier fluid through three flow lines directly managed into the cell and the heat-carrier fluid is thermo-regulated using a thermostat bath circulator (Julabo MC F25) with a temperature stability of 0.01 K. The temperature inside the cell is measured by a high precision thermometer Model PN 5207, with an accuracy of 0.01 K, connected to a calibrated platinum resistance and inserted in the cell, close to the sample. The pressure is measured by a Piezoresistive silicon pressure transducer (Kulite HEM 375) fixed inside the cell that was previously calibrated and certified by an independent laboratory with IPAC accreditation, following the EN 837-1 standard and with accuracy better than 0.2%.

A fixed amount of IL, which exact mass is determined by weighting using a high weight/high precision balance (Sartorius LA200P) with an accuracy of 1 mg, is introduced into the cell. Once introduced, the IL is kept under vacuum overnight, while stirring and heating at 353 K, in order to remove interferences from atmospheric gases during the manipulation. Having degassed the IL, the gas was introduced under pressure, using a flexible pressure capillary, from an ultra light composite tank and its mass measured with the precision balance. This final step is conducted by a gas line which establishes the connection between the cell and the gas reservoir. Moreover, a pressure sensor (SETRA 204) is connected to the line to monitor the pressure and ensures that the gas movement toward the cell is done with better control.

After preparing the mixture with a known composition, the temperature is allowed to stabilize and the pressure is slowly increased until the systems become monophasic. The minimum pressure at which the last bubble disappears, for that fixed temperature and composition, is the equilibrium pressure. This procedure was repeated for all the gases (CO_2, N_2O, CH_4 and N_2) in the IL $[C_2mim][CH_3OHPO_2]$. The mass of the IL and gases measured are listed in Tables 8.2, 8.3, 8.5 and 8.7 in the appendix C.

Furthermore, the purity of the IL was verified by ^{1}H NMR, ^{13}C NMR and ^{31}P NMR at the end of the study to assure that no degradation took place.

3.3- Experimental Results and Soft-SAFT EoS Modelling.

3.3.1- CO_2 Solubility

The solubility of CO_2 in $[C_2mim][CH_3OHPO_2]$ was measured for mole fractions from 0.05 up to 0.51 in the temperature range of (293.23–363.34) K and pressures from 0.1 to 90 MPa, as reported in Table 8.2 in appendix C and depicted in Figure 3.2. The temperature increase leads to an increase on the equilibrium pressure and by increasing CO_2 concentration, the equilibrium pressure increases gradually at first, and then rapidly for higher CO_2 contents as a liquid-liquid like region is reached, as also observed previously for other ILs.[20, 129-133]

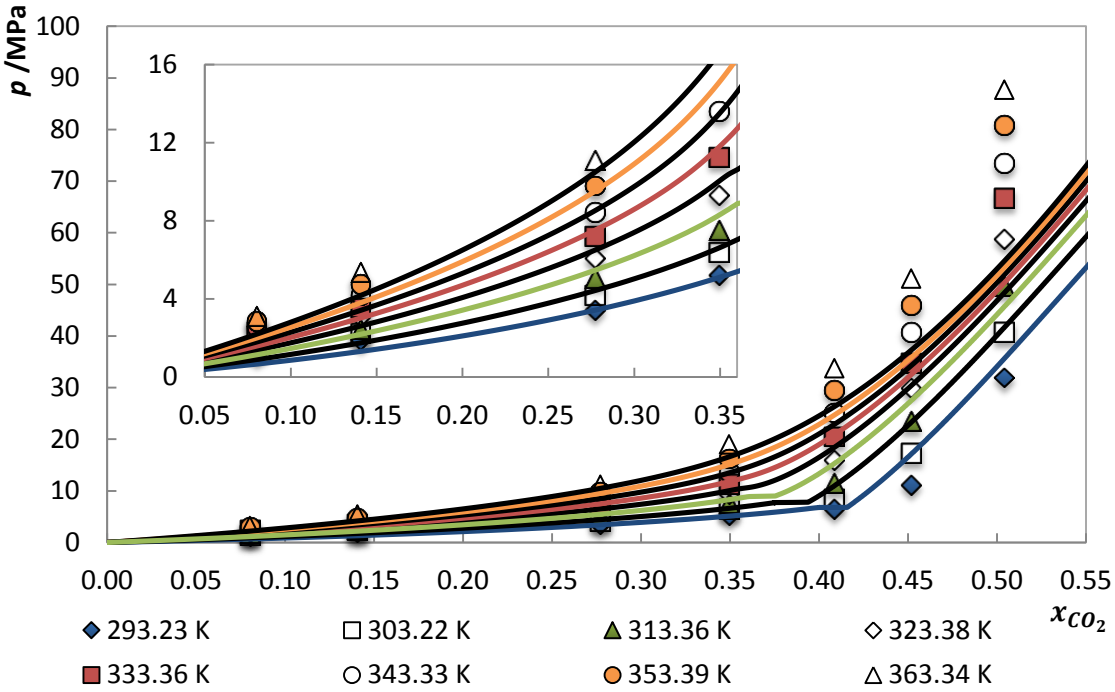

Figure 3.2- *px* diagram for the system CO_2 + $[C_2mim][CH_3OHPO_2]$ at different temperatures. Solid lines represent soft-SAFT EoS predictions using one temperature independent binary parameter (ξ=1.017).

As depicted in Figure 3.2, the soft-SAFT EoS, using one temperature independent binary parameter (ξ=1.017), provides a good description of the CO_2 + $[C_2mim][CH_3OHPO_2]$ system for gas mole fractions up to 0.35. For higher concentration, on the liquid-liquid-like region, the EoS fails to describe correctly the behaviour of the systems. In fact, for concentrations around 0.40 the model predicts a liquid-liquid region for the 293.23 K, 303.22 K and 313.36 K temperatures, as described by the depicted plateau. The temperature independent binary parameter was fitted (ξ=1.017) against the CO_2 solubility for the intermediate temperature of 323.38 K.

3.3.2- N_2O Solubility

The solubility of N_2O in $[C_2mim][CH_3OHPO_2]$ was measured for mole fractions from 0.10 up to 0.31 in the temperature range of (293.27–363.31) K and pressures from 0.1 to 57 MPa, as reported in Table 8.3 in the appendix C and in Figure 3.3. N_2O present similar solubilities to those of the CO_2 and also the temperature increase leads to an increase on the equilibrium pressures and by increasing N_2O concentration, the equilibrium pressures increases gradually at first, and then rapidly for higher N_2O contents as a liquid-liquid like region is reached.

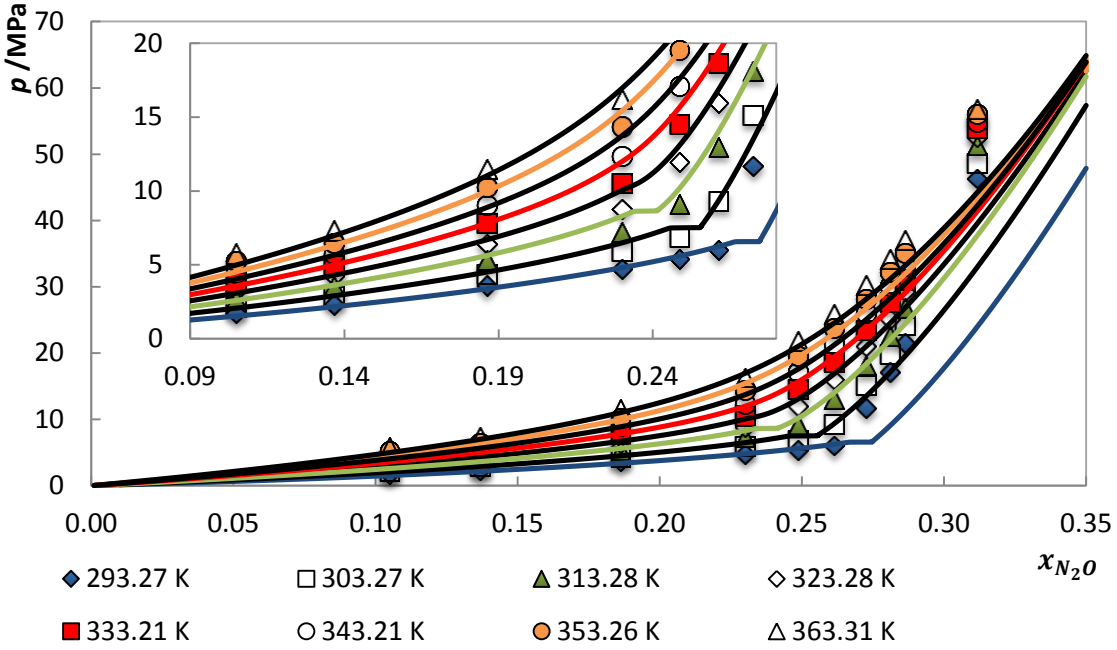

Figure 3.3- *px* diagram for the system N_2O + $[C_2mim][CH_3OHPO_2]$ at different temperatures. Solid lines represent soft-SAFT EoS predictions using one temperature independent and non-dependent binary parameter (ξ).

Soft-SAFT EoS provides a good description of the N_2O + $[C_2mim][CH_3OHPO_2]$ GLE for gas concentration up to 0.25 while for gas concentration higher than 0.25, the model under predicts the equilibrium pressures once the liquid-liquid region is reached. Similar to what is observed for the CO_2 + IL systems, the model is able to predict a liquid-liquid region for N_2O molar concentrations around 0.23 to 0.28 for the three lowest temperatures.

Moreover, a good description of the GLE data was achieved using a single temperature binary parameter for temperatures up to 323 K. For higher temperatures, the soft-SAFT EoS requires the use of a linear temperature dependent binary parameter. The binary parameters are listed in Table 8.4 in the appendix C and depicted in Figure 3.4. As described above, the temperature independent binary parameter (ξ=0.968), used for the temperature range of (293.27–323.28) K, was fitted against the N_2O solubility at 313.28 K.

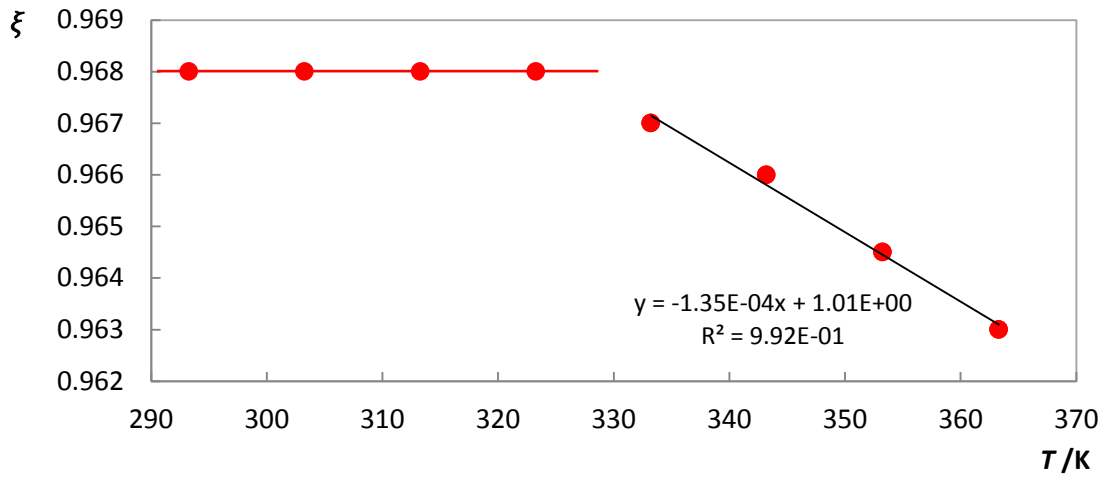

Figure 3.4- Binary parameters (ξ) used for describing the system N_2O + $[C_2mim][CH_3OHPO_2]$.

3.3.3- CH_4 Solubility

The solubility of CH_4 in $[C_2mim][CH_3OHPO_2]$ was measured for mole fractions from 0.02 up to 0.05 in the temperature range of (293.27–363.32) K and pressures from 0.1 to 20 MPa, as reported in Table 8.5 in the appendix C and depicted in Figure 3.5 and Figure 3.6.

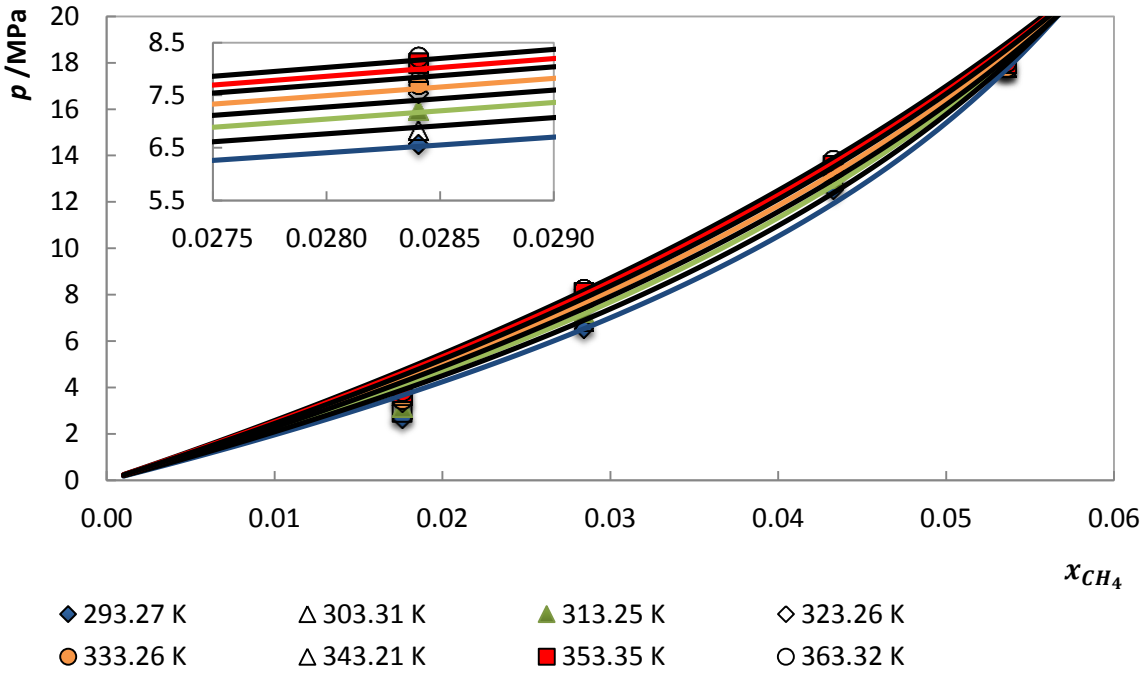

Figure 3.5- *px* diagram for the system CH_4 + $[C_2mim][CH_3OHPO_2]$ at different temperatures. Solid lines represent soft-SAFT EoS predictions using one temperature dependent binary parameters (η).

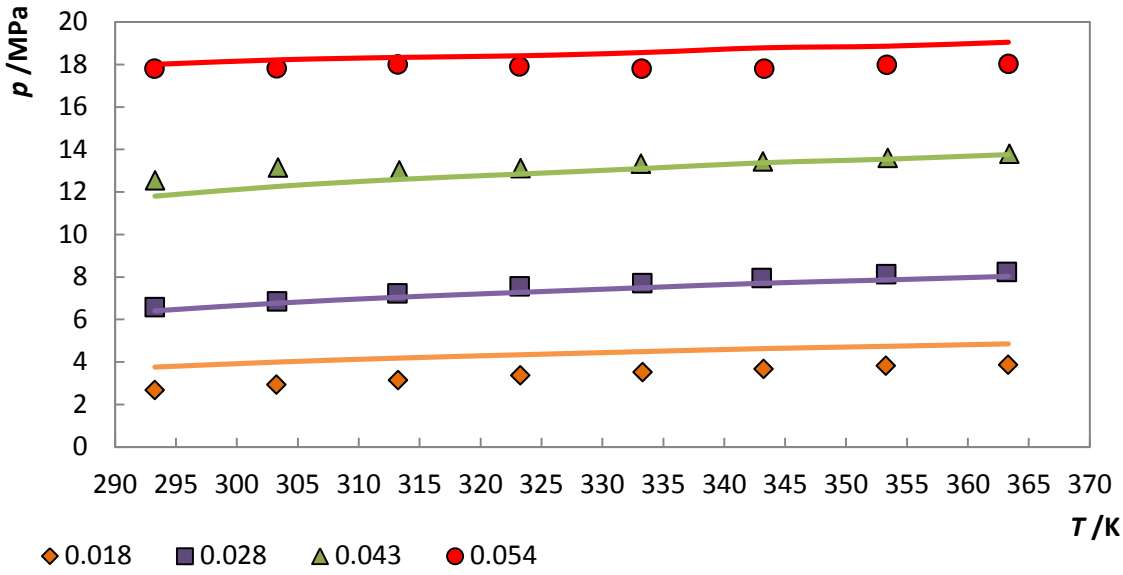

Figure 3.6- *pT* diagram for the system CH_4 + [C_2mim][CH_3OHPO_2] at different gas composition. Solid lines represent soft-SAFT EoS predictions using one temperature dependent binary parameters (η).

As depicted in Figure 3.5 and Figure 3.6, the temperature increase leads to an increase on the equilibrium pressures and, as reported for protic and NTf_2-based ILs,[6] the temperature has a very small impact on the CH_4 solubility. Nonetheless, soft-SAFT EoS provides a good description of the experimental data. This description was only achieved by using one temperature dependent binary parameter (η), listed in Table 8.6 in the appendix C and depicted in Figure 3.7, where the difference in size between the segments forming the two compound seems to have a strong influence in the model's prediction. Moreover, these parameters seem to follow a second order polynomial function with temperature.

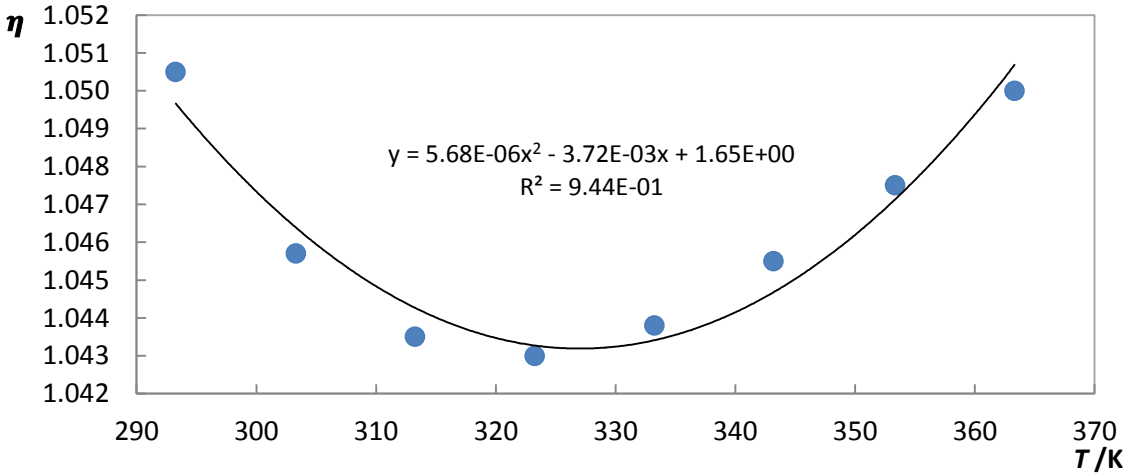

Figure 3.7- Binary parameters (η) used for describing the system CH_4 + [C_2mim][CH_3OHPO_2].

Furthermore, CH_4 has a very low solubility in $[C_2mim][CH_3OHPO_2]$ when compared with other gases such as CO_2 and N_2O, as approximately 12 MPa is required in order to achieve a CH_4 composition of 0.04 in the IL, at 293 K.

3.3.4- N_2 Solubility

The solubility of N_2 in $[C_2mim][CH_3OHPO_2]$ was measured for mole fraction from 0.01 up to 0.05 in the temperature range of (293.31–363.33) K and pressures from 14 to 90 MPa, as reported in Table 8.7 in the appendix C and in Figure 3.8. Contrary to what is commonly observed for gases, the temperature increase leads to a decrease on the equilibrium pressures. This behaviour was already reported for H_2[134, 135] and CH_4[6] systems where in certain conditions the gas shows a positive enthalpy of solution however, the reasons behind this phenomenon are not yet fully understood. Moreover, Finotello *et al.*[85] reported decreasing N_2 Henry's constant with temperature increase while an opposite behaviour was observed by Jacquemim *et al*.[76]

Apart from this, for N_2 molar concentration around 0.03 the GLE behaviour changes and contrary to what is observed for the CO_2, where the equilibrium pressure increases exponentially due to the gas complete solvation, for the N_2 the equilibrium pressure still increases but on a much less pronounced rate. Furthermore, N_2 has a very low solubility in $[C_2mim][CH_3OHPO_2]$, when compared with other gases such as CO_2 and N_2O, or even CH_4, as approximately 80 MPa is required in order to achieve a N_2 composition of 0.04 in the IL, at 293 K.

As depicted in Figure 3.8, soft-SAFT EoS is able to provide a reasonable description of the system for N_2 concentration up to 0.03 however, is not able to describe the change on the GLE behaviour for higher concentrations. Furthermore, for temperatures higher than 323K, the model provides a correct description of the effect of temperature in N_2 solubility using a single binary parameter (ξ=0.865), while for the lowest temperatures, a temperature dependent binary parameter is required to describe the system. The temperature independent binary parameter, used for the temperature range of (323.30–363.33) K, was fitted against the N_2 solubility at 323.30 K, while for remaining temperatures, one temperature dependent binary parameters (ξ) were used. The complete list of binary parameters is listed in Table 8.8 in the appendix C and depicted in Figure 3.19.

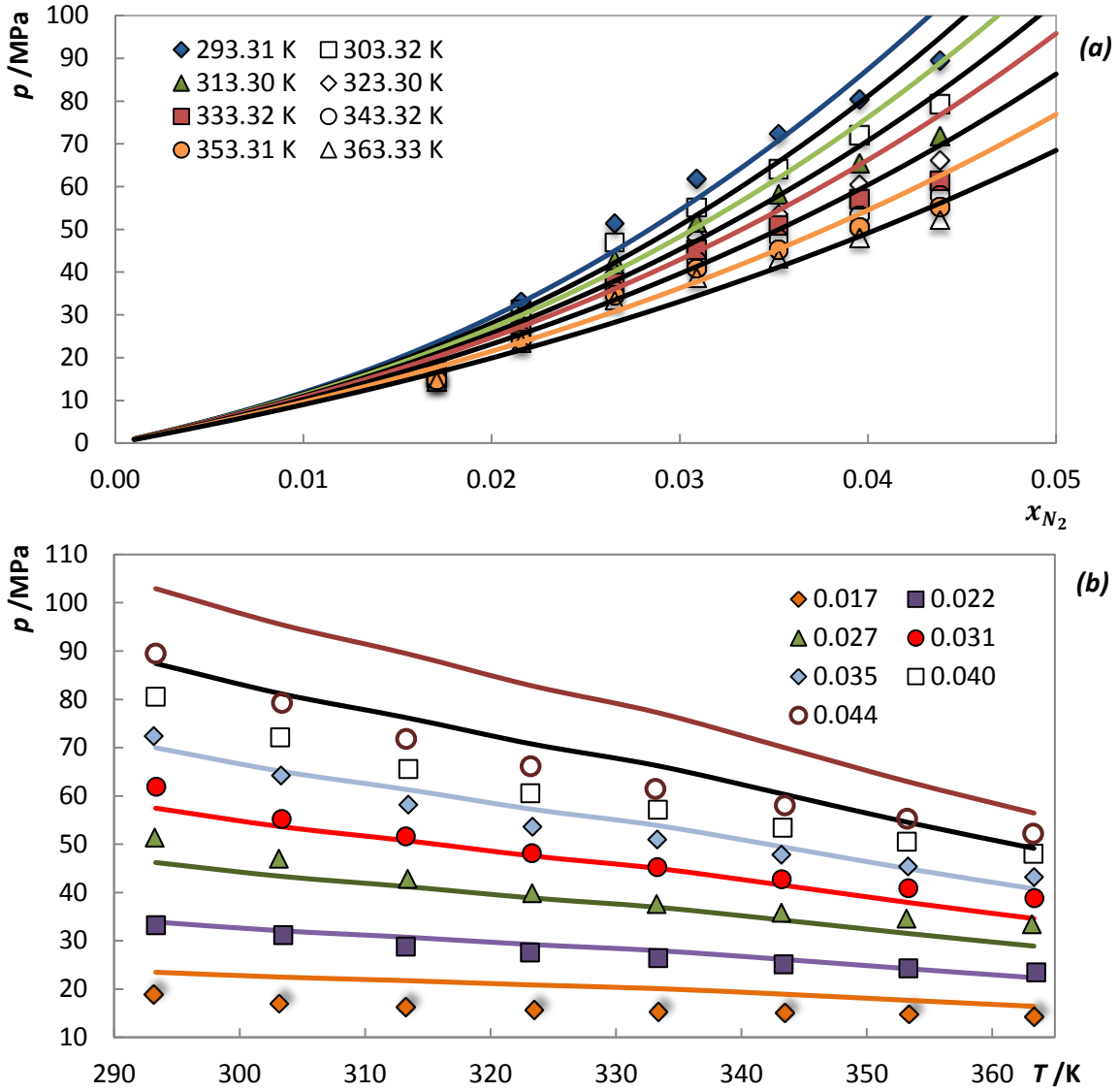

Figure 3.8- *px (a)* and *pT (b)* diagrams for the system N_2 + [C_2mim][CH_3OHPO_2]. Solid lines represent soft-SAFT EoS predictions with one temperature dependent and independent binary parameters (ξ).

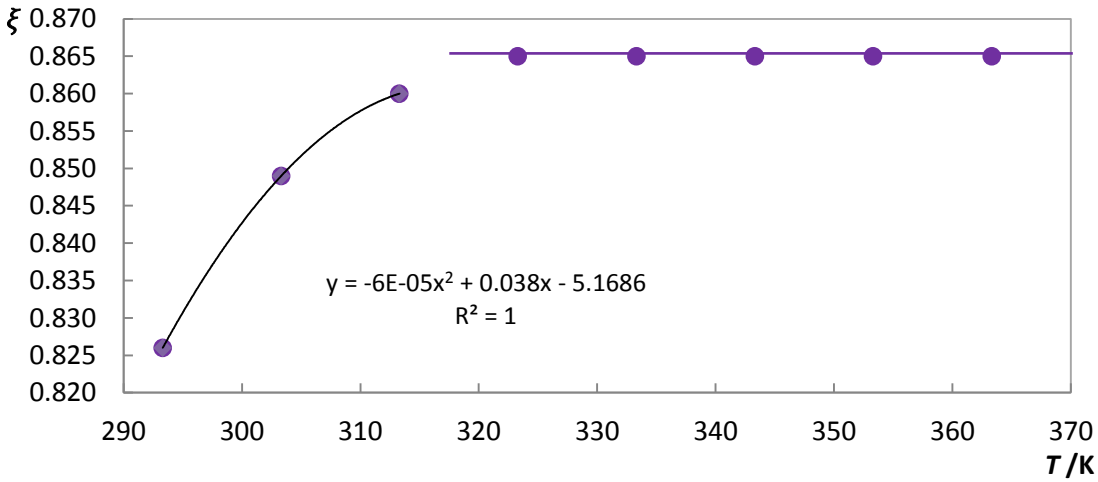

Figure 3.9- Binary parameters (ξ) used for describing the system N_2 + [C_2mim][CH_3OHPO_2].

3.4- Extension of Soft-SAFT Modelling to Other ILs + Gas Systems

3.4.1- CO_2 Solubility in Other ILs

Experimental data for the CO_2 solubility in $[C_4mim][SCN]$, $[C_4mim][BF_4]$, $[C_4mim][NTf_2]$ and $[C4mim][N(CN)_2]$ is available in the literature in a wide range of temperatures and compositions. Solubility data from Shiflett *et al.*,[17] Lee *et al.*,[19] Revelli *et al.*[15] and Carvalho *et al.*[20] were used here in order to extend the applicability of soft-SAFT EoS to other ILs systems. The phase equilibrium diagrams are depicted in Figure 3.10 to Figure 3.13.

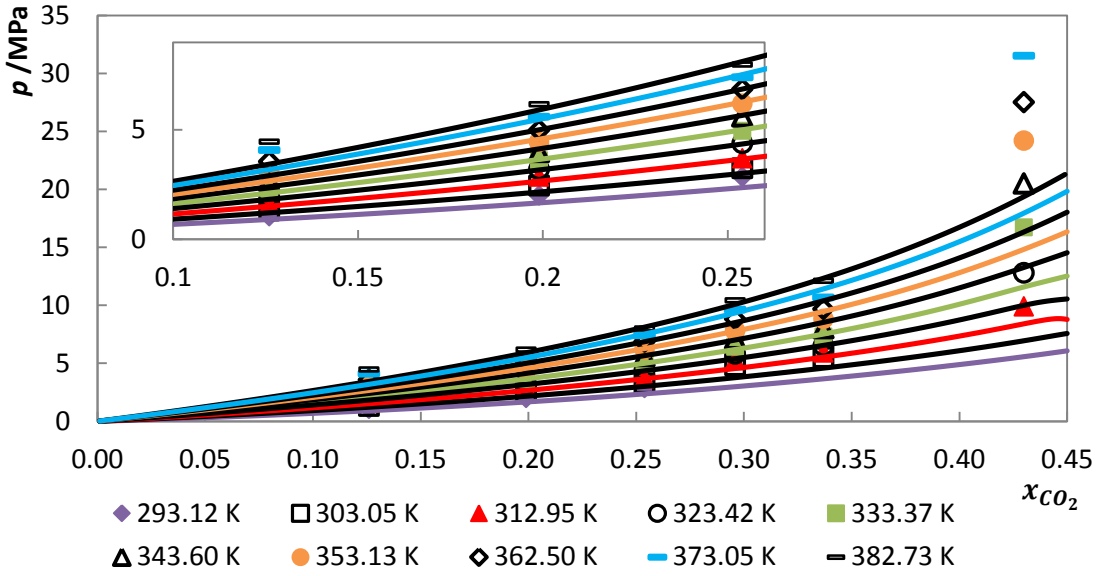

Figure 3.10- *px* diagram for the system CO_2 + $[C_4mim][SCN]$ at different temperatures.[15] Solid lines represent soft-SAFT EoS predictions using one temperature independent binary parameter (ξ=0.965).

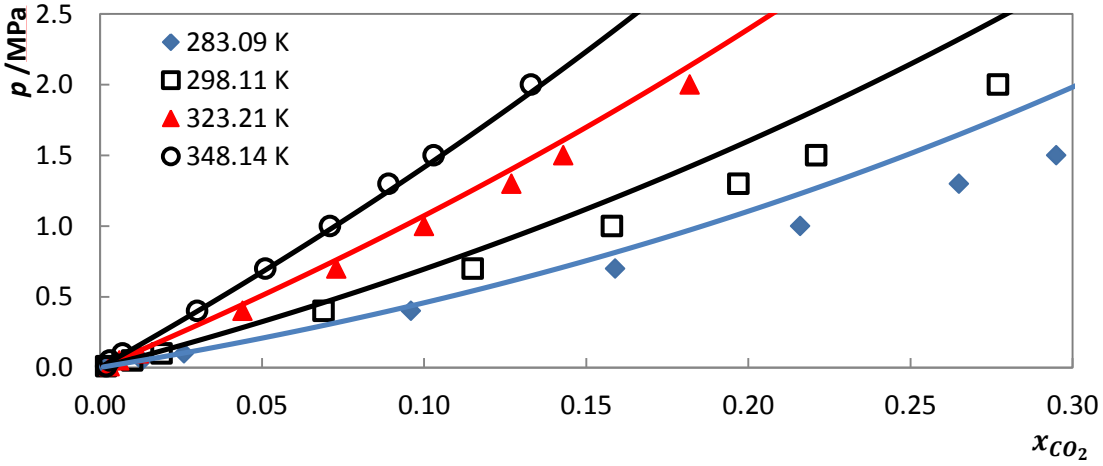

Figure 3.11- *px* diagram for the system CO_2 + $[C_4mim][BF_4]$ at different temperatures.[17] Solid lines represent soft-SAFT EoS predictions using both binary parameters (ξ and η) fixed to 1.

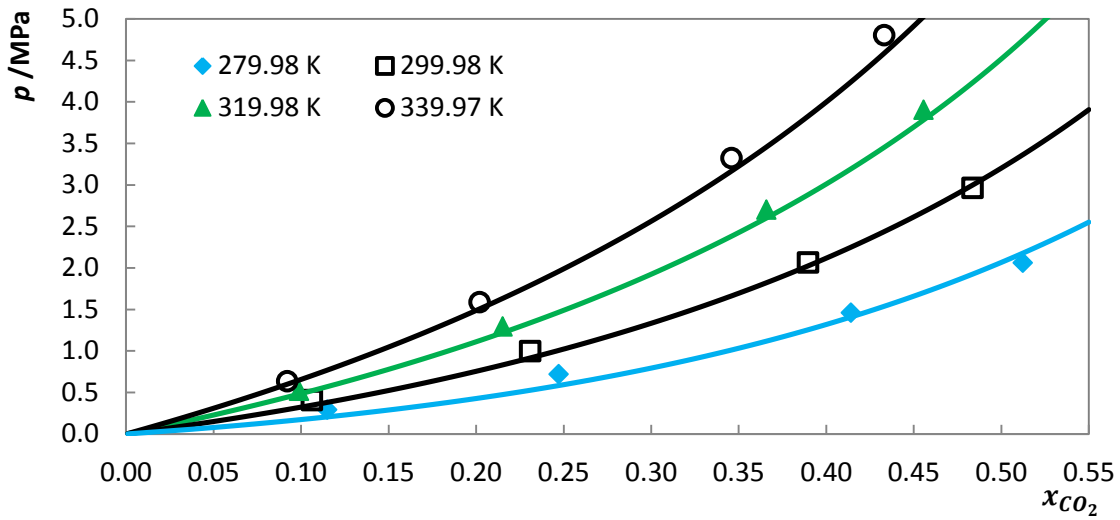

Figure 3.12- *px* diagram for the system CO_2 + [C_4mim][NTf_2] at different temperatures.[19] Solid lines represent soft-SAFT EoS predictions using one temperature independent binary parameter (ξ=0.98).

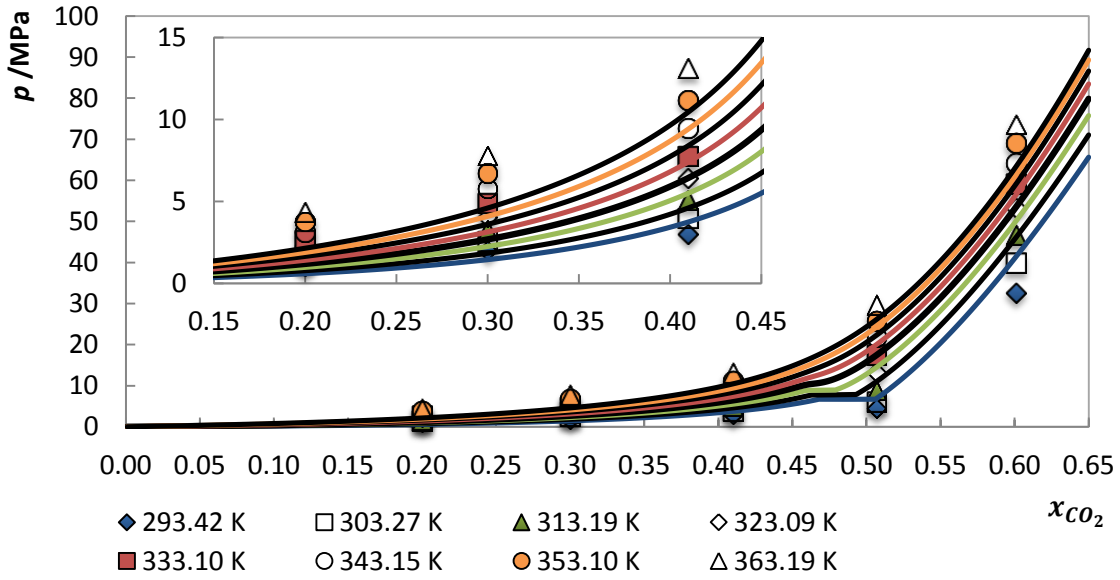

Figure 3.13- *px* diagram for the system CO_2 + [C_4mim][$N(CN)_2$] at different temperatures.[20] Solid lines represent soft-SAFT EoS predictions using one temperature independent binary parameter (ξ=0.89).

As depicted in Figure 3.10 to Figure 3.13, the temperature and CO_2 concentration increase leads to an increase in the equilibrium pressure, as previously observed for other systems, however, the liquid-liquid like region is only observed, within the studied gas mole fraction range, for the system involving the IL [C_4mim][$N(CN)_2$] (Figure 3.13).

For the system CO_2 + [C_4mim][SCN] (Figure 3.10), the model successfully captures the CO_2 phase behaviour for gas concentrations up to 0.35 by using one temperature independent binary parameter (ξ=0.965). On the other hand, it fails to describe the sudden increase of the equilibrium pressures for a gas concentration around 0.43. The temperature independent binary

parameter was fitted against the CO_2 solubility for the intermediate temperature of 333.37 K and used to predict the solubility at other temperatures.

For the systems involving the ILs [C_4mim][BF_4] and [C_4mim][NTf_2], molecular parameters available in the literature were used, providing a successful description of the binary systems either using it in a predictive manner, as depicted in Figure 3.11, or with one temperature independent binary parameter (ξ=0.98), as depicted in Figure 3.12. The temperature independent binary parameter was fitted against the CO_2 solubility for the intermediate temperature of 319.28K.

Finally, for the system CO_2 + [C_4mim][$N(CN)_2$] (Figure 3.13) the soft-SAFT EoS, using one temperature independent binary parameter (ξ=0.89), overpredicts the CO_2 solubility in the IL for gas concentrations up 0.30. Furthermore, for concentrations around 0.50 the soft-SAFT predicts a liquid-liquid region for the 293.42 K, 303.27 K and 313.19 K temperatures, as obtained for other systems. The temperature independent binary parameter was fitted against the CO_2 solubility for the intermediate temperature of 323.09 K.

3.4.2- N_2O Solubility in Other ILs

The solubility of N_2O in [C_4mim][$N(CN)_2$], depicted in Figure 3.14, was previously measured by the research group for mole fractions from 0.03 up to 0.30 in the temperature range of (303.31 –363.28) K and pressures from 0.1 to 12 MPa. N_2O presents similar solubilities to those of the CO_2 and also the temperature increase leads to an increase on the equilibrium pressures and by increasing N_2O concentration however, no liquid-liquid like region is observed within the studied gas mole fraction range.

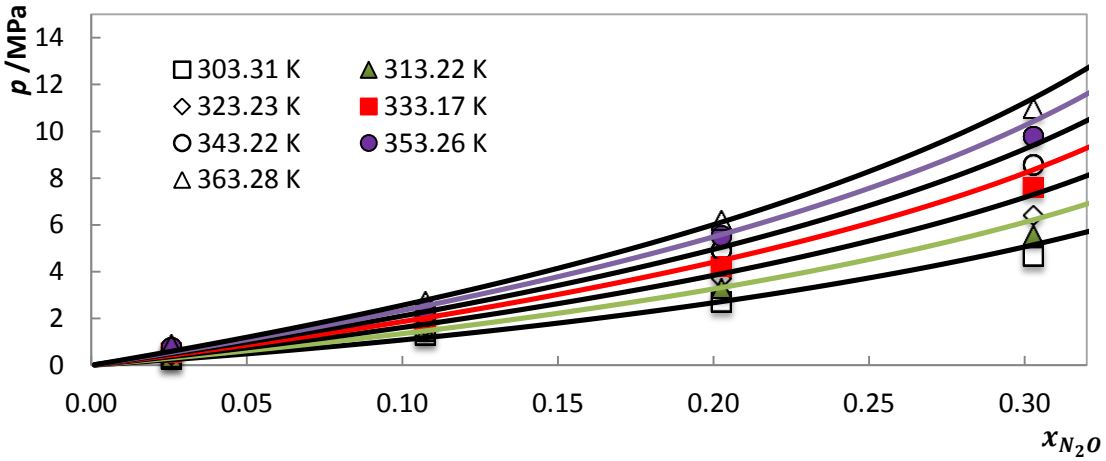

Figure 3.14- *px* diagram for the system N_2O + [C_4mim][$N(CN)_2$] at different temperatures. Solid lines represent soft-SAFT EoS predictions using one temperature independent parameter (ξ=0.915).

As illustrated in Figure 3.14, woft-SAFT EoS provides a good description of the GLE for gas concentration up to 0.30 using one temperature independent temperature binary parameter (ξ=0.915) fitted against the N_2O solubility at 323.23 K.

Experimental data for the N_2O solubility in [C_4mim][SCN], [C_4mim][BF_4] and [C_4mim][NTf_2] is available in the literature in a wide range of temperatures and compositions. Solubility data from Shiflett *et al*.[16, 18] and Revelli *et al.,*[14] depicted in Figure 3.15 to Figure 3.17, were used.

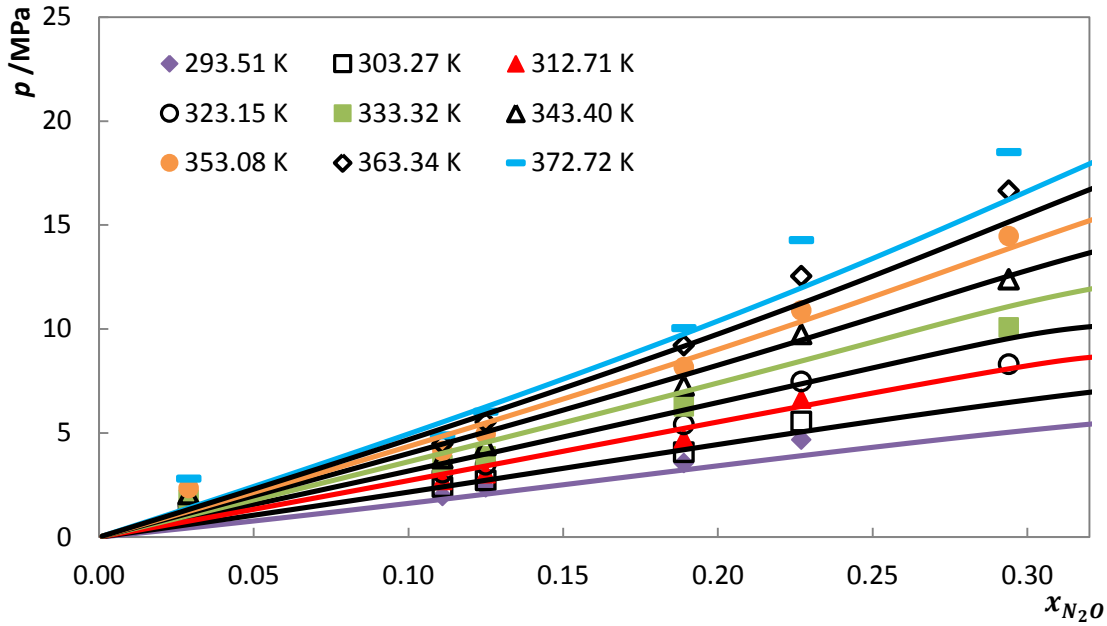

Figure 3.15- *px* diagram for the system N_2O + [C_4mim][SCN] at different temperatures.[14] Solid lines represent soft-SAFT EoS predictions using one temperature independent binary parameter (ξ=0.978).

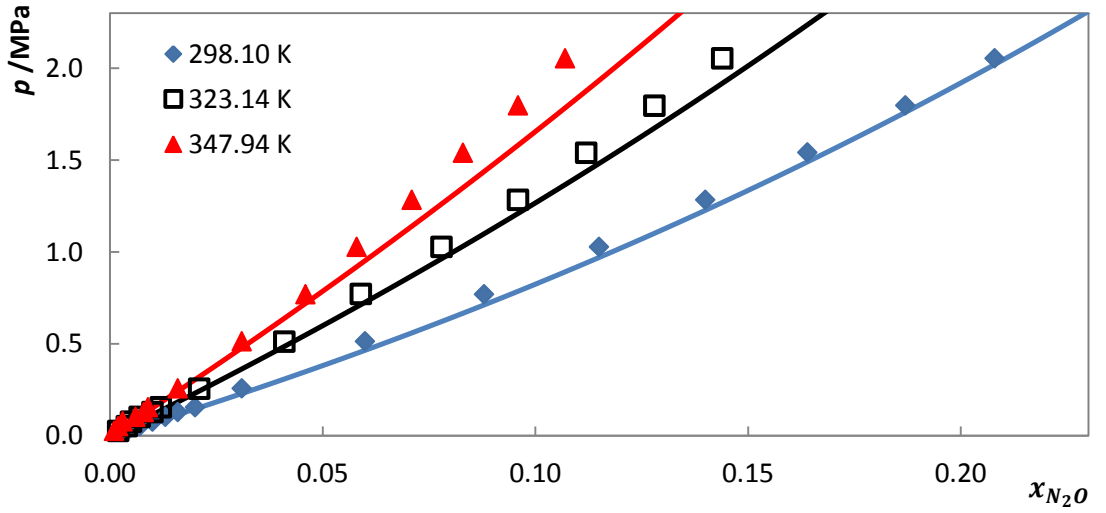

Figure 3.16- *px* diagram for the system N_2O + [C_4mim][BF_4] at different temperatures.[16] Solid lines represent soft-SAFT EoS predictions using one temperature independent binary parameter (ξ=0.978).

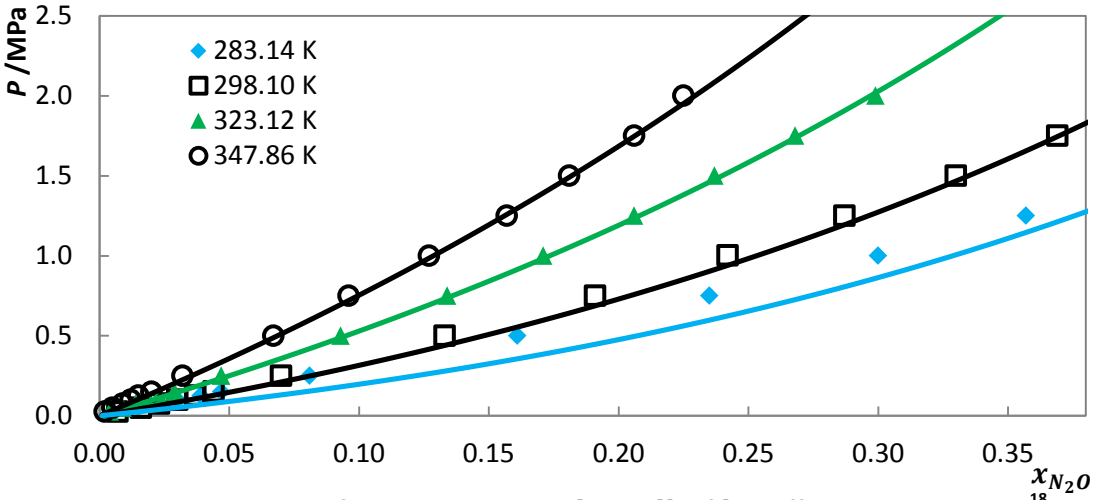

Figure 3.17- *px* diagram for the system N_2O + [C_4mim][NTf_2] at different temperatures.[18] Solid lines represent soft-SAFT EoS predictions using two temperature independent binary parameters (η=1.01 and ξ=0.98).

As depicted in Figure 3.15 to Figure 3.17, the temperature and N_2O concentration increase leads to an increase in the equilibrium pressure, as previously observed for the system [C_2mim][CH_3OHPO_2] and [C_4mim][$N(CN)_2$]. Moreover, for the system involving the IL [C_4mim][SCN] and for a gas concentration around 0.30, a decrease in the equilibrium pressure is observed for the temperatures 323.15 K and 333.32 K (Figure 3.15).

For the system N_2O + [C_4mim][SCN], soft-SAFT EoS provides a good prediction for a gas concentration within the range 0.10 to 0.23, as depicted in Figure 3.15, using one temperature independent binary parameter (ξ=0.978) fitted against the N_2O solubility at 333.32 K. Nonetheless, the model fails to predict the dilute region, gas concentration up to 0.05, and even for gas concentration above 0.30.

For the systems N_2O + [C_4mim][BF_4] and N_2O + [C_4mim][NTf_2], soft-SAFT EoS successfully describe N_2O equilibrium pressures within all temperatures and concentration range, as depicted in Figure 3.16 and Figure 3.17. Furthermore, one temperature independent binary parameter (ξ=0.978) was used for describing the system [C_4mim][BF_4] + N_2O, while for the system [C_4mim][NTf_2] + N2O two temperature independent binary parameters (η=1.01 and ξ=0.98) were required to achieve a good description of the system. The parameters for both systems were fitted against N_2O solubility at 323.12 K and 323.14 K, respectively.

3.4.3- N_2 Solubility in Other ILs

The solubility of N_2 in $[C_4mim][N(CN)_2]$, previously measured by the research group, for mole fraction from 0.01 up to 0.08 in the temperature range of (293.71–363.24) K and pressures from 0.1 to 70 MPa, as depicted in Figure 3.18, was used. Similar to what was observed for the $[C_2mim][CH_3OHPO_2]$ + N_2 system, studied here, and for some ILs + H_2[134, 135] and CH_4[6] systems, the temperature increase leads to a decrease on the equilibrium pressures. Moreover, similar to what was observed for the $[C_2mim][CH_3OHPO_2]$ + N_2 system, the $[C_4mim][N(CN)_2]$ + N_2 system also presents a less pronounced equilibrium pressure dependency with the gas composition than that observed for CO_2 and N_2O systems as well as extremely low gas solubility.

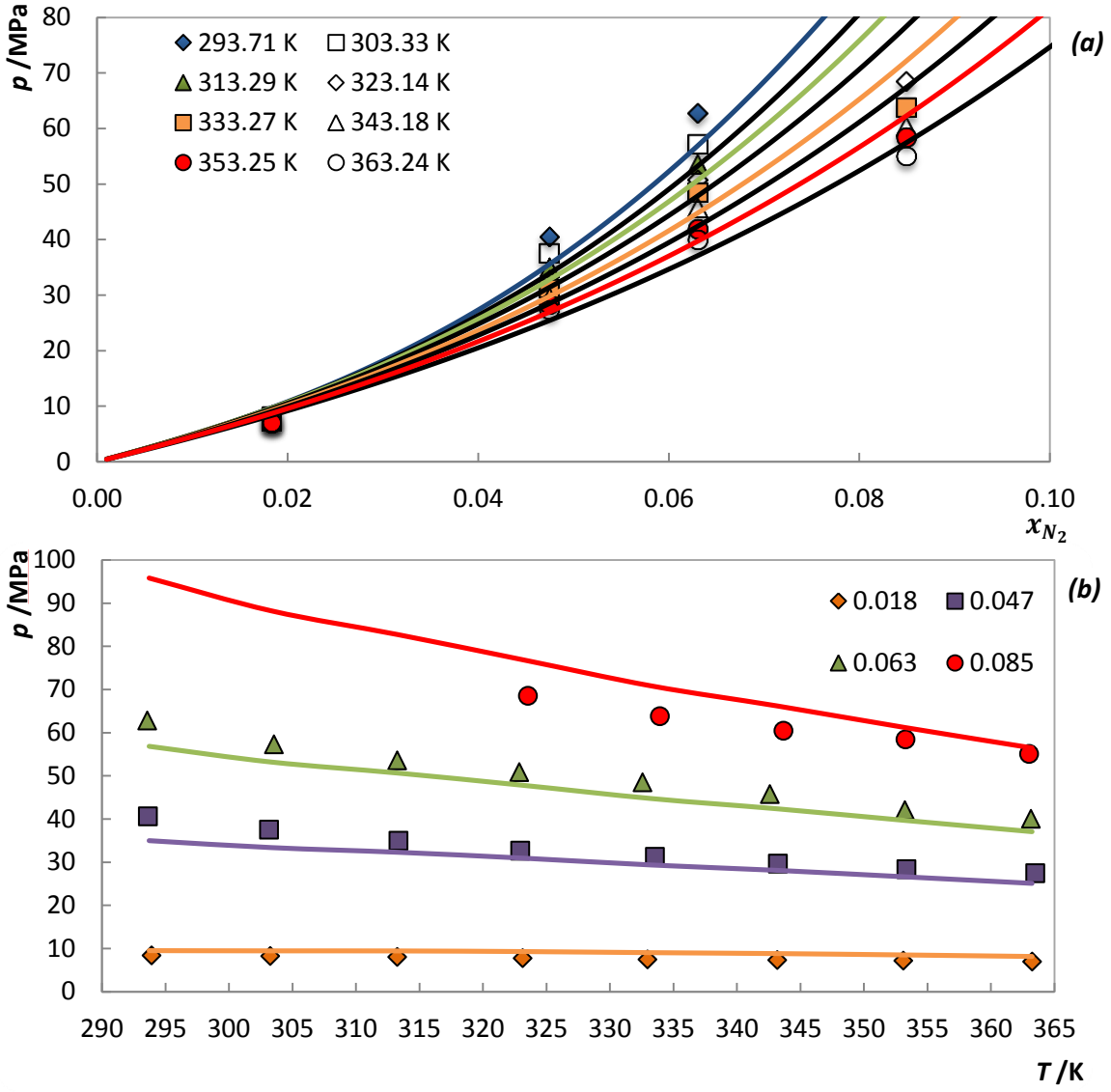

Figure 3.18- *px (a)* and *pT (b)* diagrams for the system N_2 + $[C_4mim][N(CN)_2]$. Solid lines represent soft-SAFT EoS predictions using one temperature dependent and independent binary parameters (ξ).

As depicted in Figure 3.18, soft-SAFT EoS also provides a good description of the system for a N_2 concentration up to 0.06, failing nonetheless to describe the change on the GLE behaviour for higher concentrations. Furthermore, similarly to the previously presented systems, a correct description by the model of the GLE data is achieved by using one temperature independent binary parameter (ξ=0.768) for temperatures higher than 333.27 K. For lower temperatures, one temperature dependent binary parameter was necessary for a correct description. Nonetheless, these temperature dependent binary parameters seem to be well described by a second order polynomial function, as depicted in Figure 3.19. The complete list of binary parameters for this system is listed in Table 8.8 in the appendix C.

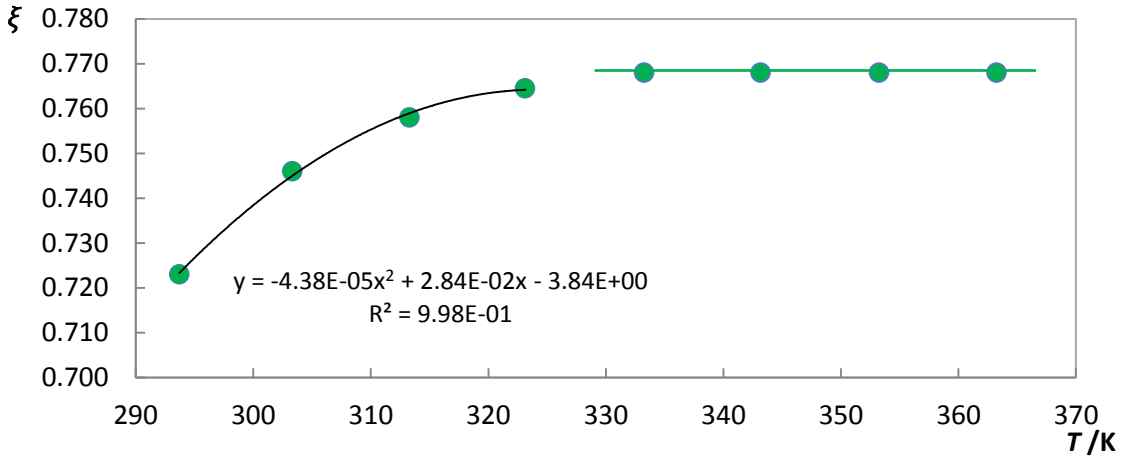

Figure 3.19- Binary parameters (ξ) used for describing the system N_2 + $[C_4mim][N(CN)_2]$.

N_2 solubility data available in literature is still scarce and huge discrepancies among different authors are common. Thus, GLE data for the $[C_4mim][SCN]$, $[C_4mim][BF_4]$ and $[C_4mim][NTf_2]$ systems is only available through its Henry's constants.[76, 85, 86] These constants will be used, further in this work, for comparing Gas/N_2 selectivities between different ILs.

4- ILs’ Capturing Efficiency and Selectivities

4.1- Introduction

Having studied the gases solubilities in different ILs, selectivity and capturing efficiency studies also stand as vital steps toward the potential use of this class of solvents as capturing agents. Therefore, ideal gas selectivities ($S_{1/2}$) are here evaluated for the three main gases of interest (CO_2, N_2O and N_2) present in post-combustion streams through the Henry's constants (H_x) determination and by the following equations:

$$S_{CO_2/N_2} = \frac{H_{N_2}}{H_{CO_2}} \quad \textbf{Eq. 4.1}$$

$$S_{N_2O/N_2} = \frac{H_{N_2}}{H_{N_2O}} \quad \textbf{Eq. 4.2}$$

$$S_{CO_2/N_2O} = \frac{H_{N_2O}}{H_{CO_2}} \quad \textbf{Eq. 4.3}$$

Moreover, these gas selectivities are compared with the ones obtained from conventional solvents like aqueous monoethanolamine (MEA) and triethylene glycol monomethyl ether (TEGMME).

MEA is a well-known solvent used in the chemical absorption of some pollutants like CO_2 and H_2S[136-144] however, MEA-based systems present several disadvantages, like large equipment sizes due to low amines/water weight relation and high solvent regeneration costs, just to mention a few.[141, 142] On the other hand, TEGMME is a physical absorbent with low vapour pressure, well-known for its strong affinity with CO_2 and N_2O[145-147] which, contrary to chemical absorption where the absorption capacity is limited by the stoichiometry of the reaction, the absorption capacity is proportional to the partial pressure of the gas. Moreover, the use of non-aqueous systems would lead to lower desorption energy consumption, making the glycols, in general, a promising alternative for MEA-based processes. [141, 147]

(a) ***(b)***

Figure 4.1- MEA *(a)* and TEGMME *(b)* molecular structures.

In addition to that, ILs capturing efficiencies are also compared with the above mentioned conventional solvents by expressing the gases solubility in terms of molality ($m_{g/s}$), moles of gas absorbed per kilogram of solvent.

4.2- Henry's Constants and Selectivities

The Henry's law relates the amount of gas dissolved in a liquid, at a constant temperature and pressure, to the fugacity (f^{L}_{1}) of that gas (1) in the liquid phase (2) and can be described as:

$$H_{12}(T,P) = \lim_{x_1 \to 0} \frac{f_i^L}{x_1} \qquad \textbf{Eq. 4.4}$$

where H_{12}(T, P) is the Henry's constant and x_1 is the mole fraction of gas dissolved in the liquid phase. Eq. 4.4 is only rigorously valid in the diluted region limit.

CO_2 and N_2O Henry's constants in the conventional solvents are available in literature[146-148] and were found to be 75.05 and 102.78 MPa in MEA (40%), respectively, and 6.80 and 7.25 MPa in TEGMME, respectively, within the temperature range of (298.15–303.00) K. Although no information was found for N_2 Henry's constant in MEA (40%), gas selectivity was taken from Xu *et al.*[149] work, where the absorption of CO_2 and N_2 in MEA (40 %) fixed in β-zeolite was study and S_{CO_2/N_2} determined, founded to be 26.67 at 303 K. This value is here used as representative selectivity and as maximum value of S_{N_2O/N_2}, since N_2O is expected to have a higher Henry's constant. On the other hand, N_2 henry constant in TEGMME was here estimated using Predictive Soave-Redlich-Kwong (PSRK) EoS[150] and a commercial simulator (ASPEN Plus 2006.5), which was previously found to accurately predict the N_2O and CO_2 + TEGMME systems, as depicted in Figure 8.2 in the appendix D. The PSRK EoS was fitted to the dilute region and the N_2 Henry's constant calculated by the limiting sloped defined in Eq. 4.4 as the solubility approaches zero, as depicted in Figure 4.2. The value for the N_2 henry's constant was found to be 52.93 MPa at 303 K.

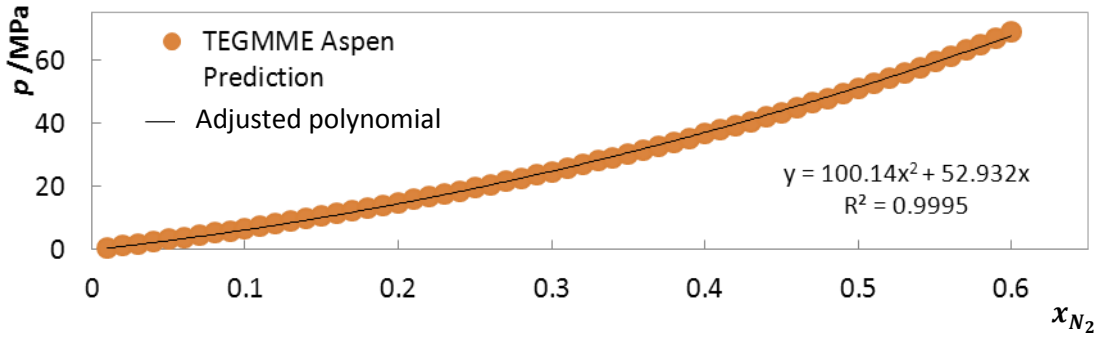

Figure 4.2- Predicted solubility of N_2 in TEGMME at 303 K using PSRK EoS and adjusted polynomial function.

The gases Henry's constant in $[C_2mim][CH_3OHPO_2]$ was here estimated, for the first time, by fitting the soft-SAFT EoS to the low pressure experimental data and calculating the limiting slope defined in Eq. 4.4 as the solubility approaches zero. The procedure is described in more detail in the appendix E, together with the molecular and binary parameters used. This approach

introduces some uncertainty on the estimated Henry's constants but the values of these constants for the studied systems are different enough to allow a discussion of the gases solubility and selectivities on the ILs based on these values. For the remaining systems, involving the ILs $[C_4mim][N(CN)_2]$, $[C_4mim][SCN]$, $[C_4mim][BF_4]$ and $[C_4mim][NTf_2]$, Henry's constants were taken from the literature,[18, 76, 85, 86] with the exception of N_2 Henry's constant in $[C_4mim][N(CN)_2]$, which was here calculated for the first time using the above mentioned approach used for the IL $[C_2mim][CH_3OHPO_2]$ and unpublished solubility data measured from our group (see appendix E). The complete list of the above mentioned Henry's constants in the ILs is listed in Table 4.1.

Table 4.1- Gases Henry's constants in the ILs within the temperature range of (298.15–303.38) K.

	$[C_2mim][CH_3OHPO_2]$	$[C_4mim][N(CN)_2]$	$[C_4mim][SCN]$	$[C_4mim][BF_4]$	$[C_4mim][NTf_2]$
CO_2	17.21	4.06	10.28	5.38	1.62
N_2O	18.14	8.69	12.78	7.86	3.21
N_2	907.41	462.03	-[a]	178.90	121.60[b]

[a] Henry's constant was not found in the literature neither solubility data that would allow its calculation.
[b] Average Henry's constant of N_2 calculated from the ones reported in $[C_2mim][NTf_2]$ (141.90 MPa)[86] and $[C_6mim][NTf_2]$ (101.30 MPa) at 298.15 K.[85]

Once all the gases Henry's constants in the different solvents are known, gas selectivities can be calculated using the equations Eq. 4.1 to Eq. 4.3, being the results depicted in Figure 4.3 and Figure 4.4.

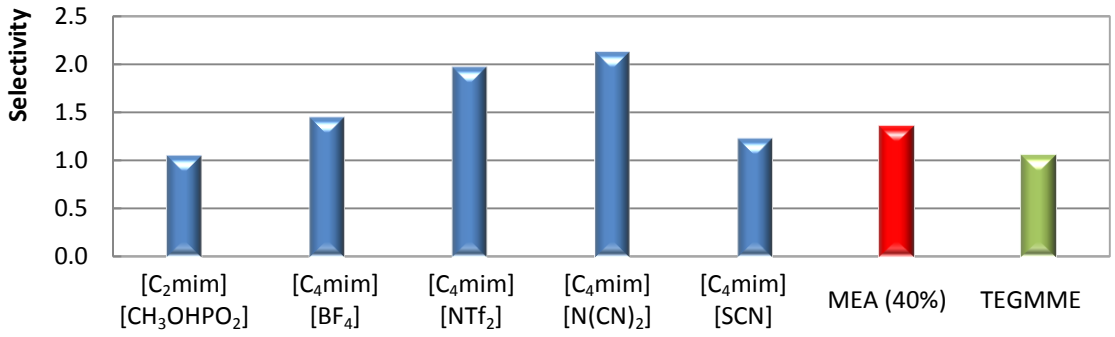

Figure 4.3- Calculated S_{CO_2/N_2O} in the different solvents within the temperature range of (298.15–303.38) K.

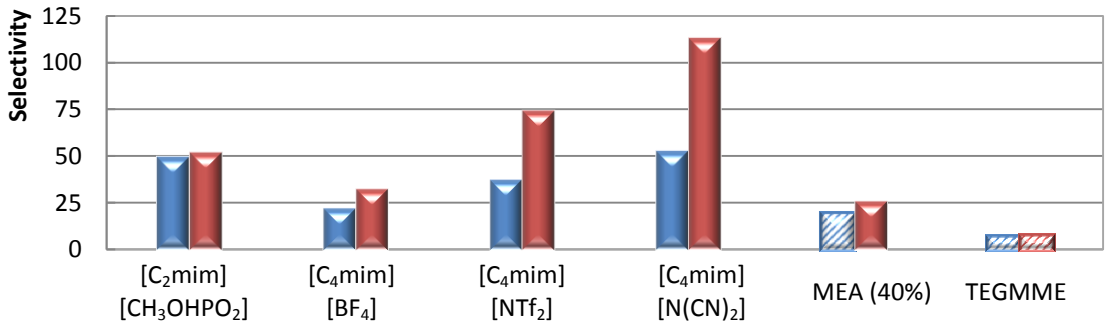

Figure 4.4- Calculated S_{N_2O/N_2}(blue) and S_{CO_2/N_2} (red) in the different solvents within the temperature range of (298.15–303.38) K.

As depicted in Figure 4.3, all the solvents considered have a low CO_2/N_2O selectivity (1 to 2.15), with the highest values obtained for the ILs $[C_4mim][N(CN)_2]$ and $[C_4mim][NTf_2]$. These low selectivities are a result of CO_2 and N_2O similar solubility either in the ILs or in the conventional solvents. In opposition, CO_2/N_2 and N_2O/N_2 selectivity in the ILs are higher than the ones obtained in the conventional solvents, in some cases in several orders of magnitude, as depicted in Figure 4.4, showing the ILs greater affinity towards CO_2 and N_2O than N_2.

According to these results, ILs and the conventional solvents present similar affinity with CO_2 and N_2O however, the extremely low solubility of N_2 in the ILs shows that these can potentially be used to remove, simultaneously, both gases from post-combustion streams with the minimum N_2 absorption.

4.3- ILs' Capturing Efficiency

In order to evaluate the ILs' capturing efficiency for N_2O and CO_2 and compare it with the conventional solvents MEA (40%) and TEGMME, gas solubilities were expressed in terms of molality, as listed in Tables 8.2, 8.3, 8.5 and 8.7 in the appendix C and depicted in Figure 4.5 and Figure 4.6, using solubility data measured here and from the literature.[16-19, 146-148]

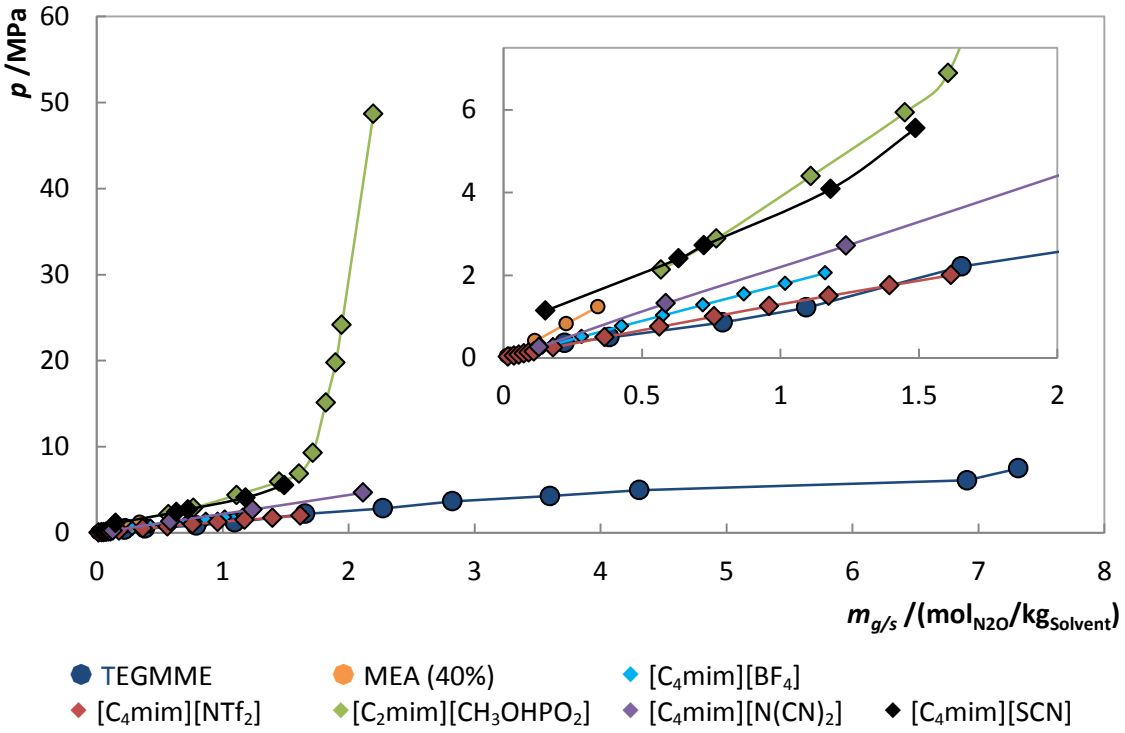

Figure 4.5- $pm_{g/s}$ diagram of N_2O in different solvents within the temperature range of (298.10–303.31) K. Solid lines are only used as guide lines.

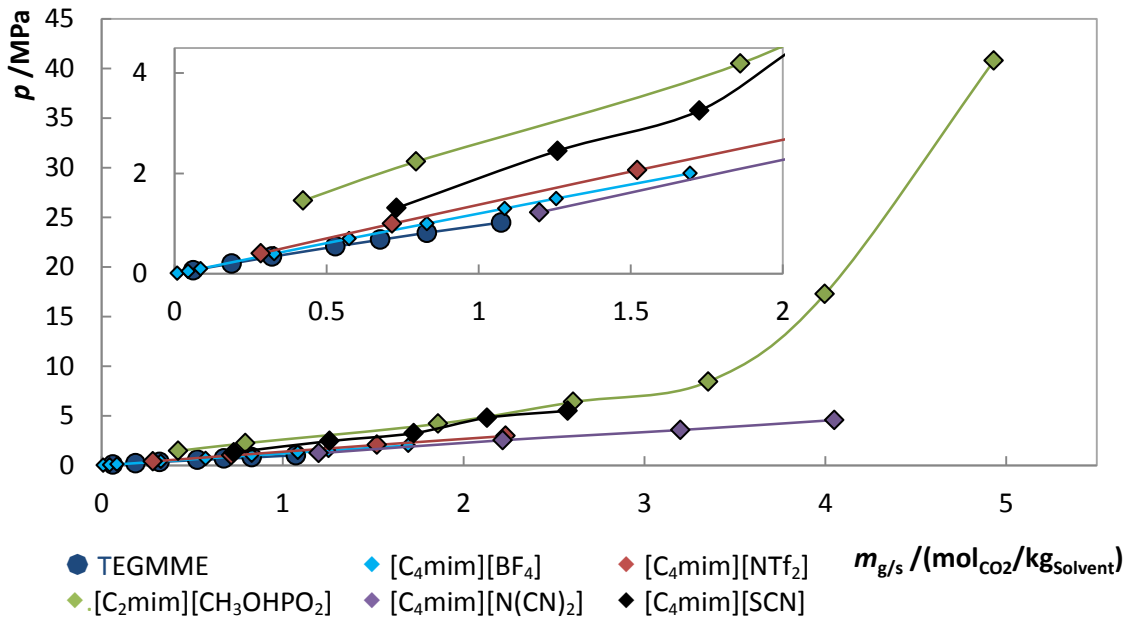

Figure 4.6- $pm_{g/s}$ diagram of CO_2 in different solvents within the temperature range of (298.11–303.22) K. Solid lines are only used as guide lines.

As depicted in Figure 4.5 and Figure 4.6, some ILs have capturing efficiencies similar to the ones of TEGMME and MEA (40%), with exception of CO_2 in MEA (40%) that is not presented in Figure 4.6, since a chemical absorption occurs and higher capturing efficiency is expected at much lower pressures. Nonetheless, as listed in Table 4.2, [C_4mim][NTf_2] is able to solubilize about 1.58 moles (69.69 grams) of N_2O per kilogram of IL, and [C_4mim][NTf_2], [C_4mim][BF_4] and [C_4mim][$N(CN)_2$] are able to solubilize about 1.49, 1.68 and 1.83 moles (65.49, 73.94 and 80.43 grams) of CO_2, respectively, per kilogram of IL, within the temperature range of (298.10–303.31) K and pressure of 2 MPa; compared to TEGMME, which is able to solubilize about 1.60 and 2.09 moles (70.23 and 90.10 grams) of N_2O and CO_2 respectively, while MEA (40%) is able to solubilize 0.55 moles (24.27 grams) of N_2O. According to these results, ILs present similar absorption capacity to TEGMME and MEA (40%) and therefore, they are feasible to be used as high efficient capturing agents at relatively low pressures.

Table 4.2- N_2O and CO_2 solubility expressed in terms of molar fraction and molality within a temperature range of (298.10–303.31) K and a pressure of 2 MPa.

	[C_4mim][NTf_2]	[C_4mim][$N(CN)_2$]	[C_4mim][BF_4]	[C_2mim][CH_3OHPO_2]	[C_4mim][SCN]	MEA (40%)	TEGMME
x_{N_2O}	0.399	0.157	0.203	0.080	0.085	0.019	0.208
$m_{g/s}(mol_{N_2O}/kg_{IL})$	1.58	0.91	1.13	0.42	0.47	0.55	1.60
x_{CO_2}	0.385	0.273	0.275	0.131	0.173	-	0.255
$m_{g/s}(mol_{CO_2}/kg_{IL})$	1.49	1.83	1.68	0.73	1.06	-	2.09

5- Conclusions

In order to overcome existent limitations in actual control processes and reduce the imminent increase in some pollutant levels, the study and proposal of alternative new methods stand as a crucial task. In this sense, solubility of common gases present in post-combustion streams in $[C_2mim][CH_3OHPO_2]$ were measured here for the first time, in a wide range of temperatures and pressures, using the synthetic method on a high pressure cell. The results showed a similar and high solubility of CO_2 and N_2O in the IL, compared to N_2 and CH_4. Moreover, a peculiar behaviour for the solubility of N_2 was observed with the solubility of the gas increasing in the IL with the temperature. In addition to that, gases solubility data in other ILs also confirm CO_2 and N_2O greater affinity to this class of solvents.

Furthermore, the model used here to describe such systems, the soft-SAFT EoS, proved to be able not only to provide a good description of the studied systems in the selected temperature and pressure ranges, but to describe both the low temperature dependence of the CH_4 + IL system and the N_2 peculiar behaviour. Therefore, despite the need in some cases of temperature dependent parameters, overall, a model as soft-SAFT EoS, without the need of ILs' critical properties, can be used not only to describe such systems but as a prediction tool for pre-selection of the better ILs to dissolve some gases, reducing the need of exhaustive and expensive data measurement.

The selectivity study performed here, showed ILs high selectivity toward pollutants like CO_2 and N_2O, greater than in conventional solvents. In addition to this, ILs showed to be able to solubilize up to 69.69 grams of N_2O and 80.43 grams of CO_2 per kilogram of IL, within the temperature range of (298.10–303.31) K and pressure of 2 MPa.

All things considered, this work proved that ILs can potentially act as capturing agent in post-combustion streams not only due their unique characteristics and high solvation capacity, but also due to their high selectivity, when compared to conventional solvents. Moreover, the decreasing of N_2 solubility in the ILs with temperature let us guess the need of reducing the gas stream temperature before treatment, in order to minimize this gas absorption. Nevertheless, the use of physical solvents, such as the ILs presented here, would allow a much lower consumption of energy for solvent regeneration, compared to chemical solvents, and a reduction in equipment size, compared to MEA-based systems.

6- Future Work

Aiming to fully understand the sorption mechanism responsible for the solubility of gases in ILs, it would be interesting to extend this type of study to other systems and test, for instance, the effect of the ILs' anion on the gases solubilities. Moreover, aiming at extending the applicability of ILs as extracting solvents to further purifications areas, it would also be interesting to study the solubilities of other gases, namely O_2 and O_3, acid gases like HCl and HF and hazardous air pollutants like dioxins and furans, using the same procedure followed here.

It would always be important to use a model to describe and predict the above mentioned systems, namely, the soft-SAFT EoS.

7- References

1. Seinfeld, J. H. and Spyros, N. P., *Atmospheric chemestry and physics: from Air Pollution to climate change*, 2006, John Wiley & Sons. p. Chapter 1 and 2.
2. Charles, B. *Everything you need to know about NOx: Controlling and minimizing pollutant emissions is critical for meeting air quality regulations.* Metal Finishing, 2005. **103**(11): p. 18-24.
3. Favre, E. *Carbon dioxide recovery from post-combustion processes: Can gas permeation membranes compete with absorption?* Journal of Membrane Science, 2007. **294**(1–2): p. 50-59.
4. U. S. Environmental Protection Agency, *AP-42, Compilation of Air Pollutant Emission Factors.* 1998. Available from: http://www.epa.gov/ttn/chief/ap42/ch01/index.html.
5. Anthony, J. L.; Anderson, J. L.; Maginn, E. J. and Brennecke, J. F. *Anion Effects on Gas Solubility in Ionic Liquids.* The Journal of Physical Chemistry B, 2005. **109**(13): p. 6366-6374.
6. Carvalho, P. J. and Coutinho, J. A. P. *The polarity effect upon the methane solubility in ionic liquids: a contribution for the design of ionic liquids for enhanced CO2/CH4 and H2S/CH4 selectivities.* Energy & Environmental Science, 2011. **4**(11): p. 4614-4619.
7. Carvalho, P. J. and Coutinho, J. A. P. *On the Nonideality of CO2 Solutions in Ionic Liquids and Other Low Volatile Solvents.* The Journal of Physical Chemistry Letters, 2010. **1**(4): p. 774-780.
8. Carvalho, P. J. and Coutinho, J. A. P. *Non-ideality of Solutions of NH3, SO2, and H2S in Ionic Liquids and the Prediction of Their Solubilities Using the Flory–Huggins Model.* Energy & Fuels, 2010. **24**(12): p. 6662-6666.
9. Vitu, S.; Jaubert, J.-N.; Pauly, J.; Daridon, J.-L. and Barth, D. *Phase equilibria measurements of CO2 + methyl cyclopentane and CO2 + isopropyl cyclohexane binary mixtures at elevated pressures.* The Journal of Supercritical Fluids, 2008. **44**(2): p. 155-163.
10. Pauly, J.; Coutinho, J. A. P. and Daridon, J.-L. *High pressure phase equilibria in methane + waxy systems: 1. Methane + heptadecane.* Fluid Phase Equilibria, 2007. **255**(2): p. 193-199.
11. Ventura, S. P. M.; Pauly, J.; Daridon, J. L.; Lopes da Silva, J. A.; Marrucho, I. M.; Dias, A. M. A. and Coutinho, J. A. P. *High pressure solubility data of carbon dioxide in (tri- iso-butyl(methyl)phosphonium tosylate + water) systems.* The Journal of Chemical Thermodynamics, 2008. **40**(8): p. 1187-1192.
12. Dias, A. M. A.; Carrier, H.; Daridon, J. L.; Pàmies, J. C.; Vega, L. F.; Coutinho, J. A. P. and Marrucho, I. M. *Vapor−Liquid Equilibrium of Carbon Dioxide−Perfluoroalkane Mixtures: Experimental Data and SAFT Modeling.* Industrial & Engineering Chemistry Research, 2006. **45**(7): p. 2341-2350.
13. Ventura, S. P. M.; Pauly, J.; Daridon, J. L.; Marrucho, I. M.; Dias, A. M. A. and Coutinho, J. A. P. *High-Pressure Solubility Data of Methane in Aniline and Aqueous Aniline Systems.* Journal of Chemical & Engineering Data, 2007. **52**(3): p. 1100-1102.
14. Revelli, A.-L.; Mutelet, F. and Jaubert, J.-N. l. *Reducing of Nitrous Oxide Emissions Using Ionic Liquids.* The Journal of Physical Chemistry B, 2010. **114**(24): p. 8199-8206.
15. Revelli, A.-L.; Mutelet, F. and Jaubert, J.-N. l. *High Carbon Dioxide Solubilities in Imidazolium-Based Ionic Liquids and in Poly(ethylene glycol) Dimethyl Ether.* The Journal of Physical Chemistry B, 2010. **114**(40): p. 12908-12913.
16. Shiflett, M. B.; Niehaus, A. M. S. and Yokozeki, A. *Separation of N2O and CO2 using room-temperature ionic liquid [bmim][BF4].* Journal of Physical Chemistry B, 2011. **115**(13): p. 3478-3487.
17. Shiflett, M. B. and Yokozeki, A. *Solubilities and Diffusivities of Carbon Dioxide in Ionic Liquids: [bmim][PF6] and [bmim][BF4].* Industrial & Engineering Chemistry Research, 2005. **44**(12): p. 4453-4464.

18. Shiflett, M.; Niehaus, A.; Elliott, B. and Yokozeki, A. *Phase Behavior of N2O and CO2 in Room-Temperature Ionic Liquids [bmim][Tf2N], [bmim][BF4], [bmim][N(CN)2], [bmim][Ac], [eam][NO3], and [bmim][SCN].* International Journal of Thermophysics, 2011: p. 1-25.
19. Lee, B.-C. and Outcalt, S. L. *Solubilities of Gases in the Ionic Liquid 1-n-Butyl-3-methylimidazolium Bis(trifluoromethylsulfonyl)imide.* Journal of Chemical & Engineering Data, 2006. **51**(3): p. 892-897.
20. Carvalho, P. J.; Álvarez, V. H.; Marrucho, I. M.; Aznar, M. and Coutinho, J. A. P. *High pressure phase behavior of carbon dioxide in 1-butyl-3-methylimidazolium bis(trifluoromethylsulfonyl)imide and 1-butyl-3-methylimidazolium dicyanamide ionic liquids.* The Journal of Supercritical Fluids, 2009. **50**(2): p. 105-111.
21. Blas, F. J. and Vega, L. F. *Prediction of Binary and Ternary Diagrams Using the Statistical Associating Fluid Theory (SAFT) Equation of State.* Industrial & Engineering Chemistry Research, 1998. **37**(2): p. 660-674.
22. Andreu, J. S. and Vega, L. F. *Capturing the Solubility Behavior of CO2 in Ionic Liquids by a Simple Model.* The Journal of Physical Chemistry C, 2007. **111**(43): p. 16028-16034.
23. Andreu, J. S. and Vega, L. F. *Modeling the Solubility Behavior of CO2, H2, and Xe in [Cn-mim][Tf2N] Ionic Liquids.* The Journal of Physical Chemistry B, 2008. **112**(48): p. 15398-15406.
24. Llovell, F.; Valente, E.; Vilaseca, O. and Vega, L. F. *Modeling Complex Associating Mixtures with [Cn-mim][Tf2N] Ionic Liquids: Predictions from the Soft-SAFT Equation.* The Journal of Physical Chemistry B, 2011. **115**(15): p. 4387-4398.
25. Llovell, F.; Marcos, R. M.; MacDowell, N. and Vega, L. F. *Modeling the Absorption of Weak Electrolytes and Acid Gases with Ionic Liquids Using the Soft-SAFT Approach.* The Journal of Physical Chemistry B, 2012.
26. Pàmies, J. C. and Vega, L. F. *Vapor−Liquid Equilibria and Critical Behavior of Heavy n-Alkanes Using Transferable Parameters from the Soft-SAFT Equation of State.* Industrial & Engineering Chemistry Research, 2001. **40**(11): p. 2532-2543.
27. Pedrosa, N.; Pàmies, J. C.; Coutinho, J. A. P.; Marrucho, I. M. and Vega, L. F. *Phase Equilibria of Ethylene Glycol Oligomers and Their Mixtures.* Industrial & Engineering Chemistry Research, 2005. **44**(17): p. 7027-7037.
28. Dässler, H.-G. and S.Börtitz, *Air pollution and its influence on vegetation*. 1 ed. Vol. 18. 1988: Springer. Chapter 1.
29. Baumbach, G., *Air Quality Control.*1996: Spinger. Chapter 2.
30. Jacob, D. J., *Introduction to Atmospheric Chemistry,* 1999: Princeton University Press. Chapter 1.
31. Herman, A. *Ambient Air Pollution and Adverse Health Effects.* Procedia - Social and Behavioral Sciences, 2010. **2**(5): p. 7333-7338.
32. World Health Organization, *The world health report 2002: Reducing risks, promoting healthy life.* 2002. Available from: http://www.who.int/whr/2002/en/.
33. Williams, M. *Air pollution and policy—1952–2002.* Science of The Total Environment, 2004. **334-335**(0): p. 15-20.
34. Samet, J. M.; Scott, L. Z. and Francesca, D. *National Morbidity, Mortality, and Air Pollution Study. Part II: Morbidity and Mortality from Air Pollution in the United States.* Health Effects Institute, 2000.
35. Romieu, I.; Samet, J. M.; Smith, K. R. and Bruce, N. *Outdoor air pollution and acute respiratory infections among children in developing countries.* Journal of occupational and environmental medicine / American College of Occupational and Environmental Medicine, 2002. **44**(7): p. 640-9.
36. Janssen, N. A. H.; Brunekreef, B.; van Vliet, P.; Aarts, F.; Meliefste, K.; Harssema, H. and Fischer, P. *The Relationship between Air Pollution from Heavy Traffic and Allergic*

Sensitization, Bronchial Hyperresponsiveness, and Respiratory Symptoms in Dutch Schoolchildren. Environmental Health Perspectives, 2003. **111**(12).

37. Nafstad, P.; Håheim, L. L.; Oftedal, B.; Gram, F.; Holme, I.; Hjermann, I. and Leren, P. *Lung cancer and air pollution: a 27 year follow up of 16 209 Norwegian men.* Thorax, 2003. **58**(12): p. 1071-1076.
38. Dadvand, P.; Rankin, J.; Rushton, S. and Pless-Mulloli, T. *Ambient air pollution and congenital heart disease: A register-based study.* Environmental Research, 2011. **111**(3): p. 435-441.
39. Per, E. and Christer, Å., *Air and the Environment,* 2004: The Swedish NGO Secretariat on Acid Rain. Chapter 3.
40. Schnelle, K. B. and Brown, C. A., *Air Pollution Control Technology Handbook*, 2002, CRC Press LLC. p. Chapter 2 and 17.
41. Davis, W. T., *Air Pollution Engineering Manual*. Second edition ed. Air & Waste Management Association2000: John Wiley & Sons.
42. *U.S Code of federal Regulations.* , 2001, U.S government Printing office: Washington.
43. Srivastava, R. K.; Nueffer, W.; Grano, D.; Khan, S.; Staudt, J. E. and Jozewicz, W. *Controlling NOx emission from industrial sources.* Environmental Progress, 2005. **24**(2): p. 181-197.
44. European Environment Agency, *Air Quality in Europe.* 2011. Available from: http://www.eea.europa.eu/publications/air-quality-in-europe-2011.
45. Ravishankara, A. R.; Daniel, J. S. and Portmann, R. W. *Nitrous oxide (N2O): the dominant ozone-depleting substance emitted in the 21st century.* Science (New York, N.Y.), 2009. **326**(5949): p. 123-5.
46. Pérez-Ramírez, J.; Kapteijn, F.; Schöffel, K. and Moulijn, J. A. *Formation and control of N2O in nitric acid production: Where do we stand today?* Applied Catalysis B: Environmental, 2003. **44**(2): p. 117-151.
47. Galle, M.; Agar, D. W. and Watzenberger, O. *Thermal N2O decomposition in regenerative heat exchanger reactors.* Chemical Engineering Science, 2001. **56**(4): p. 1587-1595.
48. U.S. Energy Information Administration, *Annual Energy Outlook 2012.* 2012. Available from: http://www.eia.gov/forecasts/aeo/er/pdf/0383er(2012).pdf.
49. Plechkova, N. V. and Seddon, K. R. *Applications of ionic liquids in the chemical industry.* Chemical Society Reviews, 2008. **37**(1): p. 123-150.
50. Walden, P. Bulletin of the Imperial Academy of Sciences in Saint Petersburg, 1914. **8**: p. 405-422.
51. Graenacher, C., *Cellulose solution*, 1934: US Pat.
52. Seddon, K. R. *Ionic Liquids for Clean Technology.* Journal of Chemical Technology & Biotechnology, 1997. **68**(4): p. 351-356.
53. Gardas, R. L. and Coutinho, J. A. P. *Group contribution methods for the prediction of thermophysical and transport properties of ionic liquids.* AIChE Journal, 2009. **55**(5): p. 1274-1290.
54. Domanska, U. *Solubilities and thermophysical properties of ionic liquids.* Pure and Applied Chemistry, 2005. **77**(3): p. 543-557.
55. Gardas, R. L. and Coutinho, J. A. P. *A Group Contribution Method for Heat Capacity Estimation of Ionic Liquids.* Industrial & Engineering Chemistry Research, 2008. **47**(15): p. 5751-5757.
56. Zhang, J.; Zhang, Q.; Qiao, B. and Deng, Y. *Solubilities of the Gaseous and Liquid Solutes and Their Thermodynamics of Solubilization in the Novel Room-Temperature Ionic Liquids at Infinite Dilution by Gas Chromatography.* Journal of Chemical & Engineering Data, 2007. **52**(6): p. 2277-2283.

57. Hu, Y.-F.; Liu, Z.-C.; Xu, C.-M. and Zhang, X.-M. *The molecular characteristics dominating the solubility of gases in ionic liquids.* Chemical Society Reviews, 2011. **40**(7): p. 3802-3823.
58. Rogers, R. D. and Seddon, K. R. *Ionic Liquids--Solvents of the Future?* Science, 2003. **302**(5646): p. 792-793.
59. Marsh, K. N.; Boxall, J. A. and Lichtenthaler, R. *Room temperature ionic liquids and their mixtures—a review.* Fluid Phase Equilibria, 2004. **219**(1): p. 93-98.
60. Chiappe, C. and Pieraccini, D. *Ionic liquids: solvent properties and organic reactivity.* Journal of Physical Organic Chemistry, 2005. **18**(4): p. 275-297.
61. Cull, S. G.; Holbrey, J. D.; Vargas-Mora, V.; Seddon, K. R. and Lye, G. J. *Room-temperature ionic liquids as replacements for organic solvents in multiphase bioprocess operations.* Biotechnology and Bioengineering, 2000. **69**(2): p. 227-233.
62. Ding, J.; Welton, T. and Armstrong, D. W. *Chiral Ionic Liquids as Stationary Phases in Gas Chromatography.* Analytical Chemistry, 2004. **76**(22): p. 6819-6822.
63. Mank, M.; Stahl, B. and Boehm, G. *2,5-Dihydroxybenzoic Acid Butylamine and Other Ionic Liquid Matrixes for Enhanced MALDI-MS Analysis of Biomolecules.* Analytical Chemistry, 2004. **76**(10): p. 2938-2950.
64. Brennecke, J. F. and Maginn, E. J. *Ionic liquids: Innovative fluids for chemical processing.* AIChE Journal, 2001. **47**(11): p. 2384-2389.
65. Kuang, D.; Comte, P.; Zakeeruddin, S. M.; Hagberg, D. P.; Karlsson, K. M.; Sun, L.; Nazeeruddin, M. K. and Grätzel, M. *Stable dye-sensitized solar cells based on organic chromophores and ionic liquid electrolyte.* Solar Energy, 2011. **85**(6): p. 1189-1194.
66. Ventura, S. P. M.; Neves, C. M. S. S.; Freire, M. G.; Marrucho, I. M.; Oliveira, J. and Coutinho, J. A. P. *Evaluation of Anion Influence on the Formation and Extraction Capacity of Ionic-Liquid-Based Aqueous Biphasic Systems.* The Journal of Physical Chemistry B, 2009. **113**(27): p. 9304-9310.
67. Welton, T. *Room-Temperature Ionic Liquids. Solvents for Synthesis and Catalysis.* Chemical Reviews, 1999. **99**(8): p. 2071-2084.
68. Wasserscheid, P. and Keim, W. *Ionic Liquids-New "Solutions" for Transition Metal Catalysis.* Angewandte Chemie (International ed. in English), 2000. **39**(21): p. 3772-3789.
69. Dupont, J.; de Souza, R. F. and Suarez, P. A. Z. *Ionic Liquid (Molten Salt) Phase Organometallic Catalysis.* Chemical Reviews, 2002. **102**(10): p. 3667-3692.
70. Visser, A. E.; Swatloski, R. P.; Reichert, W. M.; Mayton, R.; Sheff, S.; Wierzbicki, A.; Davis, J. J. H. and Rogers, R. D. *Task-specific ionic liquids for the extraction of metal ions from aqueous solutions.* Chemical Communications, 2001(1): p. 135-136.
71. Holbrey, J. D.; Visser, A. E.; Spear, S. K.; Reichert, W. M.; Swatloski, R. P.; Broker, G. A. and Rogers, R. D. *Mercury(ii) partitioning from aqueous solutions with a new, hydrophobic ethylene-glycol functionalized bis-imidazolium ionic liquid.* Green Chemistry, 2003. **5**(2): p. 129-135.
72. Bosmann, A.; Datsevich, L.; Jess, A.; Lauter, A.; Schmitz, C. and Wasserscheid, P. *Deep desulfurization of diesel fuel by extraction with ionic liquids.* Chemical Communications, 2001(23): p. 2494-2495.
73. Branco, L. C.; Crespo, J. G. and Afonso, C. A. M. *Highly Selective Transport of Organic Compounds by Using Supported Liquid Membranes Based on Ionic Liquids.* Angewandte Chemie International Edition, 2002. **41**(15): p. 2771-2773.
74. Aki, S. N. V. K.; Mellein, B. R.; Saurer, E. M. and Brennecke, J. F. *High-Pressure Phase Behavior of Carbon Dioxide with Imidazolium-Based Ionic Liquids.* The Journal of Physical Chemistry B, 2004. **108**(52): p. 20355-20365.

75. Cadena, C.; Anthony, J. L.; Shah, J. K.; Morrow, T. I.; Brennecke, J. F. and Maginn, E. J. *Why Is CO2 So Soluble in Imidazolium-Based Ionic Liquids?* Journal of the American Chemical Society, 2004. **126**(16): p. 5300-5308.
76. Jacquemin, J.; Costa Gomes, M. F.; Husson, P. and Majer, V. *Solubility of carbon dioxide, ethane, methane, oxygen, nitrogen, hydrogen, argon, and carbon monoxide in 1-butyl-3-methylimidazolium tetrafluoroborate between temperatures 283 K and 343 K and at pressures close to atmospheric.* The Journal of Chemical Thermodynamics, 2006. **38**(4): p. 490-502.
77. Jacquemin, J.; Husson, P.; Majer, V. and Costa Gomes, M. *Influence of the Cation on the Solubility of CO2 and H2 in Ionic Liquids Based on the Bis(trifluoromethylsulfonyl)imide Anion.* Journal of Solution Chemistry, 2007. **36**(8): p. 967-979.
78. Muldoon, M. J.; Aki, S. N. V. K.; Anderson, J. L.; Dixon, J. K. and Brennecke, J. F. *Improving Carbon Dioxide Solubility in Ionic Liquids.* The Journal of Physical Chemistry B, 2007. **111**(30): p. 9001-9009.
79. Shariati, A. and Peters, C. J. *High-pressure phase equilibria of systems with ionic liquids.* The Journal of Supercritical Fluids, 2005. **34**(2): p. 171-176.
80. Shiflett, M. B.; Drew, D. W.; Cantini, R. A. and Yokozeki, A. *Carbon Dioxide Capture Using Ionic Liquid 1-Butyl-3-methylimidazolium Acetate.* Energy & Fuels, 2010. **24**(10): p. 5781-5789.
81. Wappel, D.; Gronald, G.; Kalb, R. and Draxler, J. *Ionic liquids for post-combustion CO2 absorption.* International Journal of Greenhouse Gas Control, 2010. **4**(3): p. 486-494.
82. Shiflett, M. B. and Yokozeki, A. *Solubility of CO2 in Room Temperature Ionic Liquid [hmim][Tf2N].* The Journal of Physical Chemistry B, 2007. **111**(8): p. 2070-2074.
83. Jalili, A. H.; Mehdizadeh, A.; Shokouhi, M.; Ahmadi, A. N.; Hosseini-Jenab, M. and Fateminassab, F. *Solubility and diffusion of CO2 and H2S in the ionic liquid 1-ethyl-3-methylimidazolium ethylsulfate.* The Journal of Chemical Thermodynamics, 2010. **42**(10): p. 1298-1303.
84. Anderson, J. L.; Dixon, J. K. and Brennecke, J. F. *Solubility of CO2, CH4, C2H6, C2H4, O2, and N2 in 1-Hexyl-3-methylpyridinium Bis(trifluoromethylsulfonyl)imide: Comparison to Other Ionic Liquids.* Accounts of Chemical Research, 2007. **40**(11): p. 1208-1216.
85. Finotello, A.; Bara, J. E.; Camper, D. and Noble, R. D. *Room-Temperature Ionic Liquids: Temperature Dependence of Gas Solubility Selectivity.* Industrial & Engineering Chemistry Research, 2008. **47**(10): p. 3453-3459.
86. Finotello, A.; Bara, J. E.; Narayan, S.; Camper, D. and Noble, R. D. *Ideal Gas Solubilities and Solubility Selectivities in a Binary Mixture of Room-Temperature Ionic Liquids.* The Journal of Physical Chemistry B, 2008. **112**(8): p. 2335-2339.
87. Yuan, X.; Zhang, S.; Chen, Y.; Lu, X.; Dai, W. and Mori, R. *Solubilities of Gases in 1,1,3,3-Tetramethylguanidium Lactate at Elevated Pressures.* Journal of Chemical & Engineering Data, 2006. **51**(2): p. 645-647.
88. Hert, D. G.; Anderson, J. L.; Aki, S. N. V. K. and Brennecke, J. F. *Enhancement of oxygen and methane solubility in 1-hexyl-3-methylimidazolium bis(trifluoromethylsulfonyl) imide using carbon dioxide.* Chemical Communications, 2005(20): p. 2603-2605.
89. Rahmati-Rostami, M.; Ghotbi, C.; Hosseini-Jenab, M.; Ahmadi, A. N. and Jalili, A. H. *Solubility of H2S in ionic liquids [hmim][PF6], [hmim][BF4], and [hmim][Tf2N].* The Journal of Chemical Thermodynamics, 2009. **41**(9): p. 1052-1055.
90. Anderson, J. L.; Dixon, J. K.; Maginn, E. J. and Brennecke, J. F. *Measurement of SO2 Solubility in Ionic Liquids.* The Journal of Physical Chemistry B, 2006. **110**(31): p. 15059-15062.

91. Kumełan, J.; Pérez-Salado Kamps, Á.; Tuma, D. and Maurer, G. *Solubility of the single gases H2 and CO in the ionic liquid [bmim][CH3SO4].* Fluid Phase Equilibria, 2007. **260**(1): p. 3-8.
92. Shaharun, M. S.; Mukhtar, H. and Dutta, B. K. *Solubility of carbon monoxide and hydrogen in propylene carbonate and thermomorphic multicomponent hydroformylation solvent.* Chemical Engineering Science, 2008. **63**(11): p. 3024-3035.
93. Kumełan, J.; Kamps, Á. P.-S.; Tuma, D. and Maurer, G. *Solubility of CO in the ionic liquid [bmim][PF6].* Fluid Phase Equilibria, 2005. **228-229**(0): p. 207-211.
94. Vega, L. F.; Vilaseca, O.; Llovell, F. and Andreu, J. S. *Modeling ionic liquids and the solubility of gases in them: Recent advances and perspectives.* Fluid Phase Equilibria, 2010. **294**(1-2): p. 15-30.
95. Vega, L. F.; Vilaseca, O.; Valente, E.; Andreu, J. S.; Llovell, F. and Marcos, R. M., *Using Molecular Modelling Tools to Understand the Thermodynamic Behaviour of Ionic Liquids*, in *Ionic Liquids: Theory, Properties, New Approaches*, A. Kokorin, Editor 2011.
96. Arce, P. F.; Robles, P. A.; Graber, T. A. and Aznar, M. *Modeling of high-pressure vapor–liquid equilibrium in ionic liquids + gas systems using the PRSV equation of state.* Fluid Phase Equilibria, 2010. **295**(1): p. 9-16.
97. Chapman, W. G.; Gubbins, K. E.; Jackson, G. and Radosz, M. *SAFT: Equation-of-state solution model for associating fluids.* Fluid Phase Equilibria, 1989. **52**(0): p. 31-38.
98. Chapman, W. G.; Gubbins, K. E.; Jackson, G. and Radosz, M. *New reference equation of state for associating liquids.* Industrial & Engineering Chemistry Research, 1990. **29**(8): p. 1709-1721.
99. Chapman, W. G.; Jackson, G. and Gubbins, K. E. *Phase equilibria of associating fluids.* Molecular Physics, 1988. **65**(5): p. 1057-1079.
100. Huang, S. H. and Radosz, M. *Equation of state for small, large, polydisperse, and associating molecules.* Industrial & Engineering Chemistry Research, 1990. **29**(11): p. 2284-2294.
101. Wertheim, M. S. *Fluids with highly directional attractive forces. I. Statistical thermodynamics.* Journal of Statistical Physics, 1984. **35**(1): p. 19-34.
102. Wertheim, M. S. *Fluids with highly directional attractive forces. II. Thermodynamic perturbation theory and integral equations.* Journal of Statistical Physics, 1984. **35**(1): p. 35-47.
103. Wertheim, M. S. *Fluids with highly directional attractive forces. III. Multiple attraction sites.* Journal of Statistical Physics, 1986. **42**(3): p. 459-476.
104. Wertheim, M. S. *Fluids with highly directional attractive forces. IV. Equilibrium polymerization.* Journal of Statistical Physics, 1986. **42**(3): p. 477-492.
105. Felipe J, B. and Lourdes F, V. *Thermodynamic behaviour of homonuclear and heteronuclear Lennard-Jones chains with association sites from simulation and theory.* Molecular Physics, 1997. **92**(1): p. 135-150.
106. Blas, F. J. and Vega, L. F. *Critical behavior and partial miscibility phenomena in binary mixtures of hydrocarbons by the statistical associating fluid theory.* Journal of Chemical Physics, 1998. **109**: p. 7405-7413.
107. Johnson, J. K.; Zollweg, J. A. and Gubbins, K. E. *The Lennard-Jones equation of state revisited.* Molecular Physics, 1993. **78**(3): p. 591-618.
108. Hansen, J. P. and McDonald, I. R., *Theory of simple liquids*: London Academic Press.
109. Pedrosa, N.; Vega, L. F.; Coutinho, J. A. P. and Marrucho, I. M. *Modeling the Phase Equilibria of Poly(ethylene glycol) Binary Mixtures with soft-SAFT EoS.* Industrial & Engineering Chemistry Research, 2007. **46**(13): p. 4678-4685.
110. Chetty, N. and Couling, V. W. *Measurement of the electric quadrupole moment of N2O.* Journal of Chemical Physics, 2011. **134**: p. 144307.

111. Leung, H. O. *The rotational spectrum and nuclear quadrupole hyperfine structure of CO2–N2O.* Journal of Chemical Physics, 1998. **108**(10): p. 3955-3961.
112. Press, W. H.; Teulosky, S. A.; Vetterling, W. T. and Flannery, B. P. *Numerical Recipes In Frontan.* Cambrige University Press: Cambridge, U.K., 1986.
113. Blas, F. J. and Vega, L. F. *Improved vapor–liquid equilibria predictions for Lennard-Jones chains from the statistical associating fluid dimer theory: Comparison with Monte Carlo simulations.* Journal of Chemical Physics, 2001. **115**(4355).
114. Pàmies, J. C., 2003, Thesis, Universitat Rovira i Virgili, Tarragona: Spain.
115. Seddon Kenneth, R.; Stark, A. and Torres, M.-J., *Viscosity and Density of 1-Alkyl-3-methylimidazolium Ionic Liquids*, in *Clean Solvents*2002, American Chemical Society. p. 34-49.
116. Jacquemin, J.; Husson, P.; Padua, A. A. H. and Majer, V. *Density and viscosity of several pure and water-saturated ionic liquids.* Green Chemistry, 2006. **8**(2): p. 172-180.
117. Tariq, M.; Serro, A. P.; Mata, J. L.; Saramago, B.; Esperança, J. M. S. S.; Canongia Lopes, J. N. and Rebelo, L. P. N. *High-temperature surface tension and density measurements of 1-alkyl-3-methylimidazolium bistriflamide ionic liquids.* Fluid Phase Equilibria, 2010. **294**(1–2): p. 131-138.
118. Gardas, R. L.; Freire, M. G.; Carvalho, P. J.; Marrucho, I. M.; Fonseca, I. M. A.; Ferreira, A. G. M. and Coutinho, J. A. P. *High-Pressure Densities and Derived Thermodynamic Properties of Imidazolium-Based Ionic Liquids.* Journal of Chemical & Engineering Data, 2006. **52**(1): p. 80-88.
119. Ab Rani, M. A.; Brant, A.; Crowhurst, L.; Dolan, A.; Lui, M.; Hassan, N. H.; Hallett, J. P.; Hunt, P. A.; Niedermeyer, H.; Perez-Arlandis, J. M.; Schrems, M.; Welton, T. and Wilding, R. *Understanding the polarity of ionic liquids.* Physical Chemistry Chemical Physics, 2011. **13**(37): p. 16831-16840.
120. Lungwitz, R.; Strehmel, V. and Spange, S. *The dipolarity/polarisability of 1-alkyl-3-methylimidazolium ionic liquids as function of anion structure and the alkyl chain length.* New Journal of Chemistry, 2010. **34**(6): p. 1135-1140.
121. Freire, M. G.; Teles, A. R. R.; Rocha, M. A. A.; Schröder, B.; Neves, C. M. S. S.; Carvalho, P. J.; Evtuguin, D. V.; Santos, L. M. N. B. F. and Coutinho, J. A. P. *Thermophysical Characterization of Ionic Liquids Able To Dissolve Biomass.* Journal of Chemical & Engineering Data, 2011. **56**(12): p. 4813-4822.
122. Carvalho, P. J.; Regueira, T.; Santos, L. M. N. B. F.; Fernandez, J. and Coutinho, J. A. P. *Effect of Water on the Viscosities and Densities of 1-Butyl-3-methylimidazolium Dicyanamide and 1-Butyl-3-methylimidazolium Tricyanomethane at Atmospheric Pressure.* Journal of Chemical & Engineering Data, 2009. **55**(2): p. 645-652.
123. Benavides, A. L.; Guevara, Y. and Estrada-Alexanders, A. F. *A theoretical equation of state for real quadrupolar fluids.* The Journal of Chemical Thermodynamics, 2000. **32**(8): p. 945-961.
124. Afeefy, H. Y.; Liebman, J. F. and Stein, S. E. *Neutral Thermochemical Data in NIST Chemistry WebBook,*. NIST Standard Reference Database Number 69 June 2005 Available from: http://webbook.nist.gov/chemistry/.
125. Arce, P. and Aznar, M. *Modeling of critical lines and regions for binary and ternary mixtures using non-cubic and cubic equations of state.* The Journal of Supercritical Fluids, 2007. **42**(1): p. 1-26.
126. Freire, M. G.; Carvalho, P. J.; Fernandes, A. M.; Marrucho, I. M.; Queimada, A. J. and Coutinho, J. A. P. *Surface tensions of imidazolium based ionic liquids: Anion, cation, temperature and water effect.* Journal of Colloid and Interface Science, 2007. **314**(2): p. 621-630.

127. Huddleston, J. G.; Visser, A. E.; Reichert, W. M.; Willauer, H. D.; Broker, G. A. and Rogers, R. D. *Characterization and comparison of hydrophilic and hydrophobic room temperature ionic liquids incorporating the imidazolium cation.* Green Chemistry, 2001. **3**(4): p. 156-164.
128. Seddon, K. R.; Stark, A. and Torres, M.-J. *Influence of chloride, water, and organic solvents on the physical properties of ionic liquids.* Pure and Applied Chemistry, 2000. **72**(12): p. 2275-2287.
129. Carvalho, P. J.; Álvarez, V. H.; Machado, J. J. B.; Pauly, J.; Daridon, J.-L.; Marrucho, I. M.; Aznar, M. and Coutinho, J. A. P. *High pressure phase behavior of carbon dioxide in 1-alkyl-3-methylimidazolium bis(trifluoromethylsulfonyl)imide ionic liquids.* The Journal of Supercritical Fluids, 2009. **48**(2): p. 99-107.
130. Carvalho, P. J.; Álvarez, V. H.; Marrucho, I. M.; Aznar, M. and Coutinho, J. A. P. *High carbon dioxide solubilities in trihexyltetradecylphosphonium-based ionic liquids.* The Journal of Supercritical Fluids, 2010. **52**(3): p. 258-265.
131. Carvalho, P. J.; Ferreira, A. R.; Oliveira, M. B.; Besnard, M.; Cabaço, M. I. and Coutinho, J. A. P. *High Pressure Phase Behavior of Carbon Dioxide in Carbon Disulfide and Carbon Tetrachloride.* Journal of Chemical & Engineering Data, 2011. **56**(6): p. 2786-2792.
132. Mattedi, S.; Carvalho, P. J.; Coutinho, J. A. P.; Alvarez, V. H. and Iglesias, M. *High pressure CO2 solubility in N-methyl-2-hydroxyethylammonium protic ionic liquids.* The Journal of Supercritical Fluids, 2011. **56**(3): p. 224-230.
133. Carvalho, P. J.; Álvarez, V. H.; Schröder, B.; Gil, A. M.; Marrucho, I. M.; Aznar, M.; Santos, L. M. N. B. F. and Coutinho, J. A. P. *Specific Solvation Interactions of CO2 on Acetate and Trifluoroacetate Imidazolium Based Ionic Liquids at High Pressures.* The Journal of Physical Chemistry B, 2009. **113**(19): p. 6803-6812.
134. Kumełan, J.; Pérez-Salado Kamps, Á.; Tuma, D. and Maurer, G. *Solubility of H2 in the Ionic Liquid [bmim][PF6].* Journal of Chemical & Engineering Data, 2006. **51**(1): p. 11-14.
135. Kumełan, J.; Pérez-Salado Kamps, Á.; Tuma, D. and Maurer, G. *Solubility of H2 in the Ionic Liquid [hmim][Tf2N].* Journal of Chemical & Engineering Data, 2006. **51**(4): p. 1364-1367.
136. Rao, A. B. and Rubin, E. S. *A Technical, Economic, and Environmental Assessment of Amine-Based CO2 Capture Technology for Power Plant Greenhouse Gas Control.* Environmental Science & Technology, 2002. **36**(20): p. 4467-4475.
137. McCann, N.; Maeder, M. and Attalla, M. *Simulation of Enthalpy and Capacity of CO2 Absorption by Aqueous Amine Systems.* Industrial & Engineering Chemistry Research, 2008. **47**(6): p. 2002-2009.
138. Abu-Zahra, M. R. M.; Niederer, J. P. M.; Feron, P. H. M. and Versteeg, G. F. *CO2 capture from power plants: Part II. A parametric study of the economical performance based on mono-ethanolamine.* International Journal of Greenhouse Gas Control, 2007. **1**(2): p. 135-142.
139. Freguia, S. and Rochelle, G. T. *Modeling of CO2 capture by aqueous monoethanolamine.* AIChE Journal, 2003. **49**(7): p. 1676-1686.
140. Zhang, Y.; Chen, H.; Chen, C.-C.; Plaza, J. M.; Dugas, R. and Rochelle, G. T. *Rate-Based Process Modeling Study of CO2 Capture with Aqueous Monoethanolamine Solution.* Industrial & Engineering Chemistry Research, 2009. **48**(20): p. 9233-9246.
141. Perry, R. J. and Davis, J. L. *CO2 Capture Using Solutions of Alkanolamines and Aminosilicones.* Energy & Fuels, 2012. **26**(4): p. 2512-2517.
142. Perry, R. J.; Wood, B. R.; Genovese, S.; O'Brien, M. J.; Westendorf, T.; Meketa, M. L.; Farnum, R.; McDermott, J.; Sultanova, I.; Perry, T. M.; Vipperla, R.-K.; Wichmann, L. A.; Enick, R. M.; Hong, L. and Tapriyal, D. *CO2 Capture Using Phase-Changing Sorbents.* Energy & Fuels, 2012. **26**(4): p. 2528-2538.

143. Aronu, U. E.; Gondal, S.; Hessen, E. T.; Haug-Warberg, T.; Hartono, A.; Hoff, K. A. and Svendsen, H. F. *Solubility of CO2 in 15, 30, 45 and 60 mass% MEA from 40 to 120°C and model representation using the extended UNIQUAC framework.* Chemical Engineering Science, 2011. **66**(24): p. 6393-6406.
144. Manning, F. and Thompson, R., *Oil Field Processing of Petroleum*1991, Tulsa, OK: Penwell Publishing Co
145. Henni, A. and Mather, A. E. *The solubility of CO2 in triethylene glycol monomethyl ether.* The Canadian Journal of Chemical Engineering, 1995. **73**(1): p. 156-158.
146. Henni, A. and Mather, A. E. *Solubility of Nitrous Oxide in Triethylene Glycol Monomethyl Ether at Elevated Pressures.* Journal of Chemical & Engineering Data, 1995. **40**(5): p. 1158-1160.
147. Henni, A.; Tontiwachwuthikul, P. and Chakma, A. *Solubilities of Carbon Dioxide in Polyethylene Glycol Ethers.* The Canadian Journal of Chemical Engineering, 2005. **83**(2): p. 358-361.
148. Penttilä, A.; Dell'Era, C.; Uusi-Kyyny, P. and Alopaeus, V. *The Henry's law constant of N2O and CO2 in aqueous binary and ternary amine solutions (MEA, DEA, DIPA, MDEA, and AMP).* Fluid Phase Equilibria, 2011. **311**(0): p. 59-66.
149. Xu, X.; Zhao, X.; Sun, L. and Liu, X. *Adsorption separation of carbon dioxide, methane and nitrogen on monoethanol amine modified β-zeolite.* Journal of Natural Gas Chemistry, 2009. **18**(2): p. 167-172.
150. Holderbaum, T. and Gmehling, J. *PSRK: A Group Contribution Equation of State Based on UNIFAC.* Fluid Phase Equilibria, 1991. **70**(2–3): p. 251-265.

8- Appendix

Appendix A- Atmospheric Nitrogen Cycle

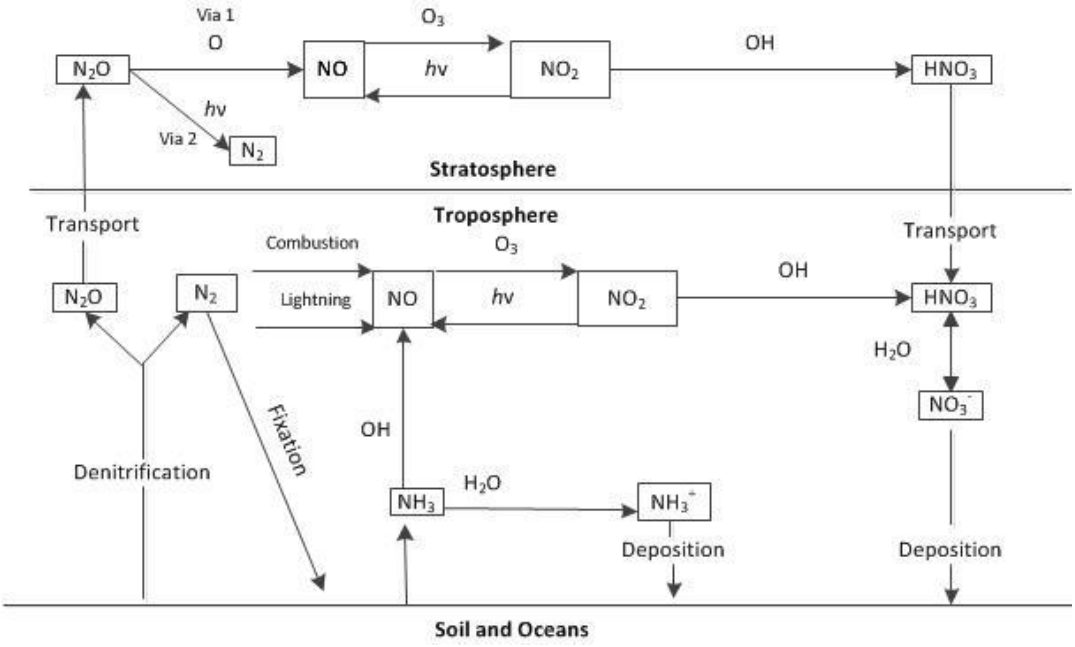

Figure 8.1- Diagram of the Atmospheric nitrogen cycle, adapted from Seinfeld *et al.*[1]

Appendix B- Adjusted Molecular Parameters for N_2O

Table 8.1- Full list of adjusted molecular parameters for N_2O.

Set	*m*	*σ* (Å)	*ε/k_B* (K)	*x_p*	*Q* (10^{-40} C m^2)	*Q_{exp}* [a] (10^{-40} C m^2)	*%AAD P* (%)	*%AAD D* (%)
1	1.272	3.520	166.18	½	5.00	10.00	7.70	1.70
2 [b]	1.197	3.612	167.42	½	5.50	11.00	7.65	1.73
3 [b]	1.130	3.699	168.83	½	6.00	12.00	7.55	1.76
4	1.111	3.725	169.26	½	6.15	12.30	7.51	1.76
5 [b]	1.751	3.078	159.90	⅓	3.67	11.01	7.07	1.39
6 [b]	1.656	3.153	159.83	⅓	4.10	12.30	7.29	1.51
7 [b]	1.415	3.306	190.43	⅓	4.10	12.30	0.77	2.64
8	1.579	3.219	159.54	⅓	4.50	13.50	7.44	1.53
9	1.333	3.402	185.00	⅓	5.00	15.00	1.39	2.16
10 [b]	1.490	3.300	159.44	⅓	5.00	15.00	7.55	1.60
11	1.411	3.378	159.42	⅓	5.50	16.50	7.61	1.65
12	1.341	3.453	159.48	⅓	6.00	18.00	7.62	1.69
13 [b]	1.655	3.105	192.48	-	-	-	6.73	2.91
14 [b]	2.484	2.646	158.82	-	-	-	4.54	0.98
15	1.570	3.168	197.69	-	-	-	7.29	3.21

[a] Q_{exp} is calculated using Eq. 1.9 in section 1.7

[b] Best suitable molecular parameters for N_2O

Appendix C- IL and Gas Mass, Experimental Bubble Point Data and Soft-SAFT EoS Binary Parameters

Table 8.2- Bubble point data and IL and gas mass of the system CO_2 + [C_2mim][CH_3OHPO_2].

x_{CO_2}	T (K)	p (Mpa)	x_{CO_2}	T (K)	p (Mpa)	x_{CO_2}	T (K)	p (Mpa)
$m_{g/s}$=0.423 $mol_{CO2}.Kg_{IL}^{-1}$			$m_{g/s}$ =0.795 $mol_{CO2}.Kg_{IL}^{-1}$			$m_{g/s}$ =1.861$mol_{CO2}.Kg_{IL}^{-1}$		
	293.21	1.16		293.29	1.88		293.16	3.42
	303.41	1.46		303.15	2.24		303.41	4.19
	313.45	1.76		313.46	2.45		313.52	5.08
0.080	323.40	1.99	0.141	323.43	3.05	0.277	323.39	6.08
	333.29	2.31		333.46	3.56		333.32	7.21
	343.28	2.56		343.35	4.17		343.18	8.41
	353.50	2.85		353.31	4.75		353.33	9.80
	363.45	3.12		363.38	5.36		363.38	11.11
$m_{g/s}$=2.607 $mol_{CO2}.Kg_{IL}^{-1}$			$m_{g/s}$=3.353 $mol_{CO2}.Kg_{IL}^{-1}$			$m_{g/s}$=3.997 $mol_{CO2}.Kg_{IL}^{-1}$		
	293.17	5.21		293.28	6.45		293.32	11.00
	302.90	6.38		303.18	8.45		303.25	17.26
	313.23	7.54		313.18	11.48		313.29	23.51
0.350	323.37	9.32	0.409	323.30	15.91	0.452	323.49	29.82
	333.23	11.27		333.24	20.47		333.53	34.67
	343.34	13.61		343.31	25.13		343.55	40.64
	353.32	16.20		353.46	29.45		353.46	45.99
	363.28	18.92		363.17	33.68		363.43	51.09
$m_{g/s}$=4.932 $mol_{CO2}.Kg_{IL}^{-1}$						m_{IL} (g)	m_{CO2} (g)	
	293.18	31.91						
	303.26	40.79					0.245	
	313.41	49.64					0.460	
0.504	323.31	58.70					1.077	
	333.35	66.69				13.153	1.509	
	343.31	73.43					1.941	
	353.34	80.89					2.314	
	363.32	87.65					2.855	

Table 8.3- Bubble point data and IL and gas mass of the system N_2O + [C_2mim][CH_3OHPO_2].

x_{N_2O}	T (K)	p (Mpa)	x_{N_2O}	T (K)	p (Mpa)	x_{N_2O}	T (K)	p (Mpa)
$m_{g/s}$=0.569 $mol_{N2O}.Kg_{IL}^{-1}$			$m_{g/s}$=0.769 $mol_{N2O}.Kg_{IL}^{-1}$			$m_{g/s}$=1.110 $mol_{N2O}.Kg_{IL}^{-1}$		
0.105	293.35	1.71	0.137	293.42	2.30	0.186	293.40	3.58
	303.37	2.13		303.30	2.88		303.22	4.39
	313.30	2.67		313.30	3.55		313.20	5.35
	323.32	3.22		323.13	4.23		323.34	6.42
	333.14	3.80		333.23	5.00		333.28	7.81
	343.25	4.45		343.25	5.71		343.23	9.04
	353.27	5.25		353.14	6.47		353.29	10.24
	363.40	5.75		363.39	7.32		363.47	11.47
$m_{g/s}$=1.450 $mol_{N2O}.Kg_{IL}^{-1}$			$m_{g/s}$=1.606 $mol_{N2O}.Kg_{IL}^{-1}$			$m_{g/s}$=1.716 $mol_{N2O}.Kg_{IL}^{-1}$		
0.230	293.12	4.73	0.249	293.16	5.40	0.261	293.27	6.01
	303.26	5.93		303.41	6.88		303.19	9.31
	313.26	7.21		313.28	9.10		313.33	12.98
	323.28	8.76		323.23	11.93		323.14	15.95
	333.42	10.54		333.14	14.56		333.16	18.67
	343.18	12.36		343.10	17.08		343.25	21.30
	353.45	14.36		353.28	19.53		353.28	23.73
	363.37	16.23		363.29	21.74		363.24	25.87
$m_{g/s}$=1.819 $mol_{N2O}.Kg_{IL}^{-1}$			$m_{g/s}$=1.897 $mol_{N2O}.Kg_{IL}^{-1}$			$m_{g/s}$=1.946 $mol_{N2O}.Kg_{IL}^{-1}$		
0.273	293.17	11.68	0.281	293.30	17.06	0.286	293.30	21.52
	303.22	15.15		303.26	19.78		303.11	24.18
	313.27	18.11		313.21	22.56		313.27	26.72
	323.30	20.98		323.16	25.15		323.25	29.25
	333.15	23.50		333.14	27.66		333.15	31.06
	343.22	25.95		343.19	30.05		343.16	33.07
	353.22	28.17		353.15	32.21		353.29	35.12
	363.25	30.19		363.11	34.13		363.14	36.99
$m_{g/s}$=2.196 $mol_{N2O}.Kg_{IL}^{-1}$						m_{IL} (g)	m_{N2O} (g)	
0.312	293.25	46.28				13.978	0.350	
	303.31	48.66					0.473	
	313.37	51.26					0.683	
	323.49	52.47					0.892	
	333.24	53.85					0.988	
	343.29	54.85					1.056	
	353.18	56.07					1.119	
	363.40	56.75					1.167	
							1.197	
							1.351	

Table 8.4- Soft-SAFT Eos temperature dependent binary parameters (ξ) used for the system N_2O + [C_2mim][CH_3OHPO_2] at average temperatures (T_a).

T_a (K)	ξ
293.27	0.968
303.27	0.968
313.28	0.968
323.26	0.968
333.21	0.967
343.21	0.966
353.26	0.965
363.31	0.963

Table 8.5- Bubble point data and IL and gas mass of the system CH_4 + [C_2mim][CH_3OHPO_2].

x_{CH_4}	T (K)	p (Mpa)	x_{CH_4}	T (K)	p (Mpa)	x_{CH_4}	T (K)	p (Mpa)
$m_{g/s}$=0.087 $mol_{CH4}.Kg_{IL}^{-1}$			$m_{g/s}$=0.142 $mol_{CH4}.Kg_{IL}^{-1}$			$m_{g/s}$=0.220 $mol_{CH4}.Kg_{IL}^{-1}$		
0.018	293.27	2.67	0.028	293.27	6.57	0.043	293.30	12.54
	303.25	2.93		303.32	6.84		303.38	13.14
	313.25	3.14		313.20	7.22		313.34	13.00
	323.29	3.36		323.22	7.55		323.31	13.12
	333.32	3.51		333.29	7.71		333.18	13.32
	343.25	3.66		343.08	7.94		343.19	13.42
	353.29	3.81		353.30	8.12		353.44	13.59
	363.31	3.86		363.21	8.23		363.43	13.78
$m_{g/s}$=0.274 $mol_{CH4}.Kg_{IL}^{-1}$								
0.054	293.24	17.79						
	303.28	17.81						
	313.22	17.99						
	323.21	17.90						
	333.24	17.79						
	343.31	17.80						
	353.36	17.98						
	363.34	18.02						

m_{IL} (g)	m_{CH4} (g)
13.628	0.019
	0.031
	0.048
	0.060

Table 8.6- Soft-SAFT Eos temperature dependent binary parameters (η) used for the system CH4 + [C_2mim][CH_3OHPO_2] at average temperatures (T_a).

T_a (K)	η
293.27	1.0505
303.31	1.0457
313.25	1.0435
323.26	1.0430
333.26	1.0438
343.21	1.0455
353.35	1.0475
363.32	1.0500

Table 8.7- Bubble point data and IL and gas mass of the system N_2 + [C_2mim][CH_3OHPO_2].

x_{N_2}	T (K)	p (Mpa)	x_{N_2}	T (K)	p (Mpa)	x_{N_2}	T (K)	p (Mpa)
$m_{g/s}$=0.084 $mol_{N2}.Kg_{IL}^{-1}$			$m_{g/s}$=0.107 $mol_{N2}.Kg_{IL}^{-1}$			$m_{g/s}$=0.132 $mol_{N2}.Kg_{IL}^{-1}$		
	293.13	18.89		293.34	33.17		293.25	51.32
	303.13	16.99		303.50	31.12		303.14	46.93
	313.23	16.20		313.26	28.77		313.42	42.77
0.017	323.48	15.67	0.022	323.16	27.54	0.027	323.34	39.80
	333.38	15.29		333.38	26.35		333.26	37.57
	343.46	15.14		343.38	25.10		343.22	35.79
	353.37	14.79		353.32	24.23		353.18	34.54
	363.33	14.33		363.53	23.41		363.19	33.38
$m_{g/s}$=0.155 $mol_{N2}.Kg_{IL}^{-1}$			$m_{g/s}$=0.812 $mol_{N2}.Kg_{IL}^{-1}$			$m_{g/s}$=0.912 $mol_{N2}.Kg_{IL}^{-1}$		
	293.36	61.89		293.18	72.34		293.31	80.51
	303.37	55.20		303.32	64.21		303.24	72.11
	313.26	51.58		313.45	58.11		313.45	65.53
0.031	323.30	48.12	0.035	323.35	53.55	0.040	323.18	60.50
	333.31	45.23		333.32	50.93		333.35	57.12
	343.23	42.72		343.21	47.78		343.32	53.37
	353.34	40.87		353.31	45.32		353.21	50.51
	363.38	38.76		363.35	43.14		363.30	47.96
$m_{g/s}$=1.012 $mol_{N2}.Kg_{IL}^{-1}$						m_{IL} (g)	m_{N2} (g)	
	293.31	89.43						
	303.38	79.25					0.030	
	313.30	71.79					0.038	
0.044	323.22	66.09					0.047	
	333.16	61.41				12.691	0.055	
	343.49	57.98					0.063	
	353.22	55.26					0.071	
	363.28	52.18					0.079	

Table 8.8- Soft-SAFT Eos temperature dependent binary parameters (ξ) used for the system N_2 + [C_2mim][CH_3OHPO_2] at average temperatures (T_a).

T_a (K)	ξ
293.27	0.826
303.30	0.849
313.34	0.860
323.29	0.865
333.31	0.865
343.33	0.865
353.28	0.865
363.34	0.865

Appendix D- Solubility of CO_2 and N_2O in TEGMME

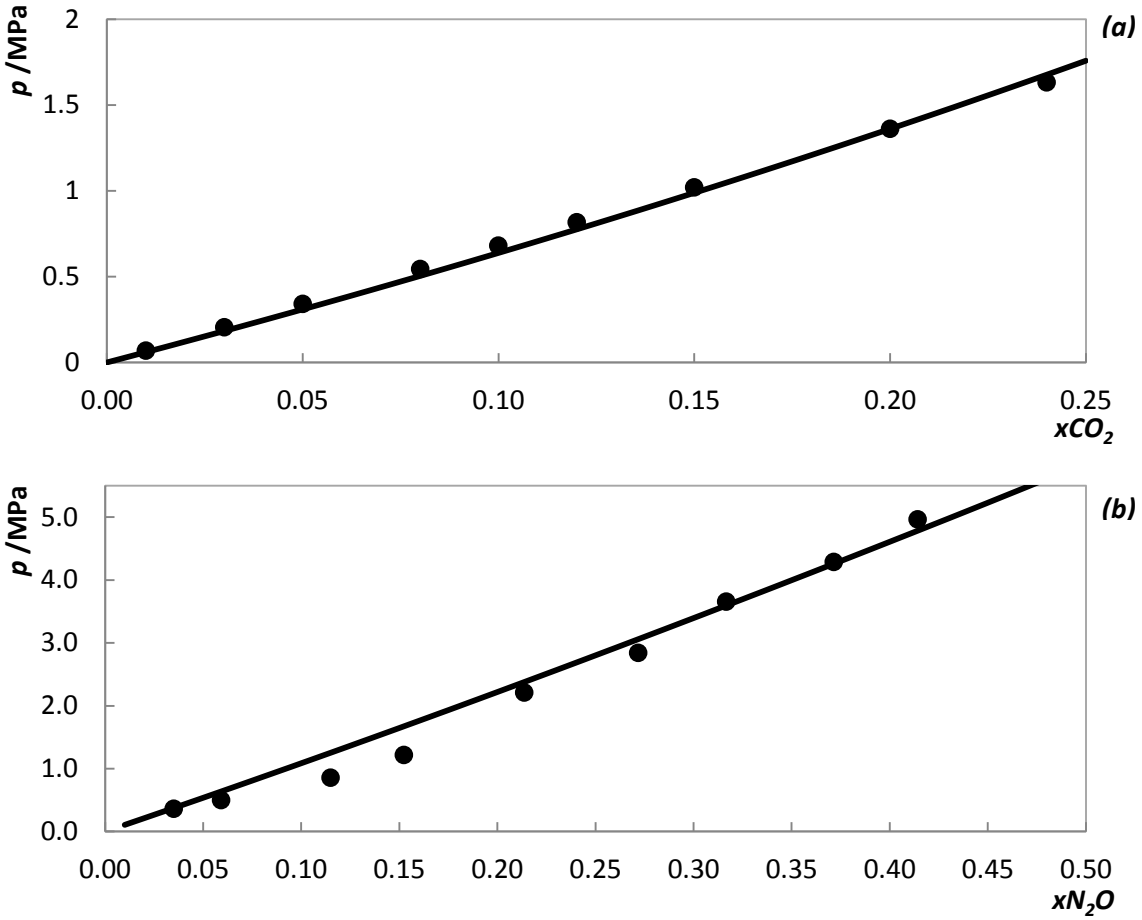

Figure 8.2- ***px*** **diagrams for the systems CO_2** ***(a)*** **and N_2O** ***(b)*** **in TEGMME at 303 K. Solid lines represent PSRK EoS predictions obtained with a commercial simulator (ASPEN Plus 2006.5). N_2O solubility data was taken from the literature,[146] while for CO_2 experimental points were calculated through the Henry's constant reported in Henni *et al.* work's.[147]**

Appendix E- Henry's Constant Calculation

Henry's constants of CO_2, N_2O and N_2 in $[C_2mim][CH_3OHPO_2]$ and N_2 in $[C_4mim][N(CN)_2]$ were determined by adjusting Soft-SAFT EoS to the lowest gas composition experimental data by using specific binary parameters and calculating the limiting slope as solubility approaches zero. The slope was calculated by fitting a linear regression to the soft-SAFT EoS prediction in the dilute region. The results are depicted in Figure 8.3 to Figure 8.6 and the calculated Henry's constants and binary parameters used are listed in Table 8.9 to Table 8.12.

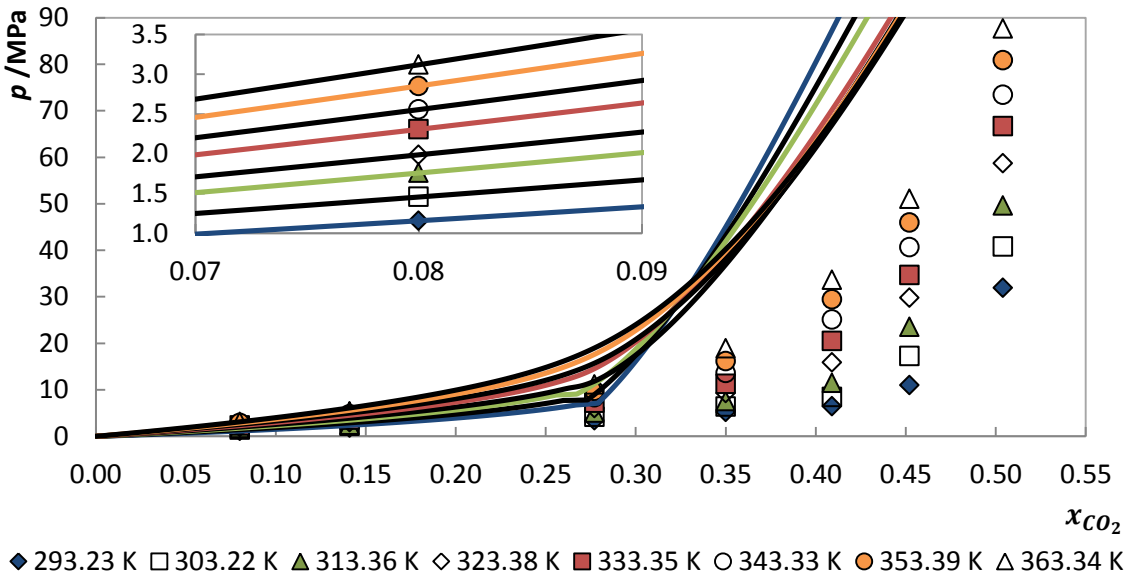

Figure 8.3- *px* diagram for the system CO_2 + $[C_2mim][CH_3OHPO_2]$ at different temperatures. Solid lines represent soft-SAFT EoS prediction adjusted for the lowest gas composition using specifics binary parameters (ξ).

Table 8.9- Calculated Henry's constants of CO_2 in $[C_2mim][CH_3OHPO_2]$ at different temperatures, minimum square error (R^2) obtained in the linear regression adjusted for a gas composition up to 0.05 and binary parameters (ξ) used in the soft-SAFT EoS predictions.

T (K)	*H* (Mpa)	R^2	ξ
293.23	13.62	0.9996	0.9735
303.22	17.21	0.9997	0.9787
313.36	20.96	0.9998	0.9816
323.38	23.76	0.9998	0.9855
333.35	27.60	0.9998	0.9843
343.33	30.57	0.9998	0.9851
353.39	34.16	0.9998	0.9837
363.34	37.28	0.9998	0.9830

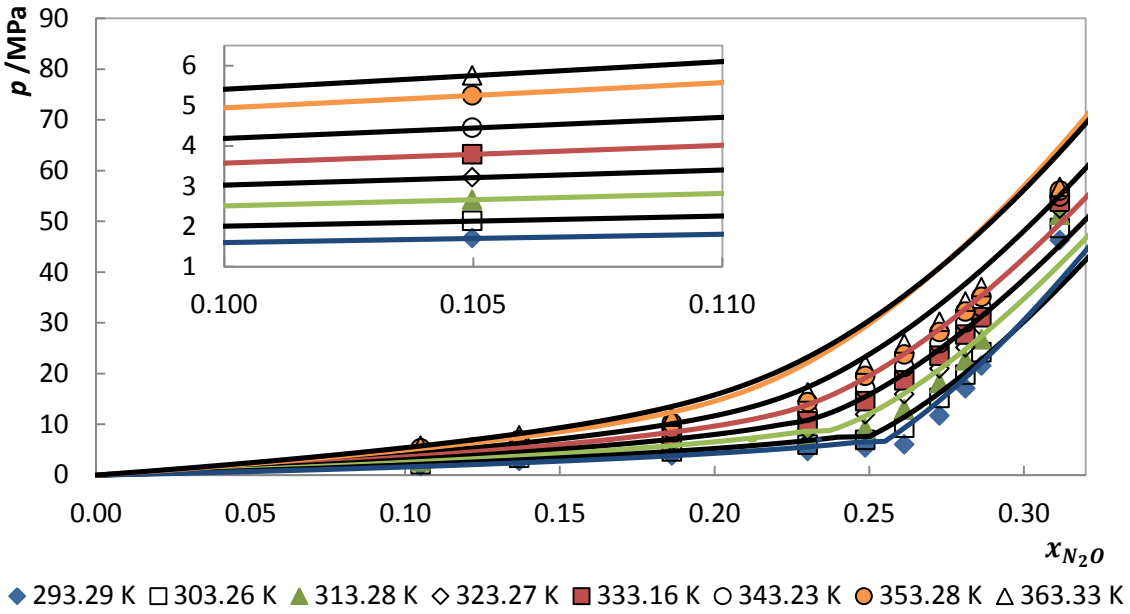

Figure 8.4- *px* diagram for the system N_2O + $[C_2mim][CH_3OHPO_2]$ at different temperatures. Solid lines represent soft-SAFT EoS prediction adjusted for the lowest gas composition using specifics binary parameters (ξ).

Table 8.10- Calculated Henry's constants of N_2O in $[C_2mim][CH_3OHPO_2]$ at different temperatures, minimum square error (R^2) obtained in the linear regression adjusted for a gas composition up to 0.05 and binary parameters (ξ) used in the soft-SAFT EoS predictions.

T (K)	*H* (Mpa)	R^2	ξ
293.29	14.24	0.9995	0.9605
303.26	18.14	0.9996	0.9658
313.28	22.80	0.9997	0.9660
323.27	27.64	0.9997	0.9649
333.16	32.59	0.9998	0.9625
343.23	38.08	0.9998	0.9587
353.28	44.71	0.9997	0.9526
363.33	48.77	0.9998	0.9513

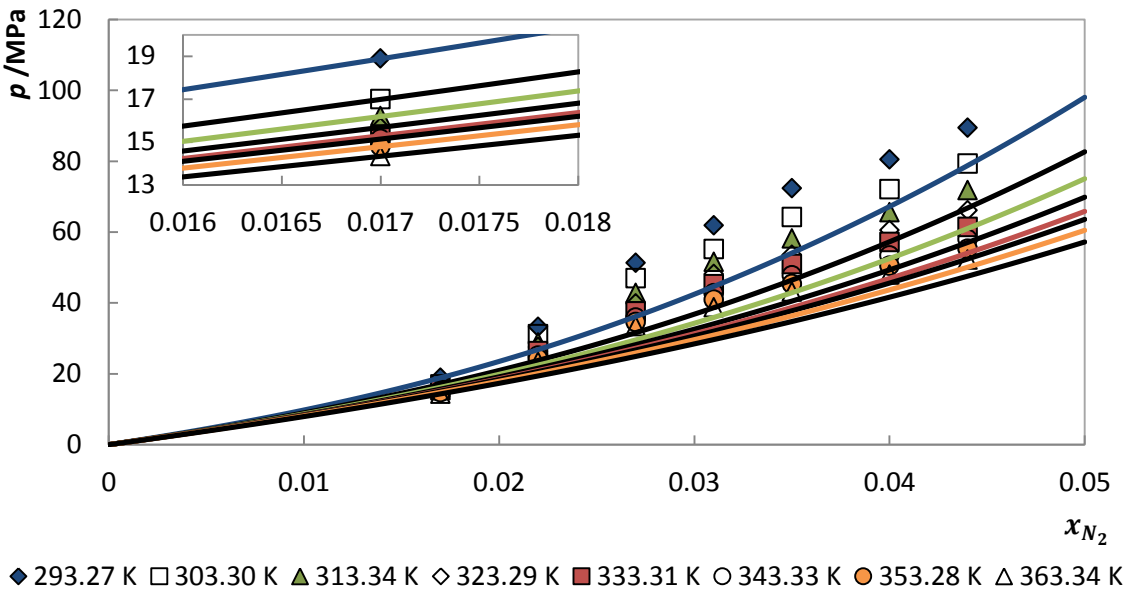

Figure 8.5- *px* diagram for the system N_2 + $[C_2mim][CH_3OHPO_2]$ at different temperatures. Solid lines represent soft-SAFT EoS prediction adjusted for the lowest gas composition using specifics binary parameters (ξ).

Table 8.11- Calculated Henry's constants of N_2 in $[C_2mim][CH_3OHPO_2]$ at different temperatures, minimum square error (R^2) obtained in the linear regression adjusted for a gas composition up to 0.01 and binary parameters (ξ) used in the soft-SAFT EoS predictions.

T (K)	*H* (Mpa)	R^2	ξ
293.27	988.58	0.9992	0.8476
303.30	907.41	0.9994	0.8780
313.34	875.19	0.9995	0.8920
323.29	855.11	0.9996	0.8975
333.31	839.58	0.9997	0.8978
343.33	835.33	0.9997	0.8933
353.28	819.84	0.9998	0.8887
363.34	798.73	0.9998	0.8840

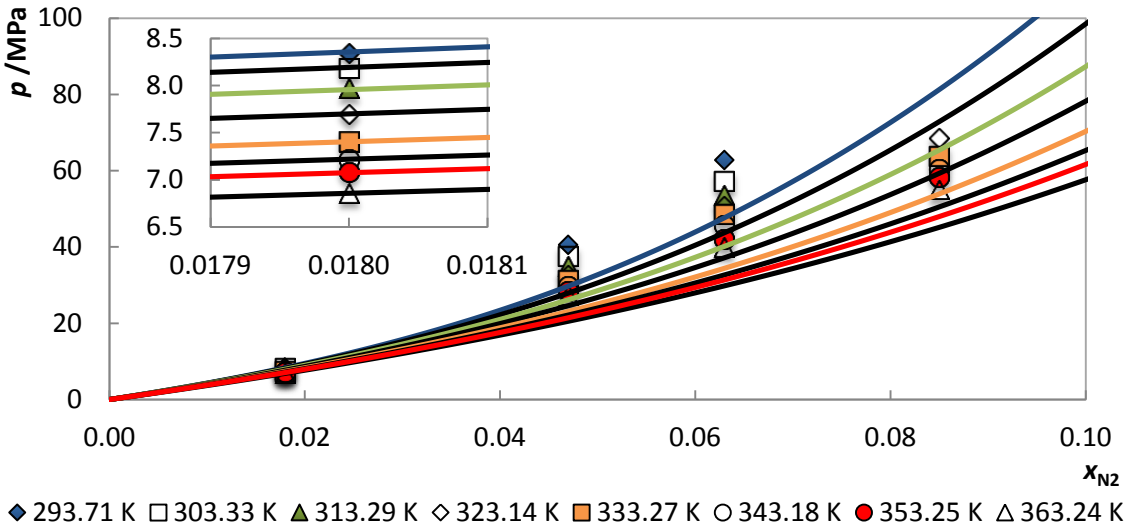

Figure 8.6- *px* diagram for the system N_2 + $[C_4mim][N(CN)_2]$ at different temperatures. Solid lines represent soft-SAFT EoS prediction adjusted for the lowest gas composition using specifics binary parameters (ξ).

Table 8.12- Calculated Henry's constants of N_2 in $[C_4mim][N(CN)_2]$ at different temperatures, minimum square error (R^2) obtained in the linear regression adjusted for a gas composition up to 0.02 and binary parameters (ξ) used in the soft-SAFT EoS predictions.

T (K)	*H* (Mpa)	R^2	ξ
293.71	472.22	0.9988	0.7400
303.33	462.03	0.9991	0.7654
313.29	447.96	0.9993	0.7820
323.14	432.88	0.9994	0.7920
333.27	415.76	0.9996	0.7985
343.18	405.01	0.9996	0.8000
353.25	396.70	0.9997	0.7987
363.24	384.20	0.9997	0.7982

9- List of Publications

1. Pereira, L. M. C.; Oliveira M. B.; Dias, A. M. A.; Llovell, F.; Vega, L. F.; Carvalho, J. P. and Coutinho, J. A. P. *High Pressure Phase Behaviour of CO_2, CH_4, N_2O and N_2 in 1-ethyl-3-methylimidazolium Methylphosphonate: Solubilities, Selectivities and soft-SAFT modelling.* (**in progress**)

2. Pereira, L. M. C.; Martins, V. F. B.; Oliveira M. B.; Dias, A. M. A.; Llovell, F.; Vega, L. F.; Carvalho, J. P. and Coutinho, J. A. P. *High Pressure Phase Behaviour of CO_2, CH_4, N_2O and N_2 in 1-methyl-3-methylimidazolium Dicyanamide: Solubilities, Selectivities and soft-SAFT modelling.* (**in progress**)